BRONSTED ACID SITE HETEROGENEITY IN ZEOLITE HZSM-5 AND SYNERGISTIC EFFECTS WITH WATER IN HYDROCARBON REACTIONS

By

MARYAM ABDOLRAHMANI

Bachelor of Science in Chemical Engineering
Mohaghegh Ardebili
Ardebil, Iran
2006

Master of Science in Chemical Engineering
Iran University of Science & Technology
Tehran, Iran
2009

Submitted to the Faculty of the
Graduate College of the
Oklahoma State University
in partial fulfillment of
the requirements for
the Degree of
DOCTOR OF PHILOSOPHY
May, 2019

BRONSTED ACID SITE HETEROGENEITY IN ZEOLITE HZSM-5 AND SYNERGISTIC EFFECTS WITH WATER IN HYDROCARBON REACTIONS

Dissertation Approved:

Dr. Jeffery L. White

Dissertation Adviser

Dr. Nicholas F. Materer

Dr. Jimmie Weaver

Dr. Christopher Fennell

Dr. Clint P. Aichele

.

ACKNOWLEDGEMENTS

I would like to express the deepest appreciation to my adviser, **Dr. Jeffery L. White**, for his continuing support and meaningful assistant.

I would also like to thank my supportive husband, **Mehdi**, who has been with me and supported me in this journey.

In addition, I would like to gratefully acknowledge my family, especially my mother, and my friends, especially **Milad**, who have been journeyed with me during my PhD.

Name: MARYAM ABDOLRAHMANI

Date of Degree: MAY,2019

Title of Study: BRONSTED ACID SITE HETEROGENEITY IN ZEOLITE HZSM-5 AND SYNERGISTIC EFFECTS WITH WATER IN HYDROCARBON REACTIONS

Major Field: CHEMISTRY

Abstract: Zeolite catalysts are solid Brønsted acids whose reactivity is typically associated with the number of protons at crystalline framework bridging acid sites (BAS's) and the bonding environments around them. Direct observation of multiple reactive sites in the zeolite HZSM-5, a member of the MFI family of zeolite structures, contradicts the traditional view of only one type of active protonic species in the zeolite HZSM-5. For the first time, an acidic and reactive species has been directly observed in HZSM-5 contributed to a small population of highly deshielded acid sites arising from extra-framework (EFAl) moieties in the solid-state ^{1}H MAS NMR spectrum at 12−15 ppm. Post-synthetic treatments of HZSM-5 zeolite modify the concentration of acidic protons arising from framework (FAl) and EFAl moieties. In this work, the removal and re-creation of EFAl species in the vicinity of BAS, via chemical washing using ammonium hexafluorosilicate (AHFS) and steaming, respectively, were quantified by ^{1}H spin-counting NMR experiments on HZSM-5 with Si/Al ratio of 11.5, 15, and 40. Spin-counting data revealed that FAl protons only comprise ca. 50% of the total protons in ZSM-5 at Si/Al = 15 and the remaining 50 % is assigned to EFAl protons. Probe-molecule reactions between benzene-d_6 and HZSM-5 at Si/Al = 15 (control, washed, mild steamed, and severe steamed) carried out at low pressure and room temperature, showed that adding sub-stoichiometric amounts of water enhanced H/D exchange reaction rates in the HZSM-5 zeolites with H-EFAL species. Our data showed that the synergistic effect between EFAl and water most likely occurs due to an increase in the "vehicle hopping" proton-transfer mechanism. In control and steamed samples, maximum reaction rates were observed at water loadings of ca. 0.1 equivalents, as a result of simultaneous presence of FAl and EFAl species. On the other hand, for the washed sample with single type of acid site, framework BAS, adding water suppressed the rate of reaction. Thus, the most active catalysts in room-temperature probe reactions contain all three types of potentially reactive protons, i.e., protons from BAS's and protons from EFAl species, and protons from trace amounts of water.

TABLE OF CONTENTS

LIST OF TABLES

Table Page

LIST OF FIGURES

Figure Page

CHAPTER I

Introduction of Zeolites

1.1. Introduction

The word zeolite is formed from two Greek words “zeo” (boiling) and “lithos” (stone); to mean boiling stones. Zeolites are the types of crystalline, microporous, aluminosilicates, which are built up from primary building units of SiO_4 and AlO_4 tetrahedra-linked through corner sharing of oxygen atoms (oxygen bridges).[1] Although SiO_4 tetrahedra is charge-balanced, an AlO_4 tetrahedra has a negative charge. This negative charge is neutralized with the extra-framework cations occupying the pores of the zeolite, resulting in a net neutral framework. Overall, zeolites have a chemical formula which is written as $M_{2/n}OAl_2O_3.xSiO_2.yH_2O$, where M is a cation with charge n, mostly from group I or II, or rare earth ions or organic species that compensate for the negative charge of AlO_4 tetrahedra. These ions are located in the external surface of zeolite (as shown in Fig.1.1), bound to the aluminosilicate by the weaker electrostatic bonds. [2] Also, x represents the ratio of silicon to aluminum atoms, which should be 2 or more, and y is the number of moles of adsorbed water molecules in the voids.[3] The pores of zeolites are of molecular dimension, which contain water, exchangeable extra-framework cations, and removable template molecules.[4]

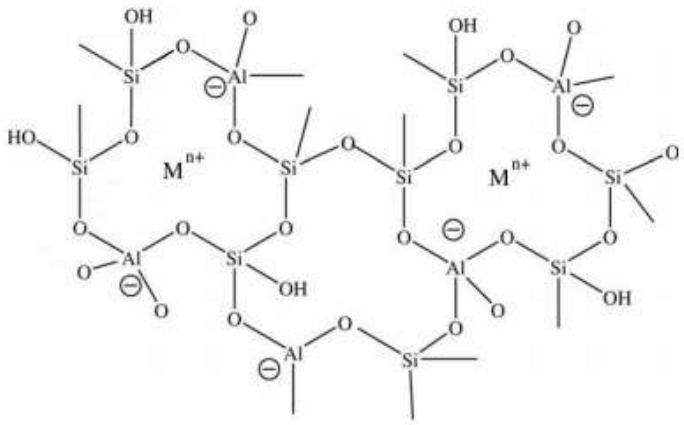

Fig. 1. 1. Two dimensional framework structure of zeolites with Si-O and Al-O bonds; M represents extra-framework cations[2] (Weckhuysen et al., *Chem. Soc. Rev.* 2015).).

1.2. Structure of zeolites

In addition to the primary building block, TO_4 tetrahedra, the secondary building units (SBUs) are characteristic of the zeolite structures, which are shown in Fig.1.2. SBUs are generated by repeating the primary building units and combining them with each other, consequently determining the type of framework type and zeolite structure. [5-6]

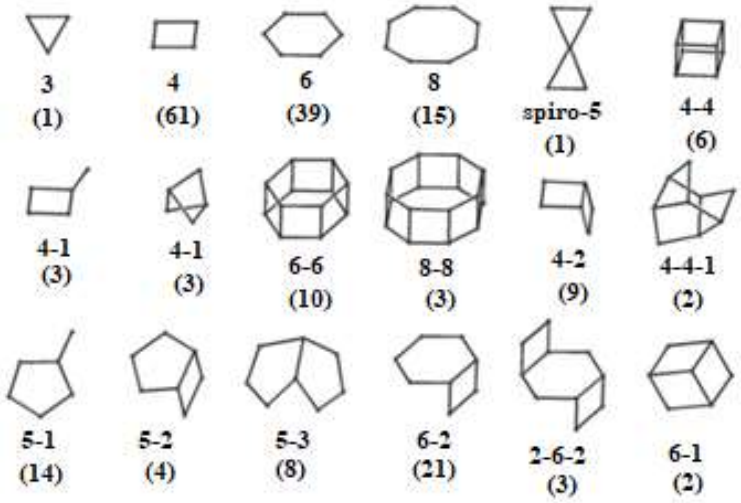

Fig. 1. 2**.** Secondary building units and their symbols; the numbers in parentheses represent the frequency of occurance[4] (Adapted from Baerlocher et al., *Elsevier, Amesterdam*).

The SBUs are in different forms such as single rings, double rings, polyhedral, and even more complex units, which are linked together in a variety of ways to produce a unique system of channels and cages.[2]

Pore diameters of three dimensional zeolite structures depend on the number of T-atoms in the ring around the pore. There are different ranges of pores depending on the number of T- atoms.

a) Small pore zeolites, 8-membered rings, such as Erionite,

b) Medium pore zeolites, 10-membered rings, such as ZSM-5, ZSM-11, MCM-23,

c) Large pore zeolites, 12-membered rings, such as mordenite, faujasite (X, Y), Beta,

d) Extra-large pore zeolites, 14-membered rings, such as CIt-5.

In the literature, various categories of the pore size are reported. Pore diameters less than 2 nm, between 2-50 nm, and larger than 50 nm are micopores, mesopores, and macropores, respectively.[7] Fig. 1.3 illustrates the various zeolite crystal structures for zeolites with different pore sizes.[2]

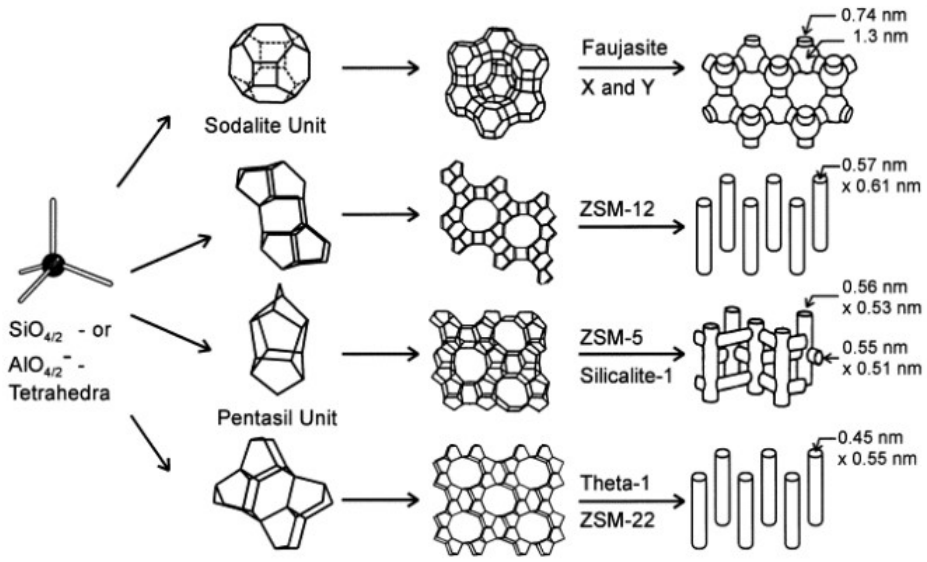

Fig. 1. 3**.** Structures of four selected zeolites and their micropore systems and dimensions[4] (Adapted from Baerlocher et al., *Elsevier, Amesterdam*).

There are more than 200 different types of zeolites, among which only 10 types are used in industrial applications. Y zeolite, ZSM-5, mordenite, MCM-22, and SAPO-34 are used as a catalyst in most of petrochemical reactions due to their large surface area, unique pore size, crystallinity, and thermal stability. In zeolites, the central atoms are Si and Al, but there are other types of zeolites in which other central atoms are possible. SAPO (in which the central atoms are Si, Al, and P), AlPO4 (in which the central atoms are Al, and P), MeAPO (in which the central atoms metal cation, Al, and P), and MeSAPO (in which the central atoms metal cation, Si, Al, and P) are known to exist.

There are more than 200 different types of zeolites, among which only 10 types are used in the industrial applications. Y zeolite, ZSM-5, mordenite, MCM-22, and SAPO-34 are used as the catalyst in the most of petrochemical reactions due to their large surface area, unique pore size, crystallinity, and thermal stability. In zeolites, the central atoms are Si and Al, but there are other types of zeolites in which other central atoms are possible. SAPO (in which the central atoms are Si, Al, and P), AlPO4 (Al, and P as the central atoms), MeAPO (Al and P as the central atoms) and MeSAPO (the central atoms are metal cation, Si, Al, and P) are known to exist.

1.3. Shape selectivity of zeolites

Shape selectivity of zeolites originates from different pore topologies and sizes in channels and pores. Steric hindrance for the reactants, products, and transition states within the channels, intersection and pores results in the selective transport of reactants and/or products through the pores.[8-10] There are basically three types of shape selectivity in HZSM-5 zeolite:

(1) Reactant shape selectivity

(2) Transition state shape selectivity

(3) Product shape selectivity

Adsorption and/or diffusion of the reactant molecules, the formation of some product molecules in the transition state, and the desorption of some product molecules are influenced by confinement arising from the size and shape of the pores.[11] As the pore size decreases, the shape selectivity in the zeolite increases. Smaller pore sizes suppress reactions by allowing only specific products to be produced. Both reactant and product shape selectivities are influenced by crystal sizes, while limited transition state selectivity does not depend on crystal size. Zeolites with smaller pore sizes and stronger interactions show higher selectivity in the products of the hydrocarbon reactions.

1.4. Three most common zeolites

1.4.1. ZSM-5

ZSM-5 (Zeolite Secondary Mobile with sequence number five) is the orthorhombic end member of the pentasil family.[11] The three-dimensional microporous structure of ZSM-5 contains straight, sinuous 10-member ring channels with a size of 5.1-5.6 Å and channel intersections with a size of about 8 Å, as shown in Fig. 1.4. According to the IZA database,[12] the maximum size of a sphere that can diffuse through the channels and intersections is 4.46-4.70 Å and 6.36 Å, respectively.[13] Also, HZSM-5 zeolite has shown unique shape-selective properties due to channels and intersections diameters.

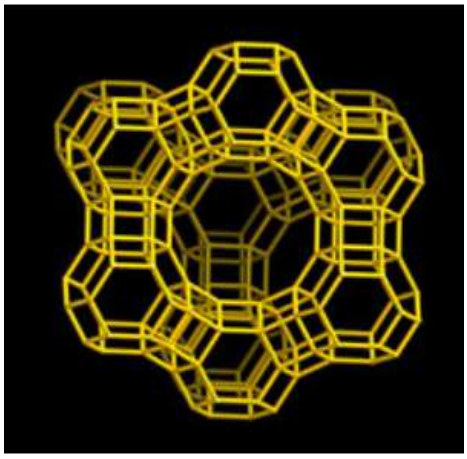

Fig. 1. 4. The framework structure of Y zeolite[12] (Adapted from www.iza-structure.org/databases).

Zeolite Y is the main active component in fluid cracking (FCC) catalyst and can effectively replace amorphous silica-alumina (the main previous catalysts in FCC). Their high activity and acidity, combined with promoted selectivity toward gasoline and lower coke formation relative to the previous generation of catalysts (amorphous silica–alumina-based catalysts), has allowed refiners to significantly increase gasoline output.[18]

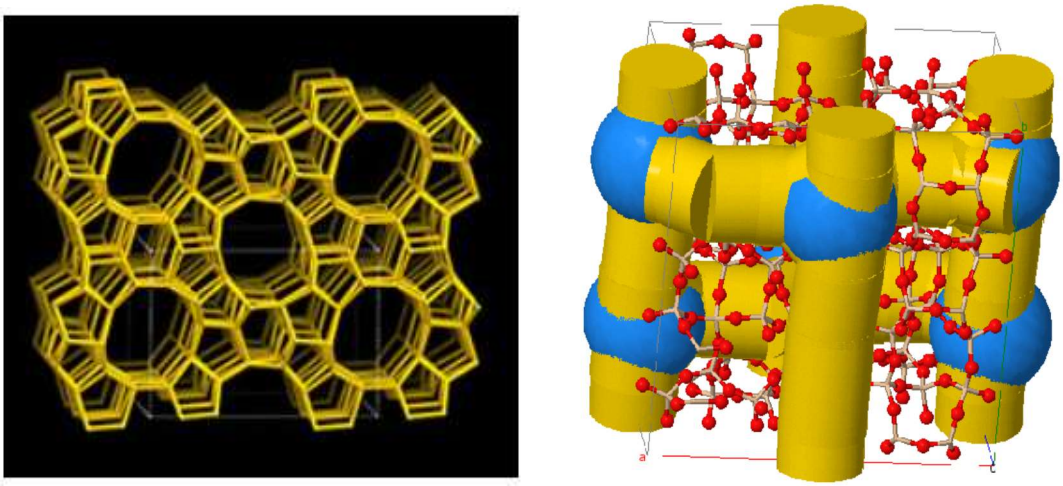

Fig. 1. 5. The framework structure of ZSM-5 zeolite[12] Adapted from www.iza-structure.org /databases).

Zeolites possess ordered micropores structures with a distribution of framework and extra-framework Brönsted acid sites. However, intracrystalline diffusion limitations and disordered distribution of acid sites limit the performance of zeolites in hydrocarbon reactions.[14-15]

HZSM-5 zeolite plays a critical role in the catalytic conversion of methanol to olefins, fluid catalytic cracking, and hydrocarbon isomerization and disproportionation reactions. HZSM-5 has attracted significant attention in the fundamental catalysis research due to its relatively simple channel structure, and wide range of accessible Si to Al lattice ratios, and spectroscopic or probe molecule evidence that it contains a single type of Brönsted acid site in its synthesized form. Recently, it has been suggested that there is more than one active acid site in the HZSM-5 zeolite.

Direct detection of at least three types of protons exhibiting Brönsted acid species in zeolite HZSM-5 has recently been reported using one- and two-dimensional ^{1}H solid-state NMR methods. HZSM-5 zeolite with low Si/Al ratios have active bridging acid site at 4.2 ppm, and extra-framework aluminol species at 2.8 ppm, 6-7 ppm, and 13-15ppm peaks respectively.[16]

1.4.2. Y

Zeolite Y, together with zeolite X are family of Faujasite type structure (FAU). One difference between zeolite Y and X is the higher ratio of silicon to aluminum in zeolite Y. FAU framework structure is composed of 24-tetrahedracuboctahedral units (sodalite cages) in the FAU framework type connected via hexagonal prisms (double 6-rings) forming a 3-dimensional porous channel structure, characterized by 12-oxygen ring window openings with the aperture of 8 Å and super cages of approximately 12 Å.[17]

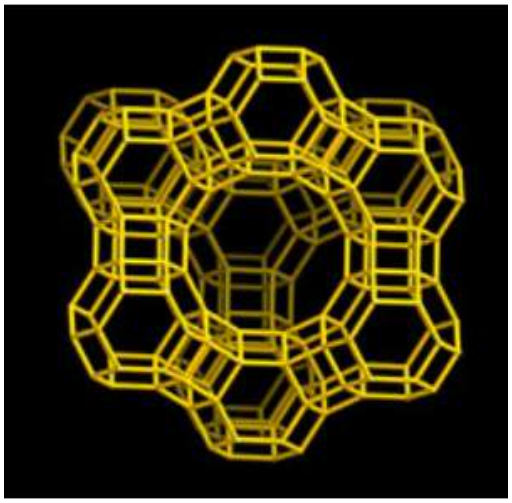

Fig. 1. 6. The framework structure of Y zeolite[12] (Adapted from www.iza-structure.org/databases).

Zeolite Y is the main active component in the fluid cracking (FCC) catalyst and can effectively replace the amorphous silica-alumina (the main previous catalysts in FCC). Their high activity and acidity, combined with promoted selectivity toward gasoline and lower coke formation

relative to the previous generation of catalysts (amorphous silica–alumina-based catalysts), has allowed refiners to significantly increase gasoline output.[18]

1.4.3. ZSM-22

The framework of ZSM-22, a member of TON family, is made up by 5-, 6-, and 10-membered rings of TO_4 tetrahedra and can be created from complex 5-1 secondary building units[19]. The 10-membered ring channels are not interconnected, so they represent a one-dimensional channel system. Its crystal structure contains needle-shaped agglomerates of individual rod-like crystals, referred to as nano-rods[3]. ZSM-22 zeolites have elliptical micropores with the diameter of 4.6 × 5.7Å, which is remarkably smaller than the 10-membered ring channels of ZSM-5 (5.1 X 5.6Å)[20].

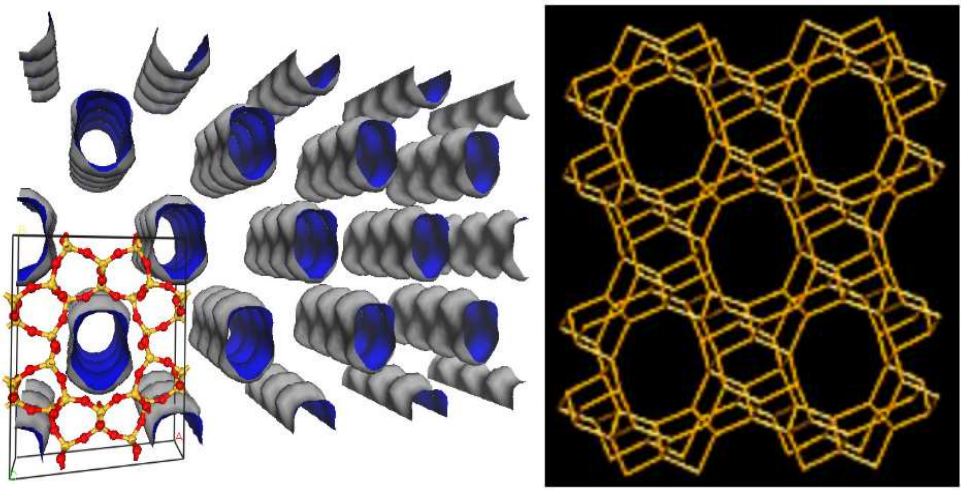

Fig. 1. 7. The framework structure of zigzag 10-ring channels of ZSM-22[12] (Adapted from www.iza-structure.org/databases).

Like ZSMS-5, ZSM-22 zeolites with unidimensional pores are interesting catalysts for methanol-to-olefins conversion.

1.5. Acid sites

The chemical and physical properties of zeolites are determined to a great extent by the amount of

aluminum in the framework of zeolite. The amount of aluminum in the zeolite framework is typically represented by the (atomic) Si/Al ratio. The Si/Al ratio affects the acidity of the zeolites: as the total number of acid sites increases, the Si/Al ratio decreases. The substitution of some of the silicon atoms by aluminum atoms in the framework forms a deficiency in the electrical charge that must be locally neutralized by the presence of an additional cation within the pore structure. These cations can be replaced relatively easily by NH_4^+ ions by ion exchange in an aqueous medium with saturated solutions of NH_4NO_3. The ammonium form of the zeolite when calcined at the sufficiently high temperatures releases NH_3 and the resulting material is the acidic form of the zeolite.[21]

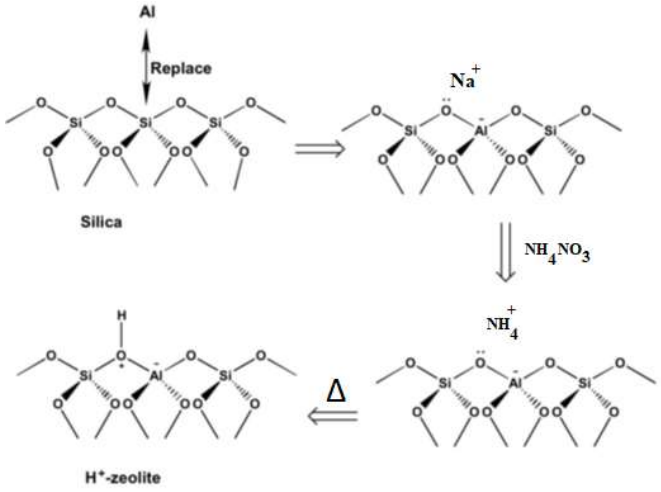

Fig. 1. 8**.** Formation of bridging hydroxyl group (Si-OH-Al) by exchanging the extra-framework cations to H^+ form[21] (Adapted from Arca et al., *Topics in Catalysis* 2018).

1.5.1. Brönsted acid sites

The acidity of zeolites refers to the type of acid site, concentration, distribution, and acid strength of them. For many catalytic applications in hydrocarbon reactions, a Brönsted acid form of a zeolite is necessary. As explained in Fig. 1.7., Brönsted acid sites in zeolites can be readily generated by introducing ammonium ions followed by heat treatment or by introducing multivalent metal

cations, typically cations of the rare-earths, again followed by heat treatment.

The principal acidity of acid zeolite catalysts is defined as Brönsted acid protons from bridging framework hydroxyls. The location and population of these hydroxyl groups in the protonated form of zeolites provide a basis for the interpretation of their properties. The protons from bridging hydroxyl groups are involved in the reactions and can be donated to the molecules to produce new products.[22]

1.5.2. Extra-framework Aluminum site (EFAl)

In the literature, it has been suggested that the distribution of acidic species is complex, including spectroscopic signals assigned to extra-lattice alumina (EFAl) sites close to lattice Brönsted sites. The distribution of Brönsted acid sites arising from extra-framework species and framework bridging acid site can be adjusted by specific post-synthesis treatments such as chemical extraction and steaming methods. The structure and nature of some selected EFAl species formed during steaming and/or preparation with Al present as cations (Al^{3+}, $Al(OH)_2^+$, AlO^+, $Al(OH)_2$) or as neutral or polymerized forms (Al_2O_3, AlO(OH), and $Al(OH)_3$) have been proposed.[23] These species, both Lewis and potential Brönsted acid sites, can be produced from the different preparation methods and/or by intentionally post-treatment procedures such as dealumination. In preparation methods, there is a preferred Si/Al ratio in the framework of every structure type. During crystallization, when the Si/Al ratio of the synthetic gel deviates from the ideal ratio, EFAl species could be formed, or the distribution of the aluminum atoms in the framework could be inhomogeneous.[24]

Thermal treatments may be used to increase the lattice Si/Al ratio of a zeolite by means of removing different fractions of framework Al-atoms, where heating of Brönsted acid sites causes dehydroxylation with the formation of an electron acceptor “Lewis acid sites” at high temperatures. This process is followed by the removal of aluminuum species (AlO^+) from the lattice structures into cationic positions, and the generated EFAl species as the true Lewis acid sites.[25]

As shown in Fig. 1.8, dealumination of zeolites usually releases aluminum atoms from the framework giving rise to EFAL.

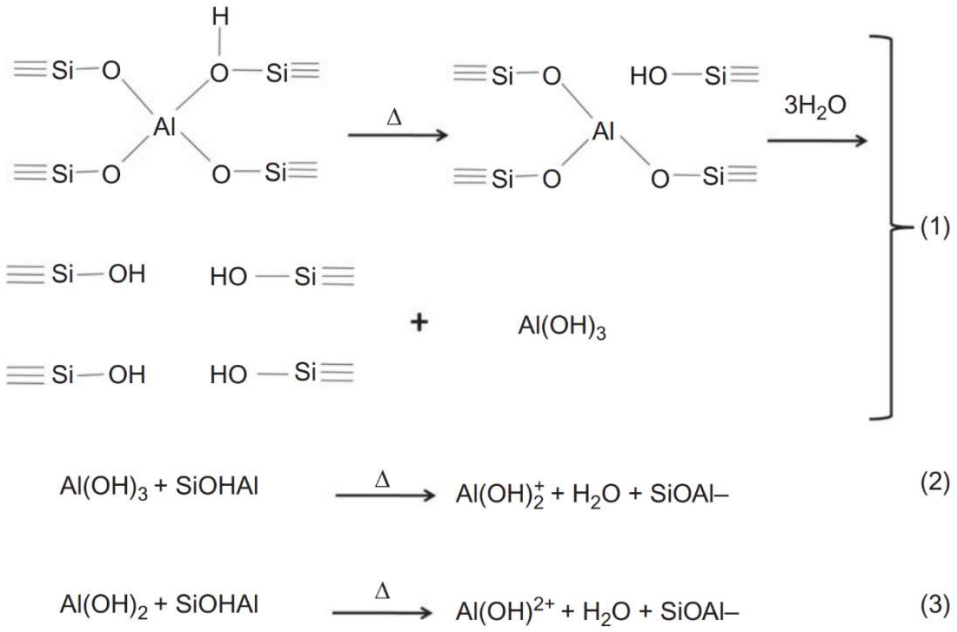

Fig. 1. 9. Dealumination and EFAl creation mechanism proposed for zeolite H-Y[26] (Adapted from Zhiwu et al., *Angew. Chem. Int. Ed*, 2010).

The creation of EFAL species improves the thermal stability and catalytic performance of zeolites. The improvement of catalytic properties can be explained by the formation of Lewis acid sites or by an increase in the Brönsted acidity due to the influence of close EFAl species.[26] It has been concluded that the role of EFAL is to stabilize the conjugated base formed upon deprotonation by hydrogen bonding and nucleophilic interaction with the framework oxygen atoms. Also, the improvement of catalytic activity arising from the presence of EFAl species is mostly related to a cooperative interaction between strong Brönsted acid sites (SBAS) and an adjacent EFAl as shown in Fig. 1.9.[27]

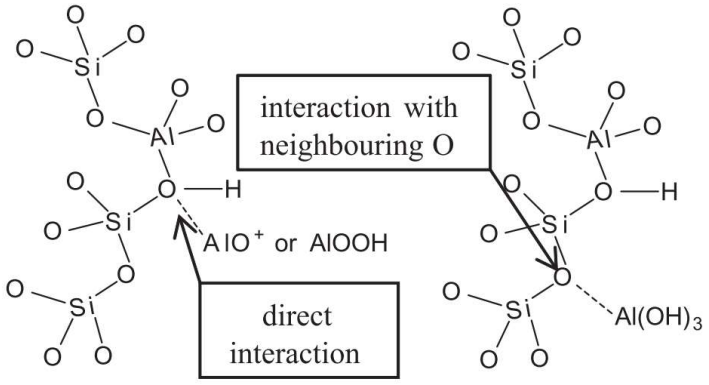

Fig. 1. 10. Possible modes for the interaction of extra-framework Al with SBAS[27] (Adapted from Schallmoser et al., *Journal of Catalysis*, 2014).

The direct interaction would involve a partial electron transfer from the hydroxyl group to the EFAl species, which has been proposed to increase its acid strength. Based on NMR experiments and DFT calculations, Li et al. have developed a modified picture of this interaction between the SBAS and EFAl, suggesting that the proton affinity of the SBAS substantially decreases even when the EFAl species are coordinated to neighboring oxygen atom.[28]

O. Lisboa et al. performed quantum-chemical calculations by using DFT method in order to model the whole EFAL formation process and concluded that the resulting EFAL in the dealumination process of H-ZSM5 zeolite are Penta- ($Al(OH)_3(OH)_2$) or threefold ($Al(OH)_3$) coordinated species. Octahedral species are not discarded because these species are formed as intermediates in the EFAL formation. A SiOH nest is also produced in the framework.[29]

It was found that all of the extra-framework aluminum species (EFAL and Lewis acid sites) are always in close proximity to the framework aluminum arising from Brönsted acid sites in both H-MOR and H-ZSM-5 zeolites. Deng et.al proposed a model to explain the Brönsted/Lewis acid synergy in the dealuminated HZSM-5 zeolite as shown in Fig. 1.10.

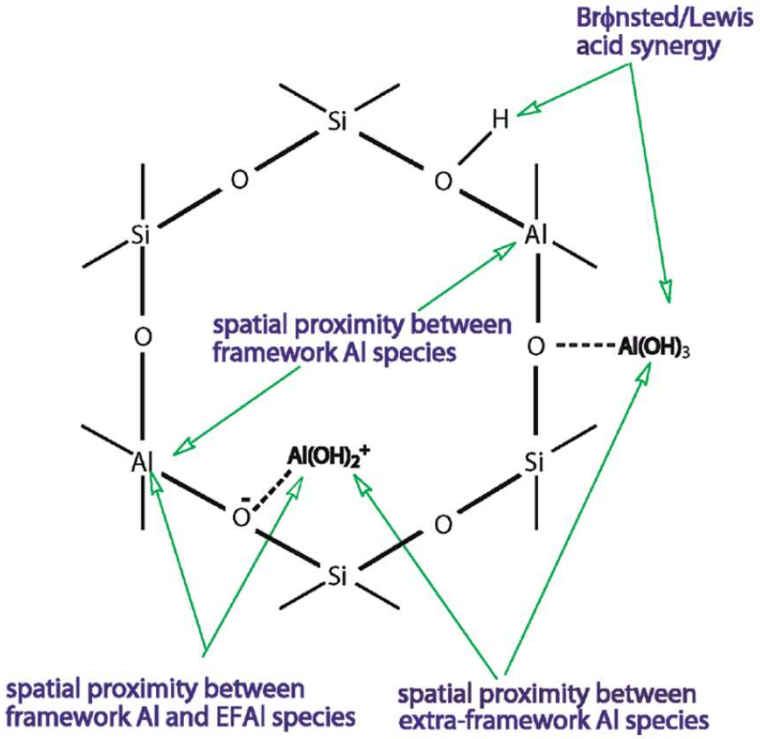

Fig. 1. 11. Scheme of Brönsted/Lewis acid synergy and experimentally observed spatial proximities of various species for dealuminated Zeolite H-ZSM-5[28] (Adapted from Li et al., *Journal of the American Chemical Society* 2007).

The Brönsted/Lewis acid synergy affects the acidic strength of the dealuminated H-ZSM5 and H-MOR zeolites by coordination of the Lewis acid site to the oxygen atom nearest to the Brönsted acid sites. In addition, the NMR characterization indicated that six-coordinate $Al(OH)_3$ and five-coordinate $Al(OH)_2^+$ are the preferred EFAl species and are in close proximity of four-coordinate framework Al species in the dealuminated zeolites.[28]

1.6. Post-synthesis treatments

The different size of the micropores causes some limitations in using zeolites as catalysts. To overcome these limitations that arise from diffusion constraints and consequently preventing access to the active acidic sites, the introduction of mesopores interconnected with the existing micropores is suggested. The acidic strength of zeolite materials is related to the number of aluminum atoms in the framework by substitution of silicon by aluminum. Each aluminum in the framework results in one bridging acid site, which is very acidic and reactive. Modification of the catalytic properties through dealumination of zeolite lattices by various treatments has therefore been a matter of considerable interest. Although ZSM-5 is more resistant to dealumination than Y or mordenite zeolites, it can be dealuminated by using different post-synthetic treatments. Different preparation methods and post-synthesis treatments such as hydrothermal treatment and calcination, steaming, and chemical washing dealumination introduce extra-framework aluminum species of low symmetry, which remain within the pores of the zeolite as catalytically active sites.[30-31] In other words, framework hydrolysis of Si–O–Al linkages can lead to the aluminum losses from the framework that enhances the catalyst activity.[27]

In the next section, different post-synthesis methods to control and modify the acidic properties arising from bridging acid sites and EFAl species are explained.

1.6.1. Steaming

Hydrothermal steaming is an effective post-synthesis treatment used for controlling the framework Si/Al ratio as it leads to the replacement of a part of the framework aluminum by silicon. Dealumination of the zeolite framework by water vapor treatment at high temperatures called steaming, can change the performance of zeolites in the reactions. Furthermore, such post-treatment processes are often used to increase the thermal stability and catalytic activity prior to their use in

hydrocarbon reactions. During steaming, the removal of Al from the tetrahedral sites results in formation of EFAl species that can be involved in the reactions.

In general, a dealumination process, that occurs through three steps, is summarized in scheme 1.1:[32]

1) Cleavage of the -O-Al-O- bonds in the framework,

2) Removal of the aluminum complexes,

3) Refilling of the empty sites by the silicon atoms and formation of the silanol nest.

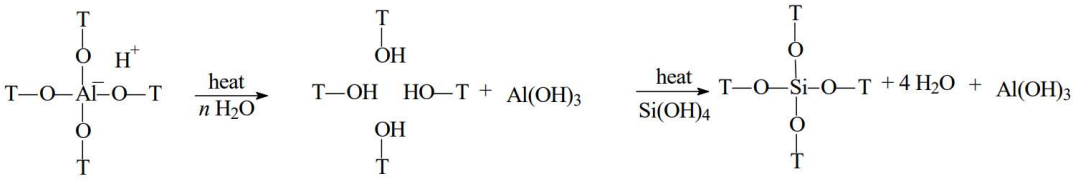

Scheme 1.1. Dealumination process by water at high temperature[32] (Adapted from Kerr et al., *American Chemical Society*, 1973).

A number of studies have observed that the degree of lattice dealumination depends on some parameters such as the type of parent zeolites, temperature (referred as "mild" when T ≤ 500 °C and "severe" for higher values), water vapor pressure, and time of steaming. In general, the resistance towards dealumination increases as the initial concentration of Al of the zeolite decreases. The removal of framework aluminum results in lower density of BAS, which also progressively decreases as the steaming treatment time increases.[33] It has been reported that for faujasite zeolites following steam treatment, higher temperatures lead to a higher degree of dealumination. As HY zeolite is dealuminated in presence of steam to convert to ultra-stable HY (USHY) zeolite, its activity increases due to an increase in the strength of its Brönsted acid sites.

Some reasons for the higher acid strength of USHY than HY zeolites are explained: First, dealumination results in an increase in the number of isolated aluminum, those with no second nearest neighbor aluminum, which are believed to be more acidic. Secondly, steam dealumination introduces non-framework aluminum species, which could withdraw electron density from nearby Brönsted acid sites, causing an enhancement in the strength of the site. The synergistic mechanism of the Lewis acid and Brönsted acid sites may enhance activity by promoting hydride abstraction and help to initiate the cracking reaction.[34-36]

Also, M. Ibáñez et al.[33] observed the dependency of the dealumination of a ZSM-5 zeolite as a function of exposure to steam at 350°C by using FTIR and solid-state NMR. The ^{29}Si MAS-NMR and ^{27}Al MAS-NMR spectra of the parent HZSM-5 (SiO_2/Al_2O_3 = 30), HZ-30, and three steamed catalysts with treatment temperature of 300ºC (ST300), 400ºC (ST400), and 500ºC (ST500) are displayed in Fig. 1.11. and Fig.1.12, respectively. The chemical shift of the ^{29}Si nuclei depends on their respective coordination with OSi, OH or OAl species. The parent catalyst shows a main peak at −118.5 ± 0.5 ppm corresponding to $Si(OSi)_4$ species (the framework tetrahedral Si species surrounded by 4 OSi) and a shoulder at −113.2 ppm corresponding to $Si(OSi)_3(OAl)$ species. As the temperature of the steaming is raised, the band corresponding to $Si(OSi)_3(OAl)$ species gradually disappears and that of the $Si(OSi)_4$ species progressively increases. It means that by increasing the steaming temperature, the tetrahedral aluminum transfers and extra-framework aluminum species including distorted four-fold, penta-coordinated or octahedral Al sites are produced.

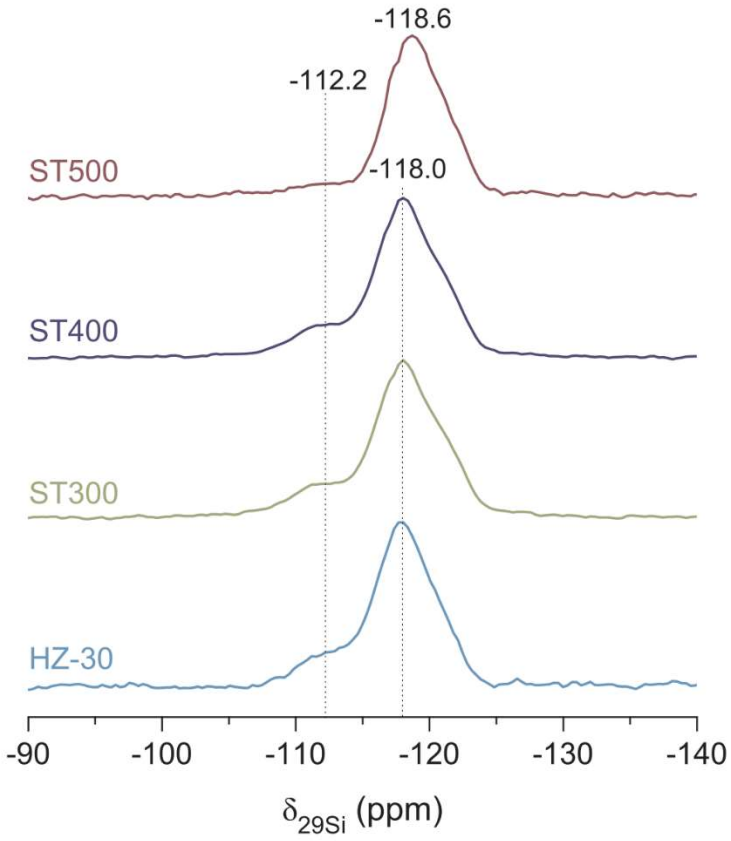

Fig. 1. 12. ^{29}Si MAS-NMR spectra of the parent and steamed HZSM-5 zeolites[33] (Adapted from Ibáñez et al., *Applied Catalysis A: General* 2017).

In Figure 1.12, ^{27}Al MAS-NMR spectra show that the parent HZ-30 sample encompasses two main peaks located at 55 ppm and 0 ppm rising from framework tetrahedral and extra-framework octahedral aluminum species, respectively. For the steamed samples at different temperatures, by increasing the steaming temperature, the peak corresponding to the tetrahedral aluminum shifts towards 53.6 ppm. Also, the intensity of extra-framework aluminum species increases and a new peak at 33.1 ppm, assigned to distorted pentahedral coordination, or distorted tetrahedral coordination aluminum, appears.

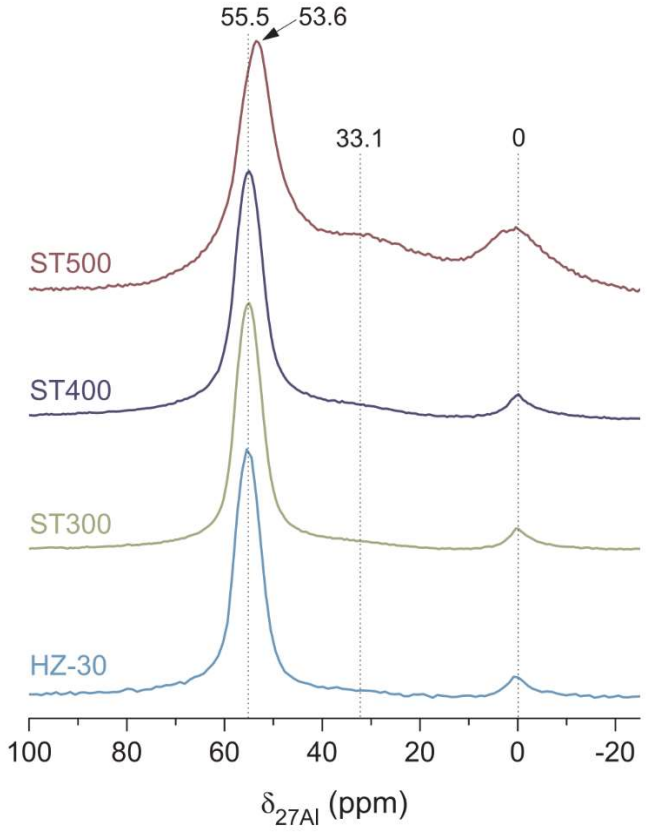

Fig. 1. 13. ^{27}Al MAS-NMR spectra of the parent and steamed HZSM-5 zeolites[33](Adapted from Ibáñez et al., *Applied Catalysis A: General* 2017).

The peak arising from the framework tetrahedral species at 55 ppm can be subdivided into two sub-peaks, which have been correlated with the different types of framework aluminum sittings: (i) 55.5 ppm, strong acid sites sometimes involving a pair framework Al site (Al-O-Si-OAl), located within the micropores of the HZSM-5 zeolite (both straight and sinusoidal pores), referred as ($\alpha + \gamma$) siting; and (ii) 53.6 ppm, weaker acid sites, involving a single framework Al site, located within the pore intersections and referred as β siting. From the combined results of Fig. 1.11. and Fig. 1.12., it is concluded that during the steaming dealumination, tetrahedral aluminum species convert to distorted and extra-framework aluminum species.

The formation mechanisms and detailed structure of these species are far from understood, due to the lack of experimental methods in order to provide the necessary information on the local structure. However, the structure and formation of these EFAl species and distorted framework sites have been addressed in several theoretical studies, often in combination with NMR spectroscopy. On the other hand, the combination of ^{27}Al DQ-MAS NMR with DFT theoretical calculations for H-Y zeolite explained the three consecutive steps for the dealumination process:[28]

- In the first step, four-coordinate framework Al is released from zeolite framework, giving rise to six-coordinate $Al(OH)_3$ EFAL species.
- In the second step, the $Al(OH)_3$ EFAL species would interact with the Brönsted acid site (SiOHAl, associated with four-coordinate framework Al), leading to the formation of five-coordinate $Al(OH)_2^+$ EFAL species by removal of one water molecule between them.
- In the third step, the interaction of the $Al(OH)_2^+$ species with the Brönsted acid sites results in the formation of four-coordinate $AlOH^{2+}$ EFAL species by eliminating another one water molecule between them.

$Al(OH)_3$, $Al(OH)_2^+$, and $AlOH^{2+}$ in the form of six-, five-, and four-coordination, respectively, are the preferred EFAL species in the dealuminated H-Y zeolites at different calcination temperatures.[28]

1.6.2. Chemical washing treatment

The amount and distribution of non-framework aluminum species formed during thermal treatments can significantly influence the activity and selectivity of zeolites in the reaction. At the same time, the large amount of non-framework Al has a deleterious effect on the catalytic and transport properties, so some post-synthesis treatments such as acid leaching and chemical washing treatments to extract them is necessary.[37] It has been reported in the literature that a modification in the distribution of aluminum by acid leaching can be controlled by the type and concentration of

the acid used, pH, temperature and duration of the treatment. A commonly used post-synthesis treatment for the removal of aluminum from the zeolite framework is using chemicals such as $SiCl_4$, $(NH_4)_2SiF_6$, HNO_3, HCl, H_3PO_4, $AgNO_3$, oxalic acid, tartaric acid, citric acid, trichloroacetic acid, among others.[33]

A. Gola et al. observed that EFAL species arising from dealumination of steamed Y zeolite (S34), as isolated cations, are resistant to strong acid leaching. Their results from subsequent leaching with nitric acid, AHFS, and Na_2H_2EDTA (EDTA) showed that both EDTA and AHFS led to progressive removal of all EFAL. However, EFAL species linked to the zeolite framework appear more resistant to these agents. In general, the EFAL concentration decreases continuously with strength of AHFS leaching, reaching a value close to zero at the point where the framework starts to get dealuminated. The general behavior for the EDTA leaching is similar to that observed for AHFS, but approximately twice the strength of leaching agent is required to achieve a similar level of EFAL.[23]

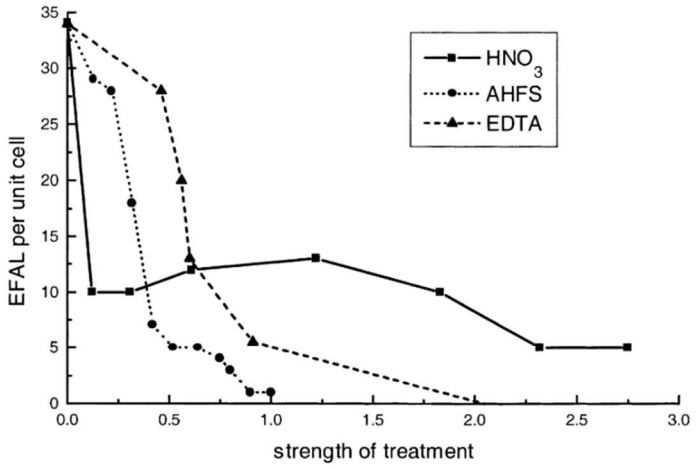

Fig. 1. 14. Concentration of EFAL following leaching by different agents (strength is expressed as the molar ratio of HNO_3, $(NH_4)_2SiF_6$ or H_2Na_2EDTA to Al in the steamed solid)[23] (Adapted from Gola et al., *Microporous and Mesoporous Materials* 2000).

The formation of EFAl species and dealumination of the framework depend on the reagents used. As has been shown in Fig. 1.13, acid-treatment of samples by AHFS resulted in a very high EFAl removal. Also, other chemicals such as oxalic acid (mild dealumination reagent) and AHFS (mild to intense dealumination reagent) have been applied on HZSM-5 zeolite to extract EFAl species. Farahani et al. reported that dealumination process can change the micropore architecture of ZSM-5 zeolite, which affects ethylbenzene disproportionation and even changes the relevant reaction mechanism. Their results showed that mild increase in the Si/Al molar ratio by one unit using oxalic acid or by 10 units by AHFS result in more than 10% increase in para-xylene selectivity.[38]

1.7. References

1. Bert M. Weckhuysen, J. Y., Recent advances in zeolite chemistry and catalysis. *Chem. Soc. Rev.* **2015**, *44*.
2. Mohau Moshoeshoe, M. S. N.-T., Veronica Obuseng, A Review of the Chemistry, Structure, Properties and Applications of Zeolites. *American Journal of Materials Science* **2017**, *7* (5), 26.
3. Sherman, J. D., Synthetic zeolites and other microporous oxide molecular sieves. *Proceedings of the National Academy of Sciences* **1999**, *96* (7), 3471-3478.
4. Ch. Baerlocher, L. B. M., D.H. Olson, Atlas of Zeolite Framework Types. *Elsevier, Amesterdam*.
5. Flanigen, E. M.; Khatami, H.; Szymanski, H. A., Infrared Structural Studies of Zeolite Frameworks. In *Molecular Sieve Zeolites-I*, AMERICAN CHEMICAL SOCIETY: **1974**; Vol. 101, pp 201-229.
6. Boscoboinik, J. A.; Yu, X.; Yang, B.; Shaikhutdinov, S.; Freund, H.-J., Building blocks of zeolites on an aluminosilicate ultra-thin film. *Microporous and Mesoporous Materials* **2013**, *165*, 158-162.
7. Borislav D. Zdravkov, J. J. C., Martin Sefara, Josef Jank, Pore classification in the characterization of porous materials: A perspective. *Central Journal of European Chemistry* **2007**, *5* (2), 11.
8. Bernauer, M.; Tabor, E.; Pashkova, V.; Kaucký, D.; Sobalík, Z.; Wichterlová, B.; Dedecek, J., Proton proximity – New key parameter controlling adsorption, desorption and activity

9. in propene oligomerization over H-ZSM-5 zeolites. *Journal of Catalysis* **2016**, *344*, 157-172.
10. Jones, A. J.; Carr, R. T.; Zones, S. I.; Iglesia, E., Acid strength and solvation in catalysis by MFI zeolites and effects of the identity, concentration and location of framework heteroatoms. *Journal of Catalysis* **2014,** *312*, 58-68.
11. Mlinar, A. N.; Zimmerman, P. M.; Celik, F. E.; Head-Gordon, M.; Bell, A. T., Effects of Brönsted-acid site proximity on the oligomerization of propene in H-MFI. *Journal of Catalysis* **2012**, *288*, 65-73.
12. Baur, W. H.; Fischer, R. X., MFI. In Zeolite-Type Crystal Structures and their Chemistry. Framework Type Codes LTA to RHO, Fischer, R. X.; Baur, W. H., Eds. Springer Berlin Heidelberg: Berlin, Heidelberg, **2006**; pp 1-31.
13. http://www.iza-structure.org/databases/.
14. Park, S.; Biligetu, T.; Wang, Y.; Nishitoba, T.; Kondo, J. N.; Yokoi, T., Acidic and catalytic properties of ZSM-5 zeolites with different Al distributions. Catalysis Today **2018**, 303, 64-70.
15. Wang, W.; Zhang, W.; Chen, Y.; Wen, X.; Li, H.; Yuan, D.; Guo, Q.; Ren, S.; Pang, X.; Shen, B., Mild-acid-assisted thermal or hydrothermal dealumination of zeolite beta, its regulation to Al distribution and catalytic cracking performance to hydrocarbons. Journal of Catalysis **2018**, 362, 94-105.
16. Sazama, P.; Pastvova, J.; Kaucky, D.; Moravkova, J.; Rathousky, J.; Jakubec, I.; Sadovska, G., Does hierarchical structure affect the shape selectivity of zeolites? Example of transformation of n-hexane in hydroisomerization. Journal of Catalysis **2018**, 364, 262-270.
17. Chen, K.; Abdolrhamani, M.; Sheets, E.; Freeman, J.; Ward, G.; White, J. L., Direct Detection of Multiple Acidic Proton Sites in Zeolite HZSM-5. *Journal of the American Chemical Society* **2017**, *139* (51), 18698-18704.

18. Julbe, A.; Drobek, M., Zeolite Y Type. In Encyclopedia of Membranes, Drioli, E.; Giorno, L., Eds. Springer Berlin Heidelberg: Berlin, Heidelberg, **2016**; pp 2060-2061.

19. Komvokis, V.; Tan, L. X. L.; Clough, M.; Pan, S. S.; Yilmaz, B., Zeolites in Fluid Catalytic Cracking (FCC). In *Zeolites in Sustainable Chemistry: Synthesis, Characterization and Catalytic Applications*, Xiao, F.-S.; Meng, X., Eds. Springer Berlin Heidelberg: Berlin, Heidelberg, **2016**; pp 271-297.

20. Marler, B., Silica-ZSM-22: synthesis and single crystal structure refinement. *Zeolites* **1987**, 7 (5), 393-397.

21. Dyballa, M.; Obenaus, U.; Rosenberger, M.; Fischer, A.; Jakob, H.; Klemm, E.; Hunger, M., Post-synthetic improvement of H-ZSM-22 zeolites for the methanol-to-olefin conversion. *Microporous and Mesoporous Materials* **2016**, 233, 26-30.

22. Arca, H. A.; Mota, C. J. A., Rearrangement of Cyclopropylcarbinyl Chloride Over Protonic Zeolites: Formation of Carbocations and Behavior as Solid Solvents. *Topics in Catalysis* **2018**, *61* (7), 616-622.

23. Brunner, E.; Ernst, H.; Freude, D.; Fröhlich, T.; Hunger, M.; Pfeifer, H., Magic-angle-spinning NMR studies of acid sites in zeolite H-ZSM-5. *Journal of Catalysis* **1991**, *127* (1), 34-41.

24. Gola, A.; Rebours, B.; Milazzo, E.; Lynch, J.; Benazzi, E.; Lacombe, S.; Delevoye, L.; Fernandez, C., Effect of leaching agent in the dealumination of stabilized Y zeolites. *Microporous and Mesoporous Materials* **2000,** 40 (1), 73-83.

25. González, M. D.; Cesteros, Y.; Salagre, P., Comparison of dealumination of zeolites beta, mordenite and ZSM-5 by treatment with acid under microwave irradiation. *Microporous and Mesoporous Materials***, 2011**, 144 (1), 162-170.

26. P.A. Jacobs and H.K. Beyer., Evidence for the Nature of True Lewis Sites in Faujasite-Type Zeolites. *J. Phys. Chem.,* **1979**, 83 (9): 1174-1177.

27. Zhiwu Yu, A.Z., Qiang Wang, Lei Chen, Jun Xu, Jean-Paul Amoureux, Feng Deng, Insights into the Dealumination of Zeolite HY Revealed by Sensitivity Enhanced 27Al DQ-MAS NMR Spectroscopy at High Field. *Angew. Chem. Int. Ed,* **2010**, *49* (46).
28. Schallmoser, S.; Ikuno, T.; Wagenhofer, M. F.; Kolvenbach, R.; Haller, G. L.; Sanchez-Sanchez, M.; Lercher, J. A., Impact of the local environment of Brönsted acid sites in ZSM-5 on the catalytic activity in n-pentane cracking. *Journal of Catalysis*, **2014**, 316 (Supplement C), 93-102.
29. Li, S.; Zheng, A.; Su, Y.; Zhang, H.; Chen, L.; Yang, J.; Ye, C.; Deng, F., Brönsted/Lewis Acid Synergy in Dealuminated HY Zeolite: A Combined Solid-State NMR and Theoretical Calculation Study. *Journal of the American Chemical Society* **2007**, *129* (36), 11161-11171.
30. Lisboa, O.; Sánchez, M.; Ruette, F., Modeling extra framework aluminum (EFAL) formation in the zeolite ZSM-5 using parametric quantum and DFT methods. *Journal of Molecular Catalysis A: Chemical* **2008**, 294 (1), 93-101.
31. Wang, Q.; Han, W.; Hu, H.; Lyu, J.; Xu, X.; Zhang, Q.; Wang, H.; Li, X., Influence of the post-treatment of HZSM-5 zeolite on catalytic performance for alkylation of benzene with methanol. Chinese Journal of Chemical Engineering **2017**, 25 (12), 1777-1783.
32. Campbell, S. M.; Bibby, D. M.; Coddington, J. M.; Howe, R. F.; Meinhold, R. H., Dealumination of HZSM-5 Zeolites: I. Calcination and Hydrothermal Treatment. *Journal of Catalysis* **1996**, 161 (1), 338-349.
33. Kerr, G.T. in: "Molecular Sieves, Advances in Chemistry, Ser. 121". W.M. Meier, J.B. Uytterhoeven (Eds.), *American Chemical Society*, Washington, **1973**, p. 219.
34. Ibáñez, M.; Epelde, E.; Aguayo, A. T.; Gayubo, A. G.; Bilbao, J.; Castaño, P., Selective dealumination of HZSM-5 zeolite boosts propylene by modifying 1-butene cracking pathway. *Applied Catalysis A: General* **2017**, 543 (Supplement C), 1-9.

35. Kuehne, M. A.; Babitz, S. M.; Kung, H. H.; Miller, J. T., Effect of framework Al content on HY acidity and cracking activity. *Applied Catalysis A: General* **1998**, 166 (2), 293-299.

36. Silaghi, M.-C.; Chizallet, C.; Sauer, J.; Raybaud, P., Dealumination mechanisms of zeolites and extra-framework aluminum confinement. *Journal of Catalysis* **2016**, 339, 242-255

37. Fyfe, C. A.; Gobbi, G. C.; Kennedy, G. J., Investigation of the conversion (dealumination) of ZSM-5 into silicalite by high-resolution solid-state silicon-29 and aluminum-27 MAS NMR spectroscopy. *The Journal of Physical Chemistry* **1984**, 88 (15), 3248-3253.

38. Yan, Z.; Ma, D.; Zhuang, J.; Liu, X.; Liu, X.; Han, X.; Bao, X.; Chang, F.; Xu, L.; Liu, Z., On the acid-dealumination of USY zeolite: a solid state NMR investigation. *Journal of Molecular Catalysis A: Chemical* **2003**, 194 (1), 153-167.

39. Shokoufeh Hosseinieh Farahani, S. M. A., Cavus Falamaki, Improved performance of HZSM-5 for the ethylbenzene/xylene isomerization reaction under industrial operating conditions. *RSC Adv.* **2017**, *7*, 21.

CHAPTER II

Overview of NMR

2.1. Introduction

Nuclear magnetic resonance (NMR) technique was invented in the 1920's by Pauli. First experiments on NMR was developed by Bloch on paraffin wax and Purcell on the water in 1945 and it has been used as one of the powerful spectroscopic instruments in the physical science. They discovered that in a magnetic field, nuclei absorb electromagnetic radiation due to the splitting of their energy levels. It was soon realized that the molecular environment of an NMR active nucleus directly affects the manner in which radio-frequency (r.f.) radiation was absorbed.[1-3]

The NMR parameters of solids are very sensitive to the changes in the local environment of nuclei and it can be affected by bond lengths, angles and molecular symmetry. The principle of basic solution-state NMR is the same as solid-state NMR, but the solid-state NMR is more complicated. In solution state, the presence of fast isotropic molecular tumbling and motion typically leads to narrow spectra and well-resolved lineshapes, as well. The rapid motion can average the lone broadening sources such as dipolar coupling and chemical shift anisotropy (CSA) causing the narrow spectra.[4] In the solid state, due to the lack of such motion, the anisotropically broadened lineshapes happen. The existence of broadenings resulting from chemical shift anisotropy, dipolar coupling, and quadruple interactions lead to broad, poorly-resolved lineshapes in the solid-state NMR spectra. As a result, the modern methods in the solid-state NMR have focused on the technique to gain high-resolution isotropic spectra in which all anisotropic line broadening is

removed. The nature of these interactions with respect to their anisotropic character, will be discussed later in this chapter. Also, Magic angle spinning (MAS) techniques are used to overcome the line broadening problem.[5-6]

2.1.1. Spin magnetization

A molecule contains an atom with protons, neutrons, and electrons. Nuclei with their characteristic spin quantum number (I) is considered as a magnet. The nucleus has a non-zero net spin only when it contains unpaired protons or neutrons. Table 2.1 shows the natural abundance, net spin, and gyromagnetic ratio for some elements, which are studied in zeolite structures.

Table 2. 1. Properties of nuclei most useful for zeolite material[7-8]

Isotope	Neutron	Proton	Natural abundance (%)	Spin Quantum Number (I)	Gyromagnetic ratio (10^{-7} rad/T sec)
^{1}H	0	1	99.9844	1/2	26.7520
^{2}H	1	1	0.0156	1	4.1067
^{13}C	7	6	1.108	1/2	6.7265
^{27}Al	14	13	100	5/2	6.9763
^{29}Si	15	14	4.67	1/2	-5.3190

All nuclear spins are oriented randomly due to the thermal effects and the net magnetization of the oppositely oriented spin vectors is zero because of cancelling each other in the opposite site. However, when a strong external magnetic field is applied, nuclei with non-zero spins will exhibit a Zeeman splitting, leaving spins oriented either partially along or opposite to the external magnetic field. The orientation of spins depends on the gyromagnetic ratio, γ. For the nuclei with positive and negative γ, the orientation is parallel and antiparallel to the external magnetic field, respectively. At equilibrium, the population of the spins in the state of lower energy (+1/2 or α) is slightly higher than that of state of higher energy level (-1/2 or β). The population difference is determined by Boltzmann distribution shown in the following equation.

$$\frac{N\alpha}{N\beta} = e^{-\frac{\Delta E}{KT}}$$

Where k is Boltzmann's constant, 1.3805×10^{-23} J/K and $\Delta E = E\alpha - E\beta$.

Therefore, in the presence of a magnetic field, the nuclear spin energies become non-degenerate, since nuclei with different nuclear spin states start to precess about the field axis. For a nucleus with nuclear spin I, there are 2I + 1 possible energy levels, each related to magnetic nuclear spin quantum number, m_I, where m_I = +I, +I – 1, +I – 2, …, -I.

As the magnetic field becomes stronger, the energy separations between the two energy levels as well as the population differences between energy levels increase.[1]

Fig. 2.1 represents the Zeeman splitting of spin ½ in presence of the magnetic field.

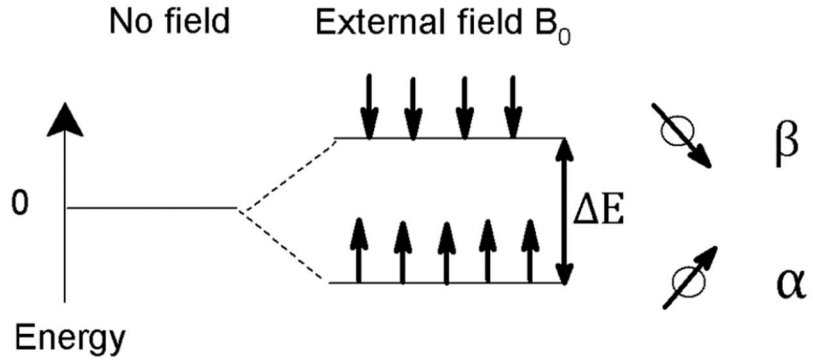

Fig. 2. 1. Population distribution under Zeeman interaction of spin ½ [1] (Adapted from Levitt, M., Chichester, West Sussex, United Kingdom, 2009).

A NMR-active nucleus possesses non-zero nuclear spin angular momentum (I) and an associated nuclear spin magnetic moment (μ) as well. The relationship between these two quantities are linear through the gyromagnetic ratio with $\mu = \gamma \times I$. When a group of nuclear spins experiences a constant external magnetic field (B_0), they start to precess about the applied field because of angular

momentum. The direction of their rotation is determined by the sign of the gyromagnetic ratio; positive γ indicates clockwise precession about B_0, while negative γ indicates counterclockwise precession about B_0.

2.1.2. Hamiltonian interaction

There are many important nuclear spin interactions, classified as either external or internal interactions. The external interactions arise from the interaction of nuclear spins with external magnetic fields (i.e., a large static magnetic field (B_0) and a smaller oscillating field, B_1). The internal interactions are related to the interactions among spins. A general Hamiltonian describing the NMR interaction is given by the following equation:

$$\hat{H}_{NMR} = \hat{H}_Z + \hat{H}_{CS} + \hat{H}_{DD} + \hat{H}_J + \hat{H}_Q$$

Where $\hat{H}_Z, \hat{H}_{CS}, \hat{H}_{DD}, \hat{H}_J, and\ \hat{H}_Q$ refer to the Zeeman, chemical shielding, direct dipolar coupling, indirect (scalar-J) spin-spin coupling and quadrupolar interactions, respectively.

The Zeeman interaction is related to the applied magnetic field and is much larger than all other external and internal interactions.

2.2. Solid-state Magic Angle Spinning (MAS) NMR

In solution, rapid molecular tumbling leads to an averaging of chemical shielding, and dipolar and first-order quadrupolar interactions, resulting in the observation of isotropic chemical shifts as sharp resonances. Magic angle spinning (MAS) is a technique in the solid state NMR in which a solid sample is rapidly spun around an axis tilted by ~54.74° with respect to the static magnetic field for removing the effects of anisotropic interactions in solid-state NMR spectra. The magnitude of the chemical shielding interaction depends on the nuclear component's symmetry and the orientation of molecule with respect to the magnetic field. This orientation dependence is assigned for the chemical shielding anisotropy (CSA)[9-10]. As mentioned before, a number of different NMR

interactions, such as chemical shielding, dipolar and first-order quadrupolar interactions, have essentially the same spatial orientational dependence of (3cos2θ-1), where θ is the angle between the internuclear vector and the magnetic field B_0. When θ = 54.74°, the term (3cos2 θ-1) = 0 and the spatial dependencies are averaged out to 0, resulting in the significant line narrowing in NMR spectra.

MAS greatly improves the spectral resolution and sensitivity in solid samples by averaging out a range of anisotropic nuclear spin interactions such as CSA and dipolar coupling[11]. For spin quantum number 1/2, I=1/2 nuclei, MAS can result in the observation of isotopic spectra, containing a sharp and resolved peaks as shown in Fig. 2.2.

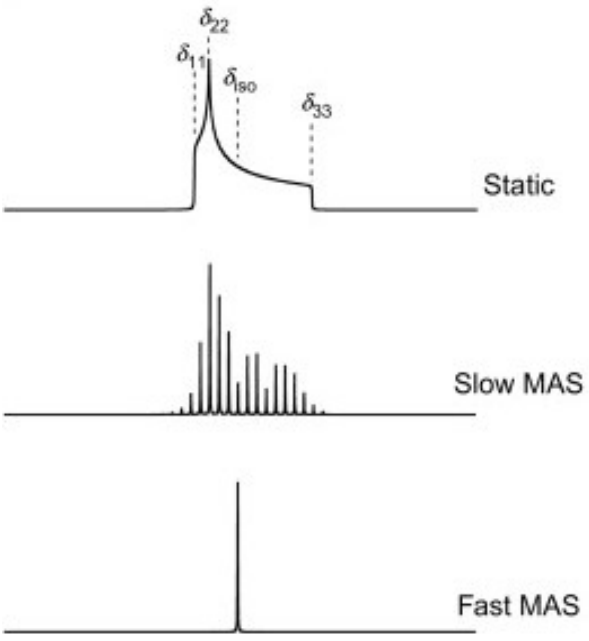

Fig. 2. 2. Schematic NMR spectra showing lineshapes of the CSA simulated under static, slow MAS and fast MAS conditions[11] (Adapted from Polenova, T., *Analytical Chemistry* 2015).

In some cases, if the sample spinning speed frequency is less than the interaction frequency,

spinning sidebands are also observed. The applied magnetic field strength can change the magnitude of the chemical shielding interactions. However, for the commonly used magnetic field strengths available on commercial spectrometers, typical values may range from a few kilohertz for lighter nuclei to tens or hundreds of kilohertz for heavier elements.[10]

2.3. NMR relaxation

NMR relaxation is a process that excited magnetization, arising from a radio frequency pulse, can be returned to its equilibrium distribution. There are two types of magnetic relaxation: spin-lattice and spin-spin relaxation.

The spin-lattice relaxation (T_1) is referred to as longitudinal relaxation. It explains the return to equilibrium distribution in the direction of the magnetic field (z-direction) and restoration of Boltzmann equilibrium. Also, T_1 relaxation quantifies the rate of energy transfer from the nuclear spin to the neighboring molecules (lattice).

$$\frac{dM_z}{dt} = \frac{M_0 - M_z}{T_1}$$

M_z and M_0 are the magnetization vector at z- direction and equilibrium value, respectively.

Energy transfer into thermal energy by using spin-lattice relaxation depends on the rate of molecular motion. The motion in the lattice (which is expected to gain or lose the energy from the nuclear spin transition) must cause a fluctuating magnetic field that effectively acts as a “local pulse” at the site of the nuclear spin involved.[12]

The spin-spin relaxation (T_2) is also related to as transverse relaxation and describes the decay of the excited magnetization perpendicular to the applied magnetic field. After applying a 90^o pulse, the net magnetization in xy plane (M_{xy}) eventually decays. The decay is due to two factors: magnetic field inhomogeneity and spin-spin relaxation. The spin-spin relaxation is caused by transient magnetic fields arising from molecular motion at any frequency. Thus T_2 keeps getting

shorter as molecular reorientation rates slow down.

$$\frac{dM_{x(y)}}{dt} = -\frac{M_{x(y)}}{T_2}$$

T_2 is less than or equal to T_1 (R = relaxation rate, $R_1 = 1/T_1$, $R_2 = 1/T_2$, $R_2 \geq R_1$), since return of magnetization to the z-direction inherently causes loss of magnetization in the x-y plane.

Relaxation is mainly affected by fluctuating magnetic fields and molecular motion, modulating the local fields. Sources for such local fields are direct dipole-dipole coupling, chemical shielding anisotropy, quadrupole coupling, paramagnetic centers or wobbling of the total field. For spin−1/2-nuclei and nuclei with a spin of I > 1/2 (additional quadrupolar contributions) the influence of the different mechanisms can be classified by their contribution:

(quadrupole) >> dipole-dipole > CSA > spin-rotation

Fig. 2.3 shows the dependency of different relaxation times on the correlation time of the molecular tumbling motion τ_c (the time it takes the average molecule to rotate one radian).

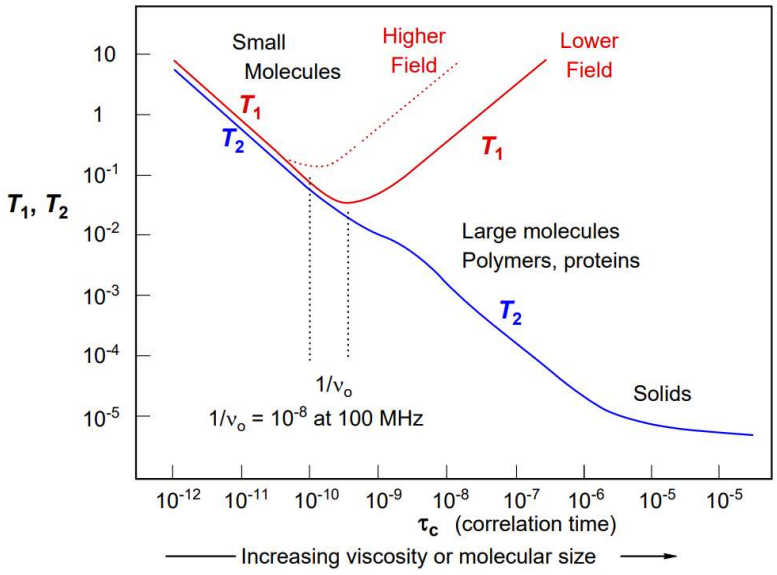

Fig. 2. 3. The dependency of T_1 and T_2 on the correlation time τ_c[12] (Adapted from Bloembergen, E.M., *Physical Review* 1948).

There are several methods to measure spin-lattice and spin-spin relaxation time constants such as spin-echo, inversion recovery and saturation recovery measurements.

2.3.1. Saturation-recovery experiment

In this research for measuring T_1 constant, the saturation-recovery sequence is used to saturate the system completely in the beginning and then followed by the recovery process. In this method, after applying a very fast series of 90°-pulses and then an evolution period during which the system is allowed to relax with T_1, the signal is recorded after a 90°-pulse as shown in Fig. 2.4.

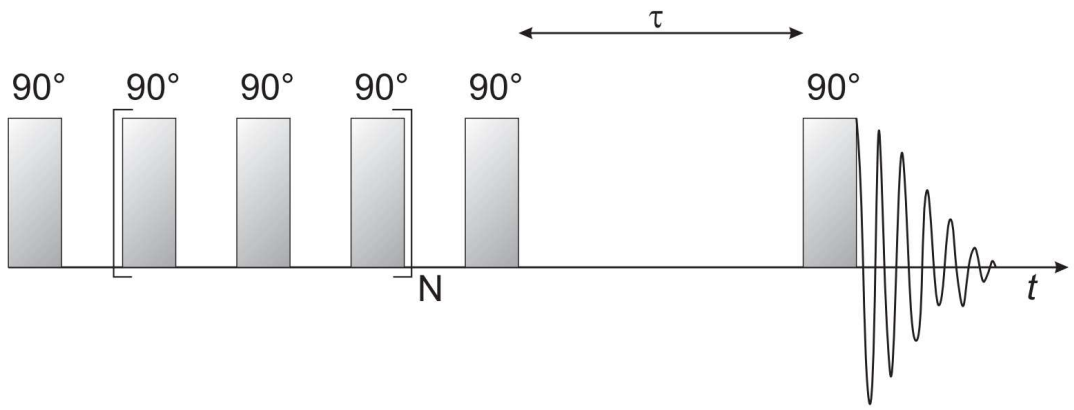

Fig. 2. 4. Scheme of the saturation-recovery sequence[13]

The advantage of this method is the short experimental repetition time. The saturation-recovery method is usually used for the materials with a very long T_1, since the system is saturated at the very beginning, there is no need to wait for the system to be fully relaxed, when accumulating experiments.[13]

2.4. Single-90° pulse sequence

Since the populations of the two levels of Zeeman interactions are not equivalent, there is a net magnetization (or bulk nuclear spin magnetic moment, M), which can be described by a vector

pointing along the z-direction. The observation of NMR signal begins by applying an oscillating r.f. pulse (the voltage in the coil is turned on and switched off very quickly, usually in the order of μs), which causes transitions between different nuclear spin energy levels. A 90° pulse along x-direction has the effect of tipping the bulk magnetization vector M from the z-axis of the lab frame into the –y direction. After that, the magnetization will start precessing around the xy plane (transverse plane) at a frequency of Ω (ω0 – ωrf) for a duration of t. In terms of relative population difference, a 90° pulse will saturate both energy levels, making them equal, which is the desirable scenario for maximum signal intensity as we detect magnetization in the transverse plane. Basically, the oscillating electric current induced by the precessing transverse magnetization is the NMR signal, or free induction decay (FID).

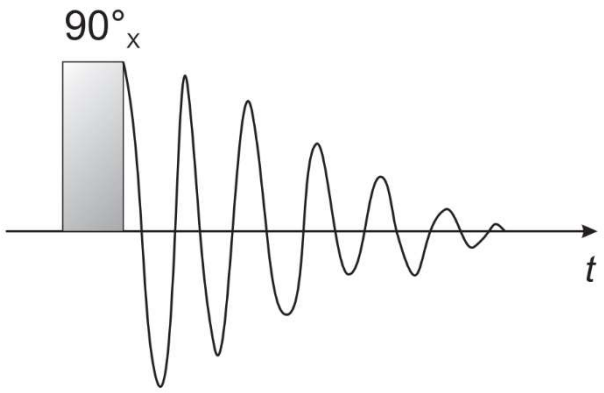

Fig. 2. 5. Single pulse experiment[13] (Adapted from Abele, M., 2012).

2.5. Characterization of zeolites by using NMR

Among a variety of techniques to characterize and determine the structure and physical-chemical properties of zeolites, the NMR technique plays an important role. This method provides useful information on the local surrounding of atoms such as silicon, aluminum, and proton[14]. It is possible to investigate the structure of the framework and non-framework species, reaction mechanism using in-situ methods, and the acidic sites by observing the magnetically active NMR nucleus. In this

section, an overview of three important NMR methods, ^{29}Si MAS NMR, ^{27}Al MAS NMR, ^{1}H MAS NMR, are described. These techniques are mostly used for characterization of structural properties of zeolites.

2.5.1. ^{29}Si MAS NMR

Zeolite structures contain both framework and extra-framework aluminum species that significantly effect the catalytic properties. It is well known that changing the Si/Al ratio can modify the thermal stability and catalytic properties of the zeolites. However, it is very essential to be able to measure the framework Si/Al ratio of zeolite and this can be achieved via ^{29}Si MAS NMR technique. In this method, the ^{29}Si nuclei, the NMR active isotope of silicon, depend on the number of aluminum atoms present as neighbors. The chemical shift ranges of ^{29}Si nuclei in a SiO_4 tetrahedra attached to the differing number of AlO_4 tetrahedra is given in Fig. 2.6.

It can be observed that by increasing the number of Al attached to SiO_4 tetrahedra, the chemical shift moves downfield.[15-17]

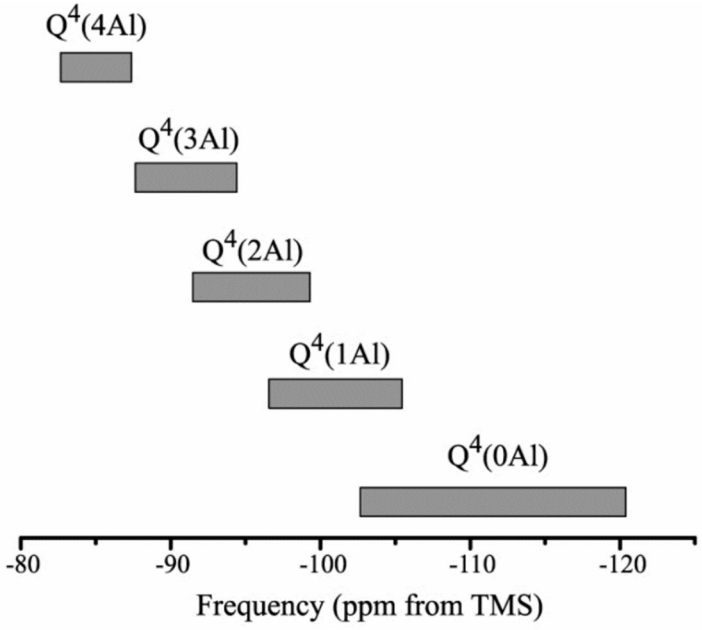

Fig. 2. 6. Chemical shift of ^{29}Si with different number of Al atoms as neighbors[15] (Adapted from Mafra, L, In *Annual Reports on NMR Spectroscopy* 2012).

To calculate the framework Si/Al ratio, the first step is to take ^{29}Si MAS NMR of zeolite to identify the peaks based on their chemical shift. For example, the ^{29}Si MAS NMR spectrum of HY zeolite is shown in Fig. 2.7. The relative concentrations of each chemical species can be calculated by measuring the peak areas under each resonance and these values can then be used to calculate the framework Si/Al ratio.[15]

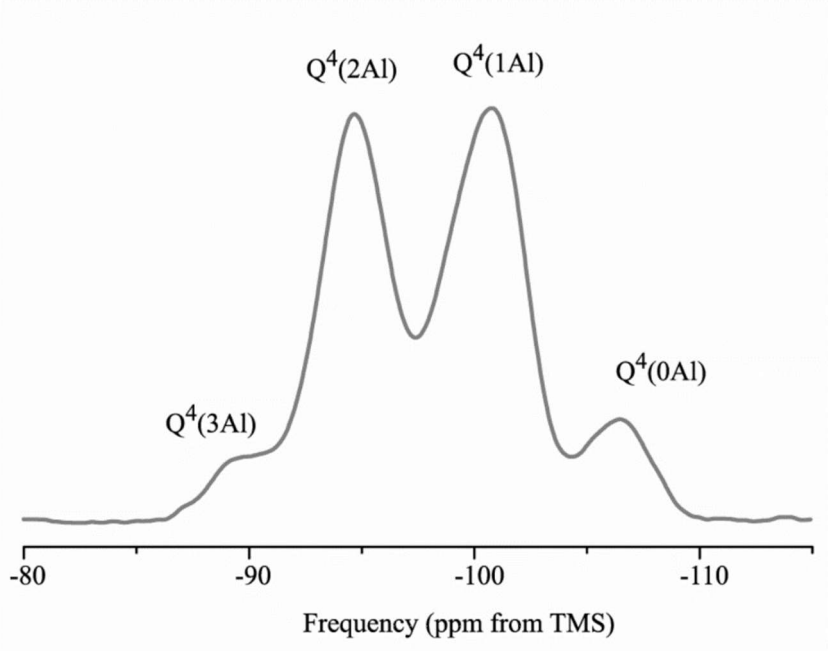

Fig. 2. 7. ^{29}Si MAS NMR spectrum of HY zeolite[15](Adapted from Mafra, L, In *Annual Reports on NMR Spectroscopy* 2012).

2.5.2. ^{27}Al MAS NMR

^{27}Al MAS NMR can give useful information about the acidity of zeolite because of its direct measurement of framework and non-framework aluminum species. A major factor in the measurement of ^{27}Al spectra is the presence of the quadrupolar interactions that complicate the experimental and theoretical interpretations. The magnitude of this interaction dominates all other interactions that the nucleus may experience such as chemical shift and dipolar couplings. The quadrupolar interaction is arising from the coupling of the quadrupole moment of the nucleus with

the electric field gradient present at the nucleus.[14, 17-18]

^{27}Al MAS NMR data are usually acquired on zeolite samples that are exposed to ambient moisture in order to eliminate lattice strain and enable detection of framework Al atoms. In completely dehydrated samples, Al observation is prevented by large quadrupole coupling constants arising from lattice distortions which its magnitude is on the order of several megahertz. For this reason, ^{27}Al NMR is not a quantitatively reliable method for measuring the acid sites quantitatively. A combination of high field strengths and magic-angle spinning is required to reduce the linewidths coming from the central transition affected by the quadrupolar coupling to the 2nd order[15].

There are two main types of aluminums in zeolite structures: framework aluminum in tetrahedral coordination (AlO_4) and extra-framework aluminums in octahedral coordination (AlO_6). As shown in Fig. 2.8, the chemical shift for the framework and extra-framework aluminum species are in the range of 50 to70 ppm and -10 to 20 ppm, respectively.[15]

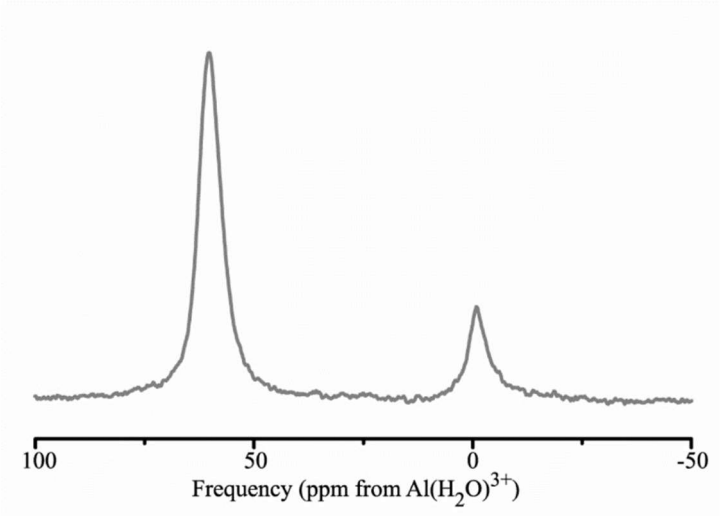

Fig. 2. 8. ^{27}Al MAS NMR spectrum of HY zeolite[15](Adapted from Mafra, L, In *Annual Reports on NMR Spectroscopy* 2012).

2.5.3. ^{1}H MAS NMR

The locus of catalytic activity in the zeolite structure is a proton, historically assumed to be a part of the bridging hydroxyl group between a Si and an Al atom. Spectroscopic detection of the variety

of protonic species that can exist in zeolites, ranging from nonacidic silanol species to acid sites, extra-framework AI-OH groups, and residual NH_4^+ is afforded by ^1H MAS NMR methods.[19]

Static ^1H NMR spectra of zeolites suffer from substantial line broadening arising from the direct dipolar interaction between the protons and the quadrupolar ^{27}Al nucleus, which limit its application in distinguishing between the different protonic species. This line-broadening problem can be resoved by applying the magic angle spinning technique.[15, 20]

Beck et.al. reported the existence of three peaks in the ^1H spectrum of commercially available HZSM-5 samples. In addition to the well-known silanol peak at 1.9-2.0 ppm and Bas peak at 4.2 ppm, a third peak located as a broad shoulder at 6.9 ppm when the temperature is reduced to 123 K.[21]

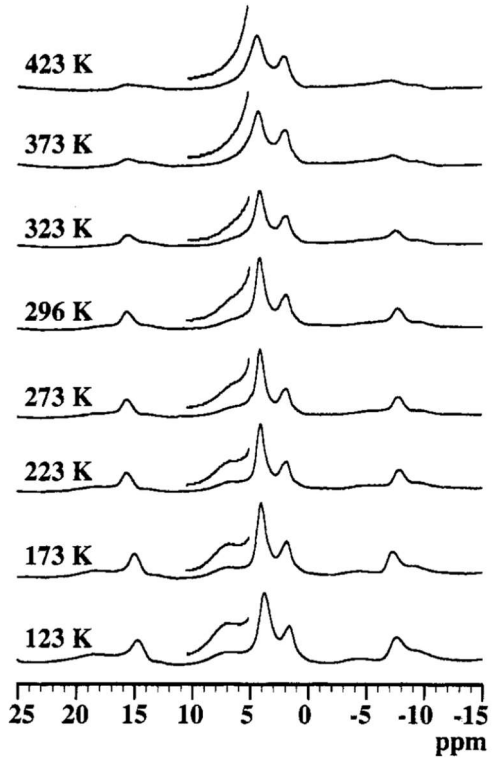

Fig. 2. 9. 'H MAS spectra of zeolite HZSM-5 over a range of temperatures[21] (Adapted from Beck, L. W., *Journal of the American Chemical Society* 1994).

2.6. References

1. Levitt, M. Spin Dynamics: Basics of Nuclear Magnetic Resonance, Second Edition.; John Wiley & Sons, Ltd.: Chichester, West Sussex, United Kingdom, **2009**.
2. Soulsby, D.; Wallner, A. S., Introduction to NMR Spectroscopy in the Undergraduate Curriculum. In NMR Spectroscopy in the Undergraduate Curriculum: First Year and Organic Chemistry Courses Volume 2, *American Chemical Society:* **2016;** Vol. 1221, pp 1-10.
3. Becker, E. D., A brief history of nuclear magnetic resonance. *Analytical Chemistry* **1993**, *65* (6).
4. Martin Dračínský, P. H., Solid-state NMR studies of nucleic acid components. *RSC Adv.* **2015**, *5*, 11.
5. Hubert Koller, M. W., Solid State NMR of Porous Materials.
6. James, T. L., Fundamentals of NMR.
7. JAMES, T. L., Fundamentals of NMR, University of California.
8. Blümich, B., Introduction to compact NMR: A review of methods. *TrAC Trends in Analytical Chemistry* **2016**, *83*, 2-11.
9. Griffin, J. M.; Ashbrook, S. E., Chapter Five - Solid-State NMR of High-Pressure Silicates in the Earth's Mantle. In *Annual Reports on NMR Spectroscopy*, Webb, G. A., Ed. Academic Press: **2013**; Vol. 79, pp 241-332.
10. ConcistrÈ, M.; Johannessen, O. G.; Carignani, E.; Geppi, M.; Levitt, M. H., Magic-Angle Spinning NMR of Cold Samples. *Accounts of Chemical Research* **2013**, *46* (9), 1914-1922.

11. Polenova, T.; Gupta, R.; Goldbourt, A., Magic Angle Spinning NMR Spectroscopy: A Versatile Technique for Structural and Dynamic Analysis of Solid-Phase Systems. *Analytical Chemistry* **2015**, 87 (11), 5458-5469.
12. Bloembergen, E.M.; Purcell, R.V.; Relaxation Effects in Nuclear Magnetic Resonance Absorption. *Physical Review* **1948**, 73, 679-746.
13. Abele, M., Solid-state NMR spectroscopy for structural investigations in materials science. **2012**.
14. Li, S.; Zhou, L.; Zheng, A.; Deng, F., Recent advances in solid state NMR characterization of zeolites. *Chinese Journal of Catalysis* **2015**, *36* (6), 789-796.
15. Mafra, L.; Vidal-Moya, J. A.; Blasco, T., Chapter Four - Structural Characterization of Zeolites by Advanced Solid State NMR Spectroscopic Methods. In *Annual Reports on NMR Spectroscopy*, Webb, G. A., Ed. Academic Press: **2012**; Vol. 77, pp 259-351.
16. Fyfe, C. A.; Feng, Y.; Grondey, H.; Kokotailo, G. T.; Gies, H., One- and two-dimensional high-resolution solid-state NMR studies of zeolite lattice structures. *Chemical Reviews* **1991**, *91* (7), 1525-1543.
17. Klinowski, J., Solid-state NMR studies of molecular sieve catalysts. *Chemical Reviews* **1991**, *91* (7), 1459-1479.
18. Jiang, Y.; Huang, J.; Dai, W.; Hunger, M., Solid-state nuclear magnetic resonance investigations of the nature, property, and activity of acid sites on solid catalysts. *Solid State Nuclear Magnetic Resonance* **2011**, *39* (3), 116-141.
19. Abdolrahmani, M.; Chen, K.; White, J. L., Assessment, Control, and Impact of Brönsted Acid Site Heterogeneity in Zeolite HZSM-5. *The Journal of Physical Chemistry C* **2018**, *122* (27), 15520-15528.
20. Hunger, M., Multinuclear solid-state NMR studies of acidic and non-acidic hydroxyl protons in zeolites. *Solid State Nuclear Magnetic Resonance* **1996**, *6* (1), 1-29.

21. Beck, L. W.; White, J. L.; Haw, J. F., 1H{27Al} Double-Resonance Experiments in Solids: An Unexpected Observation in the ^{1}H MAS Spectrum of Zeolite HZSM-5. *Journal of the American Chemical Society* **1994,** *116* (21), 9657-9661.

CHAPTER III

OBSERVATION OF MULTIPLE ACID SITES OF HZSM-5 ZEOLITES

3.1. Introduction

Zeolites catalysts are widely used in many industrial processes involving gas-phase reagents and products,[1-3] and are now increasingly the subject of research as catalysts in aqueous or biphasic reactions to transform molecules derived from biomass.[4-6] Even though they have enjoyed significant commercial success, many mechanistic aspects of hydrocarbon transformation catalyzed by solid-acid forms of zeolites are still debated, including the homogeneity of active acid sites within the zeolite lattice.[7-9] As interest continues to grow in their use as catalysts at the solid-liquid interface, understanding how active site density, distribution, and homogeneity responds to the presence of water becomes increasingly important. The acidic form of the zeolite ZSM-5, a member of the MFI family and denoted HZSM-5, has enjoyed commercial success as catalyst for hydrocarbon isomerization and disproportionation reactions, as well as the transformation of methanol to hydrocarbons including small molecule olefins, gasoline range, and aromatic hydrocarbon products. HZSM-5 has attracted significant attention in fundamental catalysis research due to its relatively simply channel structure, a wide range of accessible Si to Al lattice ratios, and spectroscopic or probe molecule evidence that it contains a single type of Brönsted acid site in its synthesized form.[10-12] The latter characteristic is attractive for fundamental mechanistic studies, as all active sites may be considered equivalent in terms of their acid strength, steric accessibility, and transition state structures. However, other evidence in the literature suggests that acid site character is potentially more complex, including increased hydrocarbon reaction rates or new spectroscopic signals assigned to the presence of extra-lattice alumina (Al_xO_y) sites close to

lattice Brönsted sites.[13-16] Additional experimental and computational studies affirms that some extra-lattice alumina species that are formed during deliberate lattice dealumination steps (steam hydrolysis, calcination, etc.) reside very close to Brönsted proton lattice sites, and a synergistic effect of having those potential Lewis sites near the Brönsted acid site have been proposed to contribute to unique reactive sites, albeit mostly in the zeolite HY.[17-19] At low Si/Al ratios, it is possible that more than one type of acid site location, i.e., channels versus channel intersections, can exist and lead to different reaction energetics in HZSM-5[20]. Recently, others have shown that adding sub-stoichiometric amounts of water can enhance reaction rates in zeolite HZSM-5, suggesting that only a small fraction of active Brönsted sites respond to water addition[21,22]. All of these studies, while suggesting the possible existence of more than one type of reactive Brönsted proton site in HZSM-5, lack direct experimental observation of actual reactive proton sites in zeolite HZSM-5. If in fact a synergistic effect of Lewis sites near Brönsted bridging acid sites (BAS) exists, the resulting deshielded hydroxyl groups should be experimentally detectable.

In this chapter, direct spectroscopic identification of at least three types of protons exhibiting Brönsted acid character in zeolite HZSM-5 is reported using one- and two-dimensional ^{1}H solid-state NMR methods, revealing for the first time a proton species characterized by a broad signal at 12-15 ppm. Multiple reactive protons are only detected in HZSM-5 whose Si/Al ratios are 25 or less. In addition to the well-known Brönsted acid site characterized by a signal at 4.2 ppm, two extra-lattice proton populations are shown to react with an alkane probe molecule at room temperature, including the ca. 13-ppm species. While the third population, an extra-lattice Al-OH species characterized by a signal at 2.8 ppm, has been previously documented in the literature, the reactivity of its hydroxyl groups is shown here for the first time. In total, all three proton types undergo proton chemical exchange with one another at room temperature, as proven by two-dimensional exchange spectroscopy. These data provide strong evidence that there is more than one active Brönsted proton site in HZSM-5, and indicate that there is a small population of sites

whose potential acid strength is significantly larger due to its 12-15 ppm chemical shift. While previous computational and experimental studies suggest this newly detected 12-15 ppm species might be hydroxonium ions stabilized in the interior lattice at a framework Al site,[23-25] the data show that its presence does not depend on the amount of water in the catalyst channels. In total, the data indicate that multiple Brönsted acid protons can exist in HZSM-5, and that some framework acid sites may experience increased acidity due to the presence of proximate extra-lattice Al-OH species.

3.2. Experimental section

3.2.1. Zeolite dehydration

Zeolite ZSM-5 samples with different aluminum content (Si/Al = 11.5 CBV 2314, Si/Al = 15 CBV 3024E, Si/Al = 25 CBV 5524G and Si/Al= 40 CBV 8014) were obtained from Zeolyst in the ammonium-exchanged form**.** The BET surface areas vary from 379-386 m^2/g independent of Si/Al ratios,[26] and SEM experiments indicated that the average particle size was 0.6-0.7 μm. Dehydrated HZSM-5 zeolite samples were prepared from the ammonium form in a glass reactor body via a stepwise vacuum procedure to a final temperature of 723 K, under 2×10^{-5} torr using an Edwards EO4K diffusion pump, as previously reported.[21] For comparison and in an effort to ensure maximum water removal, as indicated by increased T_1 values for the catalyst protons some samples were dehydrated using a flow reactor with ultrapure argon or helium gas, heated stepwise to a final temperature of 723-773 K, and held there for 24 h. This flow dehydration method follows that recently described by Grey, through which they clarified long-standing uncertainties surrounding the assignment of trace water signals.[27] A table of T_1^H values is provided in the Supporting Information for Si:Al = 15 HZSM-5 to clarify how trace water content depends on the catalyst dehydration method. For both methods, catalyst samples were sealed and immediately placed in a dry ultra-pure argon atmosphere glove box for transfer to zirconia MAS NMR rotors.

3.2.2. H/D isotopic exchange experiment

A vacuum line equipped with a CAVERN type apparatus was used for quantitative adsorption, following previously published procedures[22]. A fixed quantity of catalyst was placed in a 4-mm zirconia MAS NMR rotor in the CAVERN, evacuated and sealed. The isobutane-d_{10} gas (> 99.1%, CDN Isotopes) was then introduced in the vacuum line to an initial pressure. The adsorption was stopped at a calculated final pressure corresponding to a 1:1 ratio of isobutane:acid site, i.e., 1 equivalent (eqv) of isobutane-d_{10}.

3.2.3. NMR measurements

^{1}H MAS (magic-angle spinning) NMR data was collected on a Bruker Avance 400 spectrometer operating at 9.05 T with a 4-mm double-resonance MAS probe. When necessary, as mentioned in the text, the rotors were spun with dry nitrogen gas to avoid possibility of moisture contamination following sample sealing. Spinning speeds of 10 or 15 kHz, 32 scans and 3.9 μs π/2 excitation pulse were used for single-pulse acquisitions. Given the short acquisition times for the single-pulse ^{1}H MAS experiments, an empty rotor probe background spectrum was acquired separately for each run and subtracted from the zeolite spectrum in order to remove a small background signal near 1 ppm.

The spin-lattice relaxation time constant T_1 was measured using a modified saturation recovery pulse sequence in which the 90˚-read pulse was replaced by a composite 90˚ pulse as previously described by Cory,[28] and data were acquired with 10-kHz MAS speeds. ^{1}H/^{27}Al spin echo double resonance (SEDOR or TRAPDOR) experiments were carried out with a spinning speed of 8 kHz, 500 μs (four rotor periods), and a radio frequency field strength of 78 kHz for ^{27}Al.[29,30] The standard two-dimensional (2D) three-pulse exchange (a.k.a. NOESY) sequence[31,32] was used to monitor chemical exchange between proton sites in the catalyst, with a dwell time in the indirect dimension set to 20 μs. Typically, 32 scans were acquired for each t_1 increment, with final data sets consisting of 512 t_1 × 2048 t_2. A wide variety of experiments were run with mixing

times ranging from 1 ms to 150 ms, all of which are integral multiples of the rotor period, but only a subset of the variable mixing time data are presented herein. The recycle delays used in the 2D exchange experiments ranged from 2 to 5 s with MAS speeds equal to 10 kHz.

3.3. Results and dissection

Representative spectra for HZSM-5 catalysts in their dehydrated, acidic forms are shown in Fig.3.1 for Si:Al ratios ranging from 11.5 to 40. These spectra are, in almost every way, similar to the large number of HZSM-5 spectra previously reported in the literature, in which three main signals are detected.[8,10,11,16,27] The locus of catalytic activity is the bridging acid site (BAS), indicated by the peak at 4.2 ppm whose intensity increases as the Si:Al ratio decreases, as is expected for increasing Al incorporation into the framework and concomitant charge balance by the Brönsted proton. The silanol (SiOH) group resulting from crystallite lattice termination gives rise to the well-known peak at 1.9-2 ppm, and these hydroxyls do not exhibit Brönsted acid character. Finally, it is well established in the literature that the 2.8 ppm peak originates from hydroxyl groups on aluminum atoms that exist as extra-lattice or extra-framework aluminum (AlOH), most likely as small aluminum oxide dimers or trimers.[33] While dealumination can occur during some catalyst preparation procedures, the mild vacuum or flow temperature programmed methods used here should not lead to framework dealumination. Fig.3.1 indicates that the relative amount of extra-lattice AlOH species is largest in the Si:Al = 15 and 11.5 catalysts, and indeed, Janda and coworker have recently reported that this same Si:Al = 15 catalyst has the largest fraction of such species based on Al elemental analysis.[20] Deconvolution of the peaks for the two lowest Si:Al catalysts indicates that the area of the 2.8 ppm peak relative to the BAS and SiOH peaks is the largest for Si:Al=15 catalyst. The broad 5-9 ppm peak appearing as a shoulder downfield of the BAS peak has previously been assigned by the Grey group as strongly-bound trace water that is difficult to remove using vacuum dehydration methods.[27]

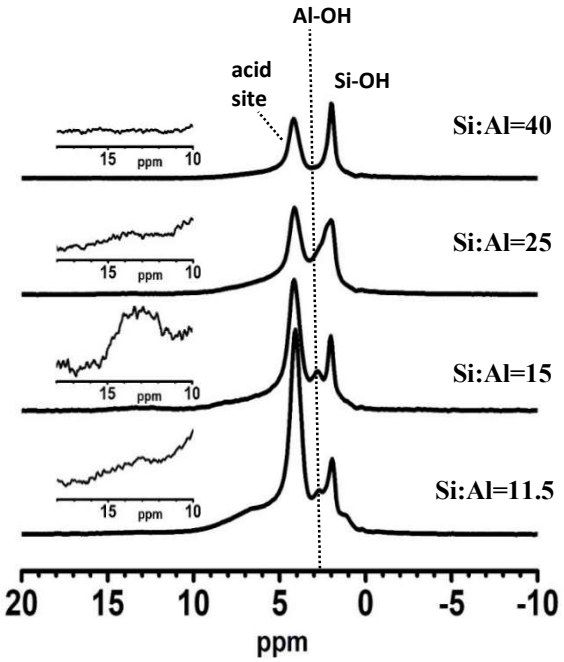

Fig. 3. 1. ^{1}H MAS NMR spectra acquired at room temperature for dehydrated HZSM-5 catalysts prepared under vacuum heating with Si/Al ratios indicated at right. Inset: The broad signal at 12-15 ppm, most visible in Si:Al=15, has not previously been reported and indicates the presence of a small population of protonic species in a strongly deshielded environment.

The new information contained in Fig.3.1 is the broad 12-15 ppm signal detected in three of the four spectra, expanded in the left insets for clarity. Given that this 12-15 ppm peak is small, in a region of a spectrum often overlapping with spinning-sidebands in previously published works (many of which were obtained at low magnetic field strengths), that it disappears in the presence of adsorbates or more than trace amounts of water loadings (*vide infra*), and that it is not detectable in Si:Al > 25 catalyst, the fact that it was unrecognized in previous works is not surprising. A chemical shift this far downfield has not been reported in acidic zeolites, but Maciel and coworkers have reported a 10.8 ppm shift for certain types of hydroxyl groups in low-surface area aluminum oxide hydroxides.[34] Comparing the top and bottom traces in Fig. 3.2 provides some information

as to the nature of the protons giving rise to the 12-15 ppm signal. The top spectrum in the overlay is a simple spin-echo spectrum for the Si:Al=15 sample, with features in every way consistent with the single-pulse MAS spectrum in Fig. 3.1. The 12-15 ppm peak is clearly visible. The bottom spectrum is acquired with the same spin-echo under the same MAS conditions, except for the application of ^{27}Al pulses during the echo evolution windows. This experimental approach, well-known in the literature as the spin-echo double resonance SEDOR[29] or TRAPDOR[30] experiment, has been used extensively to identify protons that are within a dipolar-coupling distance (2-6 Å) of an aluminum atom in inorganic oxides.[35-37] Of the four labeled peaks in the bottom spectrum of Fig. 3.2, only the Si-OH peak intensity is the same in both experiments, which is consistent with the known fact that those hydroxyl groups are not close to Al atoms. The very small decrease in the SiOH intensity is due to the loss of the 2.8 ppm extra-framework AlOH peak with which it overlaps. More importantly, the 12-15 ppm peak is completely attenuated by the double-resonance echo, which means that like the AlOH protons and the BAS protons, the protons that give rise to that signal are dipolar coupled to a nearby Al. The attenuation of the BAS and AlOH peaks, along with their known structures, coupled with no attenuation for the SiOH peak, indicates that the 12-15 is a species containing a hydroxyl group proximate to either a framework acid site Al or an extra-framework Al species. In total, the coupling with an Al atom and the strongly deshielded chemical shift value indicates that this species has to potential to act as an acid site.

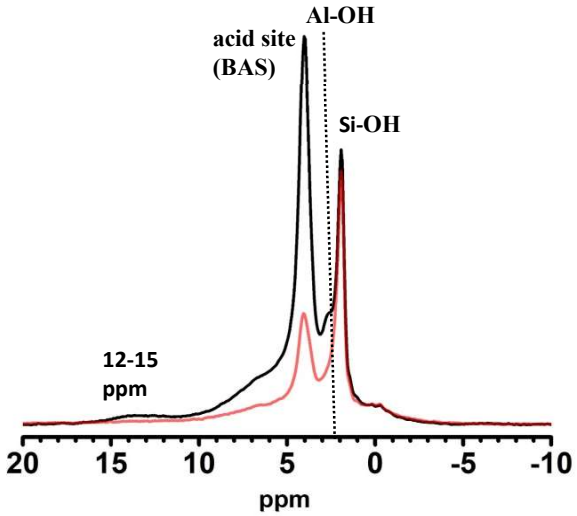

Fig. 3. 2. ^{1}H MAS NMR spectra acquired at room temperature for dehydrated Si:Al = 15 HZSM-5 using a simple spin-echo sequence (top) without and (bottom) with an ^{27}Al r.f. pulse applied during the echo evolution periods. Note the significant attenuation of all signals except the 2-ppm silanol signal, indicating that the protons in the species represented by the 13-15 ppm signal are proximate to an Al atom, as is known for the BAS and Al-OH groups.

Fig. 3.3 demonstrates that the species giving rise to the 12-15 ppm peak can also react with a hydrocarbon probe molecule. Fig. 3.3 shows selected single-pulse MAS spectra acquired following the room-temperature adsorption of isobutane-d_{10} on Si:Al=15 HZSM-5, with total reaction time for the exchange reaction increasing from bottom to top up to one hour in the upper trace. The isobutane CH_3 signal increases as the BAS signal decreases, as protons exchange from the acid site with deuterons on isobutane. The BAS/isobutane-d_{10} system is a well-documented probe of zeolite acidity,[38-41] but for the first time, the data in Fig. 3.3 also show that the 12-15 ppm species is undergoing H/D exchange with isobutane. Exchange has already occurred by the time the first (bottom) time trace is collected, as indicated by the significant isobutane CH_3 signal intensity at 1.1 ppm, thus explaining the relatively weak 12-15 ppm peak intensity. However, just like the BAS, that 12-15 ppm continues to decrease in intensity as exchange occurs. No change in the SiOH peak intensity is observed even after several hours of reaction time at room temperature. As expected based on the results of Fig.3.3, simple D_2O vapor adsorption causes a rapid decrease in the 12-15

ppm peak on the same apparent timescale as the BAS (not shown), both of which are at least one order of magnitude faster than the isotopic exchange with SiOH.

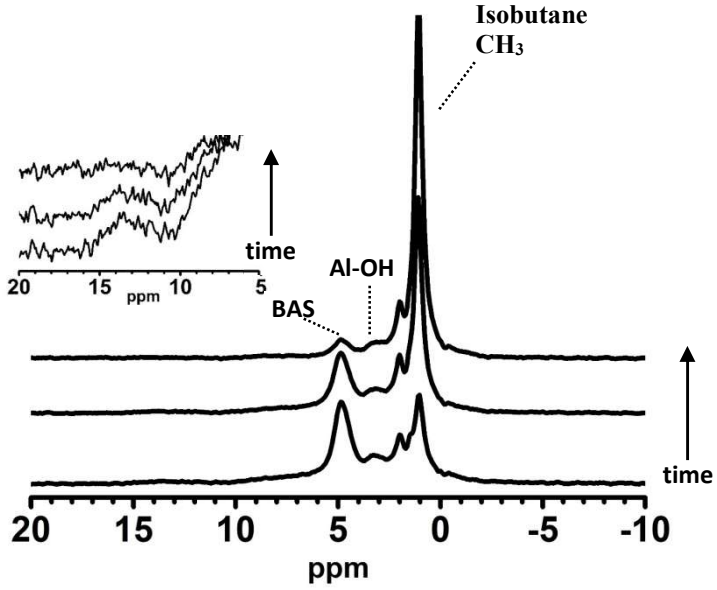

Fig. 3. 3. Selected ^{1}H MAS NMR spectra acquired following the room-temperature adsorption of isobutane-d_{10} on Si:Al=15 HZSM-5, with total reaction time for the zeolite/isobutane H/D exchange increasing from bottom to top up to one hour in the upper trace.

Identity of 12-15 ppm species. Previous studies predicted that the chemical shift for a surface-stabilized H_3O^+ species inside a zeolite would have a chemical shift in the 12-15 ppm region, from a combination of computational data and exchange-averaged NMR chemical shifts in systems with increased water content relative to that studied here.[23-25] The direct observation of a signal in the 12-15 region was not previously reported. Data reported herein are not consistent with assigning the 12-15 ppm peak to H_3O^+. Increasing the amount of water in the catalyst, such that the T_1^H relaxation time constant for all species decreases by an order of magnitude, results in no change in the peak shape or intensity of the 12-15 ppm peak as shown in Fig.3.4. For the BAS, Al-OH, and 12-15 ppm peak, the T_1's change from ca. 5-6 sec to 0.3-0.5 sec after the sealed rotor is exposed to ambient conditions for three days and the Si-OH peak decreases from 12 sec to 1 sec, relative to

the as-prepared dehydrated catalyst. However, as can be seen from the superposition of the two spectra in Fig.3.4, there is no change in the shape or intensity of the 12-15 ppm peak as might be expected if this peak originated from H_3O^+.

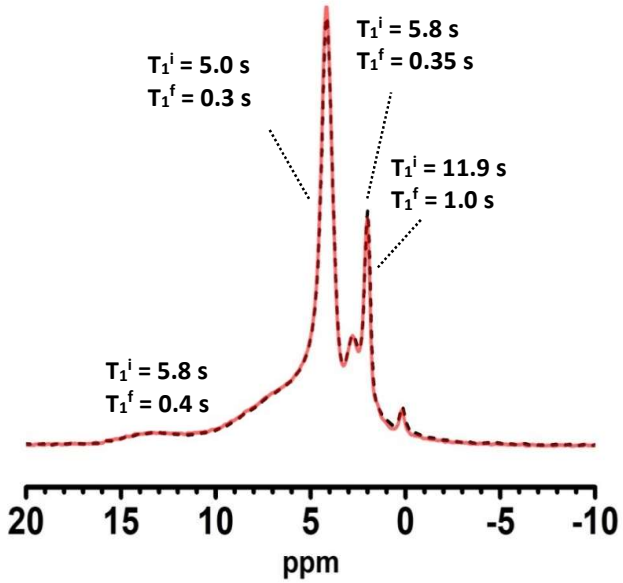

Fig. 3. 4. ^{1}H MAS NMR spectra acquired at room temperature (black dashed trace) immediately following the flow-dehydration procedure and (red solid trace) after three days of ambient atmosphere exposure in the sealed rotor. The initial (T_1^i) and final (T_1^f) values are listed above each peak. Each spectrum is quantitative based on the respective T_1 value.

Based on the previous work of Janda and coworkers, in which they found that this same Si:Al = 15 HZSM-5 catalyst contained the largest fraction of extra-lattice Al species, the data described in Figures 3.1 and 3.4, and the agreement with chemical shift data in Al_nO_mH species,[34] the most logical assignment for the acidic proton species responsible for the 12-15 ppm peak is that it is either a BAS hydroxyl group that interacts with extra-lattice aluminum species, or a hydroxyl group on extra-lattice aluminol that interacts with multiple Al centers or interacts with the BAS. Chemical washing of the Si:Al = 15 catalysts like those shown in Fig.3.4 with EDTA, aluminum salts, and

magnesium salts in an attempt to eliminate the 12-15 ppm peak caused no change in its intensity, even as the intensity of the 2.8 ppm peak decreased but was not eliminated, indicating that this species is stable. To further elucidate the structure of the highly acidic species, the as-prepared dry HZSM-5 was treated with ammonium hexafluorosilicate (AHFS) using standard published procedures[13,42,43], the results of which are shown in Fig. 3.5. The solid line is the spectrum for as-prepared catalyst, containing all of the peaks that were shown in the previous discussion to be involving in proton transfer steps, including the new 12−15 ppm peak and the 2.6 ppm peak. After washing that catalyst with AHFS, only the BAS and SiOH peaks remain (dashed spectrum), which are associated with the zeolite framework. All other peaks are removed, including the 12−15 and 2.8 ppm peaks. This proves that those species are acidic Brönsted sites arising from or associated with extra-lattice aluminol species. Moreover, the relative ratios of the BAS to the nonacidic SiOH spin populations does not change following AHFS washing, indicating that the framework BAS concentration is not perturbed.

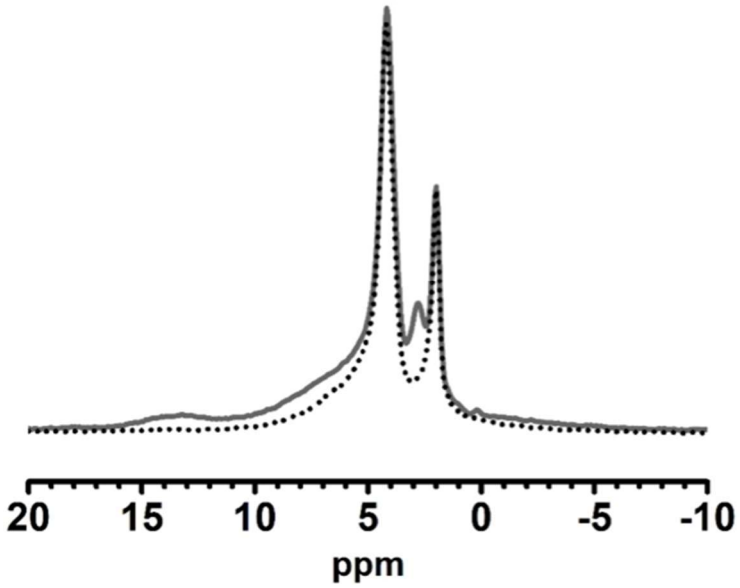

Fig. 3. 5. ^{1}H MAS NMR spectra acquired under quantitative conditions for (solid line) HZSM-5 and (dashed line) the same HZSM-5 catalyst washed with ammonium hexafluorosilicate.

As described in the Introduction, previous reports have proposed that extra-lattice aluminum oxide species, for which the Al atom coordination may vary, can work in synergy with existing Brönsted sites to create a small concentration of "strong acid" or "highly reactive" Brönsted sites. The data herein surrounding this newly detected protonic species at 12-15 ppm is consistent with these proposals, but shows for the first time that such synergy creates a strongly acidic hydroxyl group. Based on these data, the most probable structures for the Brönsted acid proton sites in HZSM-5 with Si/Al = 15 before and after washing are shown in Scheme 3.1. The 12−15 ppm signal is obviously a broad signal, and therefore it is unlikely that only one single species gives rise to it, as shown in the scheme.

Scheme 3.1. Chemical Structures for the Reactive HZSM-5 Hydroxyl Groups Leading to the Broad 12−15 ppm Signal (indicated in red), and Indicating Transformation of a Catalyst with Multiple Brönsted Acid Sites to a Single-Site Catalyst Containing only BAS's after Washing with Ammonium Hexafluorosilicate

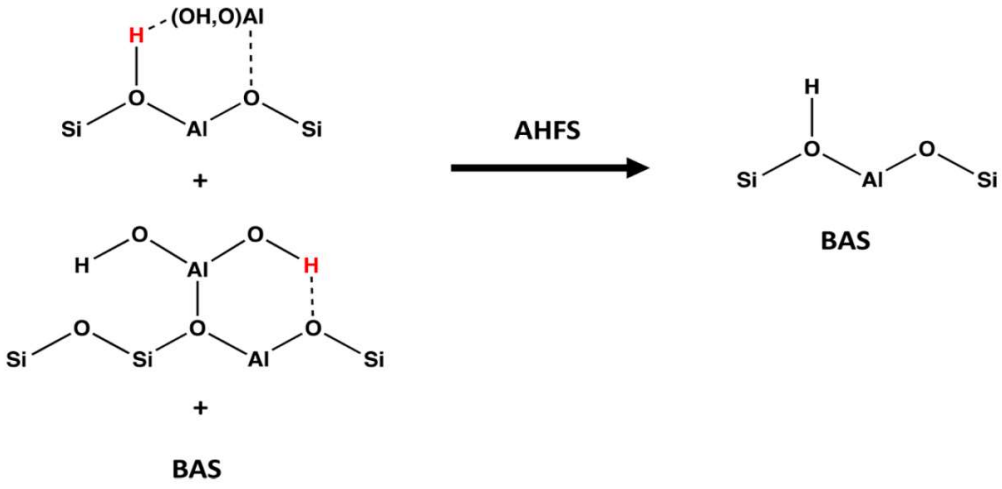

3.4. Conclusions

For the first time, an acidic species has been directly observed in HZSM-5 that gives rise to a broad peak in the solid-state ^{1}H MAS NMR spectrum at 12-15 ppm. Using a combination of 1D and 2D MAS NMR experiments along with alkane probe molecule reactions, dynamic proton

transfers and chemical exchange was observed, clearly establishing the acid character of the hydroxyl proton responsible for this highly-deshielded 12-15 ppm signal. The signal intensity was independent of ambient moisture exposure, indicating that it does not arise from surface-stabilized H_3O^+ ions. Rather, the data in total suggest that the acidic moiety is associated with either hydroxyl groups from extra-lattice aluminum oxides or from the BAS proton interacting with extra-lattice aluminum oxides. In addition to the first observation of the presence and acid character of this species, experiments also showed that previously observed extra-lattice aluminol species characterized by a signal at 2.8 ppm can undergo proton transfer, and that trace water most likely facilitates the proton scrambling between the 12-15 ppm species, the BAS, and extra-lattice aluminols.[42,43] Now that the species giving rise to 12-15 ppm signal has been observed, future computational studies coupled with heteronuclear solid-state assignment techniques can be used to further refine its structure.

3.5. References

1. Corma, A. *Chem. Rev.* **1995**, *95*, 559-614.

2. Thomas, J. M.; Thomas, W. J. *Principles and Practice of Heterogeneous Catalysis* **2005**, VCH Publishing, Weinheim, Germany.

3. Derouane, E. G.; Védrine, J. C.; Pinto, R. R.; Borges, P. M.; Costa, L.; Lemos, M. A. N. D. A.; Lemos, F.; Ribeiro, F. R. *Catalysis Reviews* **2013**, *55*, 454-515.

4. Cheng, Y.-T.; Jae, J.; Shi, J.; Fan, W.; Huber, G. W. *Angew. Chem. Int. Ed.* **2012**, *51*, 1387-1390.

5. Ennaert, T.; Van Aelst, J.; Dijkmans, J.; De Clercq, R.; Schutyser, W.; Dusselier, M.; Verboekend, D.; Sels, B. F. *Chem. Soc. Rev.* **2016**, *45*, 584-611.

6. Zapata, P. A.; Faria, J.; Ruiz, M. P.; Jentoft, R. E.; Resasco, D. E. *J. Am. Chem. Soc.* **2012**, *134*, 8570-8578.

7. Jones, A. J.; Carr, R. T.; Zones, S. I.; Iglesia, E. *J. Catal.* **2014**, *312*, 58-68.

8. Beck, L. W.; White, J. L.; Haw, J. F. 1H{27Al}c *J. Am. Chem. Soc.* **1994**, *116*, 9657-9661.

9. Gounder, R.; Iglesia, E. *J. Am. Chem. Soc.* **2009**, *131*, 1958-1971.

10. Hunger, M. *Solid State Nucl. Magn. Reson.* **1996**, *6*, 1-29.

11. Harris, K. D. M.; Xu, M. C.; Thomas, J. M. *Philosophical Magazine* **2009**, *89*, 3001-3012.

12. (a) Hadjiivanov, K. I.; Vayssilov, G. N. *Adv. Catal.* **2002**, *47*, 307-511. (b) Thomas, J. M. in *Characterization of Solid Materials and Heterogeneous Catalysts*, M. Che and J. C. Vedrine, Editors, **2012**, pp. 28, Wiley VCH, Weinheim, Germany.

13. Schallmoser, S.; Ikuno, T.; Wagenhofer, M. F.; Kolvenbach, R.; Haller, G. L.; Sanchez-Sanchez, M.; Lercher, J. A. *J. Catal.* **2014**, *316*, 93-102.

14. Yu, Z.; Li, S.; Wang, Q.; Zheng, A.; Jun, X.; Chen, L.; Deng, F. *The Journal of Physical Chemistry C* **2011**, *115*, 22320-22327.

15. DeCanio, S. J.; Sohn, J. R.; Fritz, P. O.; Lunsford, J. H. *J. Catal.* **1986**, *101*, 132-141.

16. Brunner, E.; Ernst, H.; Freude, D.; Hunger, M.; Krause, C. B.; Prager, D.; Reschetilowski, W.; Schwieger, W.; Bergk, K. H. *Zeolites* **1989**, *9*, 282-286.

17. Li, S.; Zheng, A.; Su, Y.; Zhang, H.; Chen, L.; Yang, J.; Ye, C.; Deng, F. *J. Am. Chem. Soc.* **2007**, *129*, 11161-11171.

18. Mirodatos, C.; Barthomeuf, D. *J. Chem. Soc., Chem. Commun.* **1981**, 39-40.

19. Liu, C.; Li, G.; Hensen, E. J. M.; Pidko, E. A. *ACS Catalysis* **2015**, *5*, 7024-7033.

20. Janda, A.; Bell, A. T. *J. Am. Chem. Soc.* **2013**, *135*, 19193-19207.

21. Chen, K.; Damron, J.; Pearson, C.; Resasco, D.; Zhang, L.; White, J. L. *ACS Catalysis* **2014**, *4*, 3039-3044.

22. Chen, K.; Gumidyala, A.; Abdolrhamani, M.; Villines, C.; Crossley, S.; *J. Catal.* **2017**, *351*, 130-135.

23. Ratcliffe, C. I.; Ripmeester, J. A.; Tse, J. S. *Chem. Phys. Lett.* **1985**, *120*, 427-432.

24. Sauer, J. *J. Mol. Catal.* **1989**, *54*, 312-323.

25. Batamack, P.; Doremieux-Morin, C.; Fraissard, J.; Freude, D. *The Journal of Physical Chemistry* **1991**, *95*, 3790-3796.

26. Martínez, A.; López, C. *Applied Catalysis A: General* **2005**, *294*, 251-259.

27. Huo, H.; Peng, L.; Grey, C. P. *The Journal of Physical Chemistry C* **2009**, *113*, 8211-8219.

28. Cory, D. G.; Ritchey, W. M. *Spectrosc. Lett.* **1988**, *21*, 551-558.

29. van Eck, E. R. H.; Janssen, R.; Maas, W. E. J. R.; Veeman, W. S. *Chem. Phys. Lett.* **1990**, *174*, 428-432.

30. Grey, C. P.; Vega, A. J. *J. Am. Chem. Soc.* **1995**, *117*, 8232-8242.

31. Szeverenyi, N. M.; Sullivan, M. J.; Maciel, G. E. *Journal of Magnetic Resonance (1969)* **1982**, *47*, 462-475.

32. Ernst, R. R.; Bodenhausen, G.; Wokaun, A. *Principles of Nuclear Magnetic Resonance in One and Two Dimensions,* Clarendon Press, Oxford, **1987**.

33. Sohn, J. R.; DeCanio, S. J.; Fritz, P. O.; Lunsford, J. H. *The Journal of Physical Chemistry* **1986**, *90*, 4847-4851.

34. Piedra, G.; Fitzgerald, J. J.; Dando, N.; Dec, S. F.; Maciel, G. E. *Inorg. Chem.* **1996**, *35*, 3474-3478.

35. Kalwei, M.; Koller, H. *Solid State Nucl. Magn. Reson.* **2002**, *21*, 145-157.

36. Greiser, S.; Hunger, M.; Jäger, C. *Solid State Nucl. Magn. Reson.* **2016**, *79*, 6-10.

37. Luo, Q.; Yang, J.; Hu, W.; Zhang, M.; Yue, Y.; Ye, C.; Deng, F. *Solid State Nucl. Magn. Reson.* **2005**, *28*, 9-12.

38. Sommer, J.; Habermacher, D.; Jost, R.; Sassi, A.; Stepanov, A. G.; Luzgin, M. V.; Freude, D.; Ernst, H.; Martens, J. *J. Catal.* **1999**, *181*, 265-270.

39. Haouas, M.; Walspurger, S.; Taulelle, F.; Sommer, J. *J. Am. Chem. Soc.* **2004**, *126*, 599-606.

40. Truitt, M. J.; Toporek, S. S.; Rovira-Truitt, R.; White, J. L. *J. Am. Chem. Soc.* **2006**, *128*, 1847-1852.

41. Truitt, M. J.; Toporek, S. S.; Rovira-Hernandez, R.; Hatcher, K.; White, J. L. *J. Am. Chem. Soc.* **2004**, *126*, 11144-11145.

42. Ryder, J. A.; Chakraborty, A. K.; Bell, A. T. *The Journal of Physical Chemistry B* **2000**, *104*, 6998-7011.

43. Alberti, A.; Martucci, A. *The Journal of Physical Chemistry C* **2010**, *114*, 7767-7773.

CHAPTER IV

CONTROL AND IMPACT OF BRÖNSTED ACID HETEROGENEITY OF HZSM-5 ZEOLITES BY USING POST-SYNTHETIC TREATMENTS

4.1. Introduction

Brönsted acid site density and homogeneity significantly impact catalytic activity and selectivity in zeolites, even for identical framework types.[1-3] Specific synthetic methods allow tailored acid site densities based on framework Al content. Post-synthetic processes, whether intentional or inadvertent, can lead to significant perturbations in the final acid site types and concentrations, including catalyst deactivation and regeneration, chemical treatments to vary catalyst particle hydrophilicity, chemical substitutions, or modifications to remove extra-framework Al species.[4-9] There is growing recognition that "single-site" zeolite catalysts, i.e. catalysts where all acid sites are topologically and electronically equivalent, may be rare, even in relatively simple zeolite structures like members of the MFI family.[10-14] The presence of extra-framework aluminum (EFAl) oxides and aluminols can contribute to acid site heterogeneity due to their proximity to framework acid sites, and chemical extraction methods to remove them are common to the literature.[14-17] Only recently has it been shown that the EFAl species themselves contribute Brönsted acid sites that are as, or even more, reactive than framework bridging acid sites (BAS).[18] The ability to measure and interpret the distribution of framework BAS's versus Brönsted acid sites from EFAl species is critical to defining catalyst reactivity, which is uniquely different than strictly attributing Lewis acid character to EFAl. In this contribution, several post-synthetic

treatment methods previously described in the literature are investigated in a high Al-content ZSM-5 (Si/Al = 15), with the specific goal of minimizing changes to the framework BAS while maximizing removal of Brönsted acid sites arising from EFAl.[19] In order to determine which post-synthetic routes are most effective, a quantitative assessment of all types of Brönsted species must be obtained. A simple ^{1}H magic-angle spinning (MAS) standard-addition NMR technique is demonstrated to uniquely reveal the impacts of post-synthetic treatment methods on Brönsted proton distributions,[20] which are not accessible using ^{27}Al NMR methods. Reagents including nitric acid, hydrochloric acid, EDTA (ethylenediaminetetraacetic acid), and oxalic acid are investigated, but detailed spectroscopic analysis of the fate of BAS hydroxyl groups and hydroxyl groups associated with EFAl species shows that ammonium hexafluorosilicate (AHFS) at optimized concentrations exhibits the highest specificity for complete EFAl removal with minimal impact on framework acid sites. While many commonly used methods in the literature can remove EFAl, they do so at the expense of significant reduction in the number of BAS as shown here. Other methods routinely described in the literature, like EDTA, simply do not work for removal of acid sites associated with EFAl in MFI catalysts. Probe molecule reactions involving room-temperature hydrogen-deuterium between benzene and different catalysts demonstrate the impact of post-synthetic modifications to HZSM-5 reactivity, and more importantly, reveal that dilute Brönsted acids sites that are distinct from framework BAS's comprise the most active sites.

4.2. Experimental sections

4.2.1. Catalyst post-treatment

Zeolite ZSM-5 (Si/Al = 15, CBV 3024E and Si/Al = 40, CBV 8014) samples were obtained from Zeolyst in the NH_4^+-exchanged form. Calcined zeolite samples were prepared in a glass reactor body using a gradual, stepwise vacuum calcination up to a final temperature of 500°C to yield acidic HZSM-5. Calcined samples were then treated with different leaching reagents including HCl, HNO_3, EDTA (ethylenediaminetetraacetic acid), AHFS (ammonium hexafluoroslicate), and

oxalic acid in order to probe their efficacy for selective removal of extra-framework aluminum species. In each case, HZSM-5 zeolite was mixed with deionized water at a concentration of 30 g/L to prepare the initial solution, which was subsequently treated with the specific reagents listed below. For reference, in the HZSM-5 with Si:Al = 15, the expected framework BAS density based on total Al content is 1.04 mmol/g, while in HZSM-5 with Si:Al = 40, it is 0.39 mmol/g.

Ammonium hexafluorosilicate. For AHFS treatments, 5 ml of AHFS solution was added to the mixture of NH_4^+ZSM-5 zeolite and deionized water at 90°C and stirred for 4 hours. Five samples were prepared by varying the AHFS:Al molar ratio from 1:1, 2:1, 4:1, 6:1, and 8:1. The mixture was then filtered, washed with the warm deionized water and dried overnight at 120°C.[13,14,20]

Nitric acid. The mixture of zeolite in the proton form (HZSM-5) and deionized water was heated to 90°C under vigorous agitation. Two sets of samples were prepared by using either 5 ml/g of 0.2 M or 2.0 M nitric acid solutions, with similar results observed for each. The acid solutions were added to the mixtures and stirred for 4 hours, with final mixtures filtered, washed with deionized water, and dried overnight at 120°C.[20]

Hydrochloric acid. Hydrochloric acid solution at 0.2 M concentration was added to the mixture of HZSM-5 zeolite and deionized water at 90°C and stirred for 4 hours. The suspension was filtered, washed, and dried at 120°C overnight.[16]

Ethylenediaminetetraacetic acid. The EDTA amount in the HZSM-5/wash solution mixture was chosen to obtain an EDTA:Al molar ratio equal to 1.90:1 in the solution. EDTA was added to the mixture and stirred at 75°C for 4 h, and then the suspension was filtered and washed with deionized water. In order to eliminate sodium introduced by the EDTA, the filtrate was treated with 1M ammonium nitrate solution. The exchange was carried out twice, each at 90°C for 6 hours. The sample was filtered again, washed, dried at 90°C, and calcined at 550°C for 6 h to burn off any residual EDTA.[1,20]

Oxalic acid. A 0.8M oxalic ($C_2H_2O_4$) acid solution (oxalic acid/Al=4) was prepared and added to the stirred HZSM-5 mixture at 70°C. After 4 hours of mixing, the suspension was filtered, washed, dried overnight at 120°C, and calcined at 550°C for 6 h to burn off any residual organic moeties.[22]

Prior to spectroscopic investigations, all samples were dehydrated using the same stepwise vacuum dehydration procedure as used for the unwashed HZSM-5 control sample. Dry catalyst samples were sealed and immediately placed in a dry argon glove box following activation in order to transfer to zirconia MAS rotors without exposure to ambient moisture. Complete removal of ammonium cations, organics, and water was verified by ^{1}H MAS NMR. Selected samples, as indicated in the text, were further treated by steaming with 21 torr water vapor in nitrogen flow at 15 ml/min in a flow reactor, heated stepwise to a final temperature of 773 K, and held there for 72 h. After steaming, samples were dehydrated using the flow reactor with nitrogen gas at 773 K for 5 hr.

4.2.2. NMR measurements

^{1}H MAS (magic-angle spinning) NMR data were collected on a Bruker Avance 400 spectrometer operating at 9.05 T with a 4-mm double-resonance MAS probe. Rotors were spun with -54°C dewpoint dry air, and periodically compared to dry N_2 spinning; no differences in spectra or relaxation times were observed. Spinning speeds of 10 or 15 kHz, 32 scans and 3.4-3.9 μs π/2 pulses were used for single-pulse acquisition spectra with samples packed in zirconia rotors and sealed with grooved Teflon spacers. Extremely dry HZSM-5 catalysts of the type used here can have T_{1H} values of up to 15 seconds for the terminal silanol SiOH species, but the T_{1H} values for all framework and extra-framework protons were always 10 seconds or slightly shorter.[18] As such, spectra were acquired with a 50-second delay, as all quantitative analyses focused on acidic protons and not the inert silanol species. The spin-counting or standard-addition method to quantify the distribution of protonic species in HZSM-5 based on the addition of a known amount of inert PDMS (polydimethylsiloxane) follows the procedure previously published.[20] All samples were loaded in

the glove box, and typically included 20-30 mg of zeolite with 20-40 μg of PDMS in restricted volume MAS rotors.

^{27}Al MAS NMR data were acquired on samples that were exposed to ambient moisture in order to eliminate lattice strain and enable detection of framework Al atoms. Large quadrupole coupling constants arising from lattice distortions and whose magnitude is on the order of several megahertz precludes Al observation in completely dehydrated catalysts. For this reason, ^{27}Al NMR is not a quantitatively reliable method for following how acid sites are impacted by post-synthetic treatments. Even though multiple-quantum NMR methods can help identify some "NMR-invisible" aluminum species, the quantitative distribution of acidic protons sites must be interrogated in completely dry catalysts as even ambient water levels can enable proton exchange on intermediate timescales causing signal loss. Trace water does exist as proton-exchange on the slow-exchange timescale occurs,[18] albeit in amounts that do not impact the spectral lineshapes[23]. ^{1}H MAS NMR provides the best experimental route to this information, since Brönsted acid sites are themselves protons, not Al atoms.

4.2.3. Crystallinity measurements

X-ray diffraction (XRD) was used to calculate the HZSM-5 crystallinity following some post-synthetic chemical treatments using a Philips PW 1830 diffractometer operating with a Cu Kα radiation (λ = 1.5418 Å) source. Data was gathered in the 5−70° 2θ range with step width and scanning speed set to 0.02° and 0.5 sec/step, respectively.

4.2.4. BET measurements

Surface area BET and nitrogen adsorption measurements were determined for HZSM-5 (Si/Al=15) and the same HZSM-5 treated with AHFS (AHFS:Al = 2:1) at liquid nitrogen temperature using a Quantachrome Autosorb-1 instrument. Each sample was degassed at 423 K overnight prior to nitrogen adsorption.

4.2.5. H/D isotopic exchange experiments at room-temperature

In-situ solid state ^{1}H MAS NMR methods were used to follow hydrogen/deuterium exchange reactions.[24] Typically, 1 eqv (1 benzene per Al atom in the zeolite) of C_6D_6 molecules were adsorbed on activated HZSM-5 using an evacuated and dry vacuum line. H/D isotopic exchange took place immediately after adsorptions, while the adsorption processes usually took 3-5 minutes for completion. The initial H/D exchange spectra were typically acquired 8-11 minutes following the initial exposure.

4.3. Results and discussions

4.3.1. Quantitative analysis of distribution of acidic species

The locus of catalytic activity in HZSM-5 is a proton, historically assumed to be a framework BAS species. Spectroscopic detection of the variety of protonic species that can exist in zeolites, ranging from non-acidic silanol species to acid sites, is afforded by both infrared and solid-state MAS NMR methods[25,26]. NMR offers advantages in resolution, as well as opportunity for direct quantification of all species via spin-counting or standard-addition techniques. [20] The latter method is used here to establish baseline concentrations of all proton species in HZSM-5 in order to determine if post-synthetic modifications to the catalyst are successful. Fig. 4.1.a and 4.1.b show representative quantitative ^{1}H MAS standard-addition NMR spectra for HZSM-5 with Si:Al ratios of 15 and 40, respectively. A known mass of PDMS (polydimethylsiloxane) spin-counting standard is added to a known mass of dehydrated zeolite, and the integrated areas of each peak in the spectra yield quantitative proton concentrations. The three most intense peaks are well-resolved, with the framework bridging acid site, terminal silanol groups at crystallite surfaces, and the polymer standard peaks labeled as BAS, SiOH, and PDMS, respectively. For clarity, the smaller, less-resolved peaks in the spectra are not labeled with the exception of the 12-15 ppm peak, but their deconvoluted areas are shown by the dotted traces. Four such peaks exist in the Si/Al=15 spectrum, and three in the Si/Al=40 spectrum. Based on multiple reports in the literature,[26,27] and the

quantitative analysis of the areas of all peaks in each spectrum (*vide infra*), the peaks shown by the dotted traces in Fig. 4.1 are assigned to hydroxyl groups associated with EFAl species. This includes the species at 12-15 ppm, which has only recently been revealed in the literature,[18] and 5.1 and 6.5 ppm peaks indicated by the arrows in Fig.4.1.

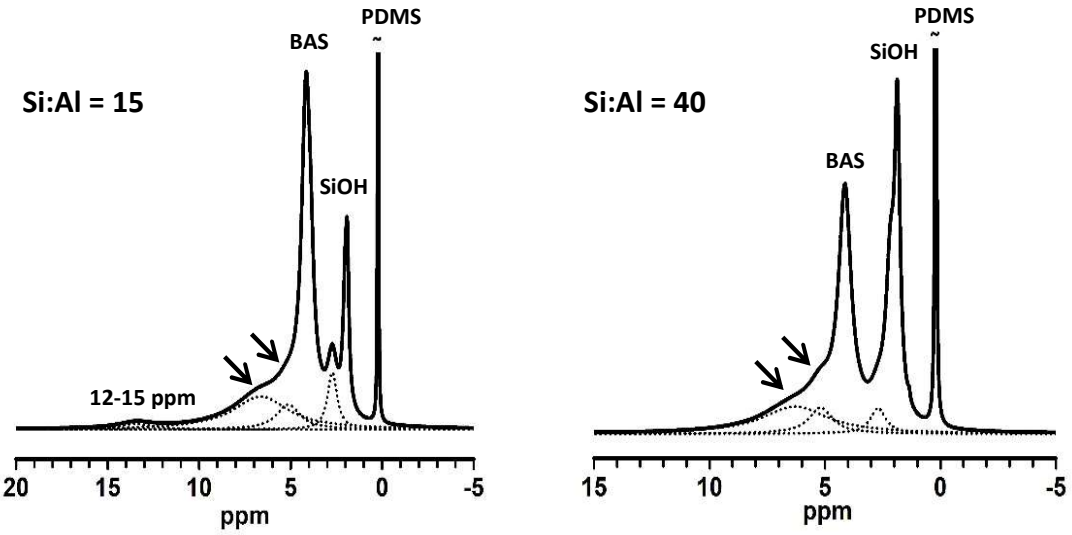

Fig. 4. 1. ^{1}H MAS NMR spectra acquired at room temperature for dehydrated HZSM-5 catalysts with Si:Al = 15 (left) and Si:Al=40 (right). The 0.2 ppm peak arising from addition of the inert PDMS is shown at less than its maximum intensity for clarity.

The broad component centered near 6.5 ppm represents the largest intensity fraction of the peaks assigned to extra-framework species, the specific assignment for which has proven controversial in previous publications. Haw and coworkers assigned the peak to hydroxyl groups in HZSM-5 arising either from distorted or associated species, proximate to Al atoms.[28] Grey and coworkers assigned the 6.5 peak as strongly bound residual water that is difficult to remove by evacuation, requiring ultra-dry helium flow to remove.[29] Recently we have shown that this peak is strongly attenuated by washing HZSM-5 with ammonium hexafluorosilicate (AHFS) followed by vacuum drying, identical to the response of the known EFAl hydroxyl peak at 2.6-2.8 ppm and the

recently assigned 12-15 ppm peaks after washing.[18] Although we followed the literature assignment[29] attributing at least some of this 6.5 ppm peak to residual water in that recent paper,[18] upon further consideration of the quantitative data following AHFS washing shown below in Figures 4.2 and 4.4, it is now clear that the majority of the species in the 5-7 ppm region cannot be attributed to water (*vide infra*).

The sum of all of the peaks denoted by the dotted lines represents essentially half of the total proton signal intensity in Fig. 4.1, excluding the silanol (SiOH) peak. Quantitative analysis of the spectra in Fig. 4.1 using the PDMS spin-counting standard yields the data shown in Table 4.1 for the two HZSM-5 catalysts. The 6.5 ppm feature is included in the 5-7 ppm intensity range in the table. Table 4.1 indicates that only about half of the theoretically maximum protons exist as BAS's (4.2 ppm peak), with the other half distributed among the other non-framework sites or other distorted framework sites. Since the SiOH group at ca. 2 ppm is not acidic and is known to be unreactive for acid catalysis, it is not considered in this analysis. If all Al atoms are incorporated in the framework, and each Al atom generates a BAS, then the expected acid site proton density in the Si/Al = 15 and = 40 catalysts is 1.04 mmol/g and 0.39 mmol/g, respectively. Although only one-half of the protons contribute to the 4.2 ppm peak, the peak assigned to BAS species, the next-to-last column in Table 4.1 shows that the total proton concentration obtained by summing the BAS and extra-framework species (columns 3-6) is very near the total expected from Al content, albeit slightly larger in both cases. This suggests that a small fraction of extra-framework Al species have more than one proton associated with them, consistent with proposed structures by Lunsford and others[5]. Obviously, there may be some EFAl species that exist as AlO^{+2} structures, or others that do not contain protons, which would not be directly counted in this analysis. However, their presence might indirectly contribute to intensity in the 5-7 or 12-15 ppm regions, and therefore be subject to perturbations following chemical washings as described below.

Table 4. 1. Distribution of species, in units of **mmol/g**, obtained from quantitative ^{1}H MAS NMR spin-counting spectra of the type shown in Fig. 4.1. Uncertainly limits were determined by triplicate or quadruplicate

catalyst	SiOH	2.6-2.8ppm	BAS	5-7ppm	12-15ppm	Sum of all species excluding SiOH	*Expected sum for H:Al=1
Si/Al=15	0.17±0.009	0.091±0.011	0.56±0.018	0.45±0.037	0.059±0.025	1.16	1.04
Si/Al=40	0.24±0.017	0.028±0.016	0.23±0.012	0.21±0.030	0	0.46	0.39

*** [Al] from total theoretical aluminum content in framework based on Si/Al, and assuming H:Al of unity in dehydrated zeolite.**

The detailed analysis and discussion above establishes a quantitative basis for evaluating if standard literature methods for post-synthetic removal of protonic species associated with EFAl (H-EFAl) are effective, and if so, can they also preserve the integrity of BAS's. The spin-counting MAS NMR approach is the only way to directly quantify protonic species in HZSM-5, independent of any assumptions about probe molecule accessibility, thus providing a convenient tool to determine if any chemical washing methods are routinely capable of generating "single-site" MFI catalysts.

4.3.2. Removal of EFAl species by using AHFS washing

Several studies have shown that AHFS washing can remove EFAl species, with some proposing that AHFS provides a silicon source to help repair framework silanol-nest defects formed during dealumination. The washing conditions, including time, temperature, pH, and concentration of AHFS vary significantly in those reports.[2,30,31] Following the procedures outlined in the Experimental section, a selected portion of the total AHFS washing results are shown in Fig. 4.2, acquired as a function of the AHFS concentration in the washing solution. From Fig. 4.2, it is clear

that the catalysts treated with AHFS solutions whose concentration corresponded to AHFS:Al molar ratios of 4 or 6 led to significant loss of BAS's, based on reduction of the 4.2 ppm and 54 ppm peaks in the ^{1}H and ^{27}Al MAS NMR spectra, respectively. Fig. 4.2a shows that AHFS:Al ratio of 2:1 leads to significant removal of H-EFAl species based on the loss of the 12-15, 5-7, and 2.6-2.8 ppm peaks, but with very little change in the area of the BAS peak in 4.2a. As stated previously, the ^{27}Al data cannot be used to quantitatively assess the amount of Al in non-tetrahedrally or non-octahedrally coordinated environments. The apparent small absolute loss in intensity of the 54-ppm peak in 4.2d, and also reduction in its linewidth, following AHFS washing arises from removal of some aluminum atoms that reside in distorted tetrahedral environments, as previously discussed.[2] Quantitative limitations of ^{27}Al NMR are well-established, which is why the ^{1}H data in Fig. 4.2a-c is uniquely critical for assessing the impact of post-synthetic treatments on the Brönsted site distribution. One observes a significant loss of the 4.2 ppm BAS peak in 4.2b and 4.2c, indicative of framework dealumination, with 4.2c showing that at sufficiently high AHFS concentrations, the dealumination is so extensive that new SiOH peaks begin to arise in the 2.2-2.5 ppm region indicative of internal "silanol nest" defects. Importantly, Fig. 4.2c does show that all intensity in

the 5-7 ppm region can be removed, further reducing the likelihood that those signals can be assigned to residual water.

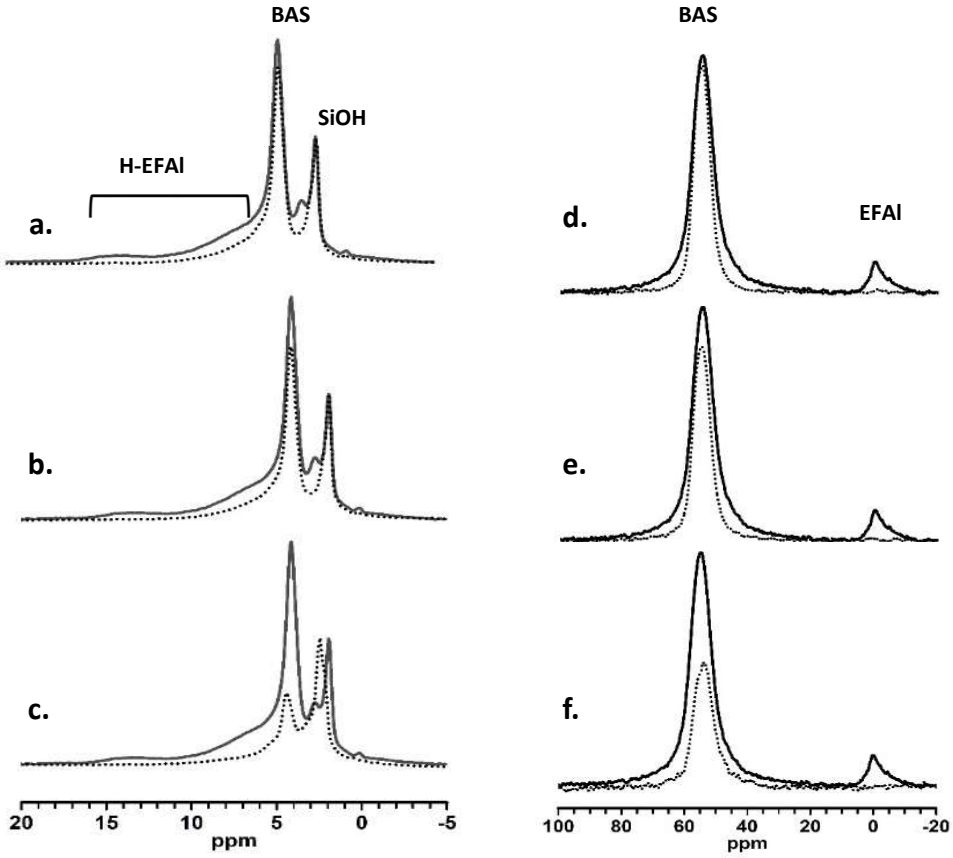

Fig. 4. 2. Comparative ^{1}H (left column) and ^{27}Al (right column) MAS NMR spectra acquired following chemical washing (dotted lines) of Si/Al = 15 HZSM-5 with AHFS concentrations corresponding to **(a,d)** 2:1 AHFS:Al, **(b,e)** 4:1 AHFS:Al, and **(c,f)** 6:1 AHFS:Al. The solid line spectra are the control data on the as-prepared HZSM-5 prior to washing. H-EFAl denotes protons from hydroxyl groups associated with EFAl species, and also includes the 2.7 ppm peak that is not labeled in order to preserve clarity in that region of the spectra.

With the AHFS time-temperature washing protocol used here, an AHFS:Al molar ratio of 2 is most effective, and XRD and BET surface area data provided in the Fig. 4.3 and Table 4.2. show that the crystalline structure is preserved. While not shown, an equimolar ratio did not lead to complete removal of the H-EFAl species, while AHFS:Al ratios of 6 or greater lead to significant crystallinity loss.

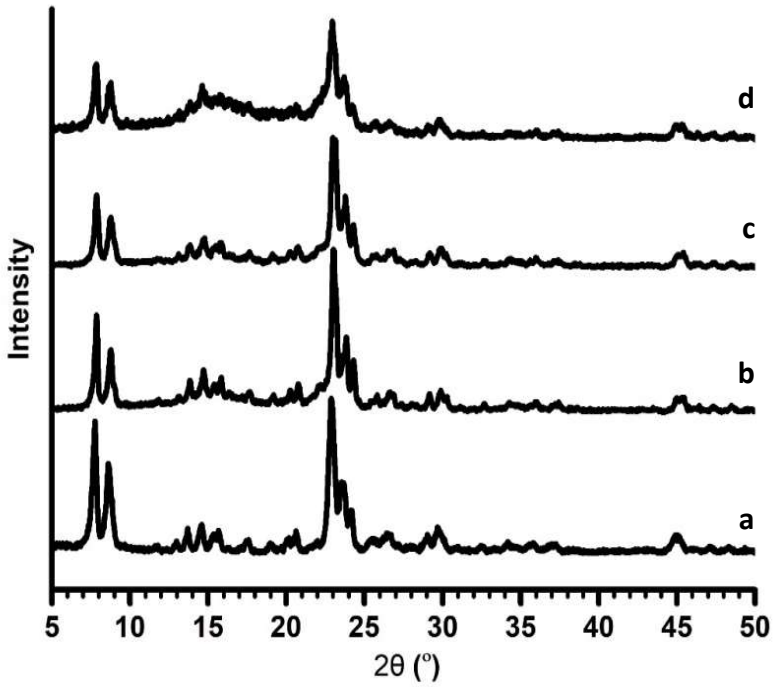

Fig. 4. 3. X-ray powder diffraction patterns for HZSM-5 catalysts with Si/Al=15 that have been washed with solutions containing an AHFS:Al ratio of **(a)** 0, **(b)** 2, **(c)** 4, and **(d)** 8.

Table 4. 2**.** Relative crystallinity (%) and surface area measurements

Sample	**Crystallinity (%)**	**Surface area (m^2/g)**
HZSM-5	100	352.5
HZSM-5-AHFS-2	99.0	315.4
HZSM-5-AHFS-4	92.0	-
HZSM-5-AHFS-8	78.8	-

Results from quantitative analyses of treatments with AHFS:Al = 2 on catalysts with Si/Al of 15 and 40, the raw data for which is shown in Fig. 4.4, are summarized in Table 4.3. All species in Fig. 4.4 are the same as previously shown in Fig. 4.1, but with the dotted-line spectra showing strong attenuation of the 12-15, 5-7, and 2.6-2.8 ppm (H-EFAl) peaks. Based on the known PDMS standard-addition method, Table 4.3 reveals that the amount of BAS protons in the framework is not changed, while the H-EFAl concentration decreases in total by ca. 60% in the Si/Al = 15 catalyst. A ca. 40% decrease in the H-EFAl is observed for the Si/Al=40 catalyst after AHFS washing, with essentially no change in the BAS concentration.

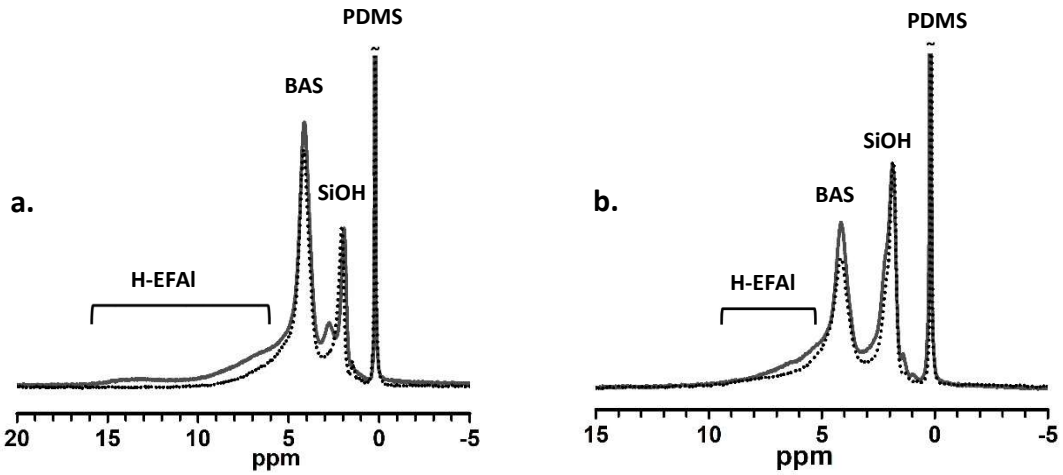

Fig. 4. 4. 1H MAS spin-counting NMR spectra acquired following AHFS treatment (dotted lines) of HZSM-5 with Si/Al equal (a) 15 and (b) 40 using AHFS:Al = 2. The solid line spectra are the control data on the as-prepared HZSM-5 prior to washing. H-EFAl denotes protons from hydroxyl groups associated with EFAl species, and also includes the 2.7 ppm peak that is not labeled here for clarity. The PDMS standard is shown at less than its maximum intensity for clarity.

From the data shown in Figures 4.2 and 4.4 and enumerated in Table 4.3, as well as the results of washing catalysts with solutions of AHFS:Al concentration less than 2 and greater than 6 that are not shown in Fig. 4.2, it is not possible to completely remove all H-EFAl species without decreasing the framework BAS concentration. Clearly, the species responsible for the 12-15 ppm peaks in Si/Al=15 spectra are completely removed, and essentially all of the 2.6-2.8 ppm species are removed. Although largely attenuated, most of the residual intensity following AHFS treatment in both HZSM-5 catalysts is in the 5-7 ppm region. Of course, all of the experimental variations of solution temperature and extraction time have not been explored for obvious practical reasons, but a range of conditions exceeding those typically discussed in the literature for AHFS extraction has been investigated. Longer extraction times at lower AHFS/catalyst solution temperatures might yield improvements.

Table 4.3. Distribution of species, in units of **mmol/g**, obtained from quantitative ^{1}H MAS NMR spin-counting spectra of two different HZSM-5 catalysts, before and after treatment with AHFS amount corresponding to AHFS:Al = 2 in the solution concentration. Uncertainly limits were determined by triplicate or quadruplicate experiments.

HZSM-5 catalyst	**SiOH**	**2.6-2.8ppm**	**BAS**	**5-7ppm**	**12-15ppm**	**Sum of all species excluding SiOH**	***Expected sum for H:Al=1**
Si/Al=15 control	0.17±0.009	0.091±0.011	0.56±0.018	0.45±0.037	0.059±0.0.025	1.16	1.04
Si/Al=15 AHFS	0.20±0.005	0.030±0.003	0.54±0.020	0.28±0.019	0	0.85	1.04
Si/Al=40	0.24±0.017	0.028±0.016	0.23±0.012	0.21±0.030	0	0.46	0.39
Si/Al=40 AHFS	0.24	0.017	0.21	0.13	0	0.36	0.39

AHFS washing did not remove all of the peak intensity assigned to H-EFAl species, and it is possible that the species responsible for the remaining intensity in the 5-7 ppm region in Figures 4.4a and 4.4b might arise from framework acid sites in distorted or coupled environments, as was originally proposed for untreated HZSM-5 catalysts.[28]

The signal at 5-7 ppm comprises a significant portion of the total proton intensity, and is reduced by almost a factor of 2 following treatment with the AHFS:Al=2 solution, as shown earlier in Table 4.3. Under these same conditions, Table 4.3 shows that the framework BAS concentration is not changed. Fig. 4.5 shows the results of a ^{1}H- ^{27}Al dipolar coupling experiment, shown here to indicate that the 5-7 ppm signal in the data above correspond to protons dipolar coupled to Al atoms. The top spectrum is acquired with a simple spin-echo pulse sequence and gives the same spectrum as those shown above that were acquired using a single pulse, while the bottom two spectra utilize the same spin-echo except for the application of ^{27}Al pulses during the echo evolution windows. This experimental approach, well-known in the literature as the spin-echo double

resonance SEDOR[33] or TRAPDOR[34] experiment, has been used extensively to identify protons that are within a dipolar-coupling distance (2-6 Å) of an aluminum atom in inorganic oxides, as that coupling attenuates the refocused echo.[35-37] Signals that arise from protons coupled to Al atoms decrease or are eliminated, while those that arise from species like the 2.0 ppm terminal silanol peak are not affected. Clearly, Fig. 4.5 shows that the 5-7 ppm peak is significantly attenuated in the bottom two spectra. While this particular result for the 5-7 ppm peak has been reported previously,[28] it is added here as a result of the review process in order to increase clarity. In the context of the new AHFS washing data and the quantitative spin-counting results summarized in Table 4.3, a more definitive assignment of the origin of those acidic protons giving rise to the 5-7 ppm peak is now possible. The Al atoms associated with these acidic protons must exist either in the framework, or as EFAl species.

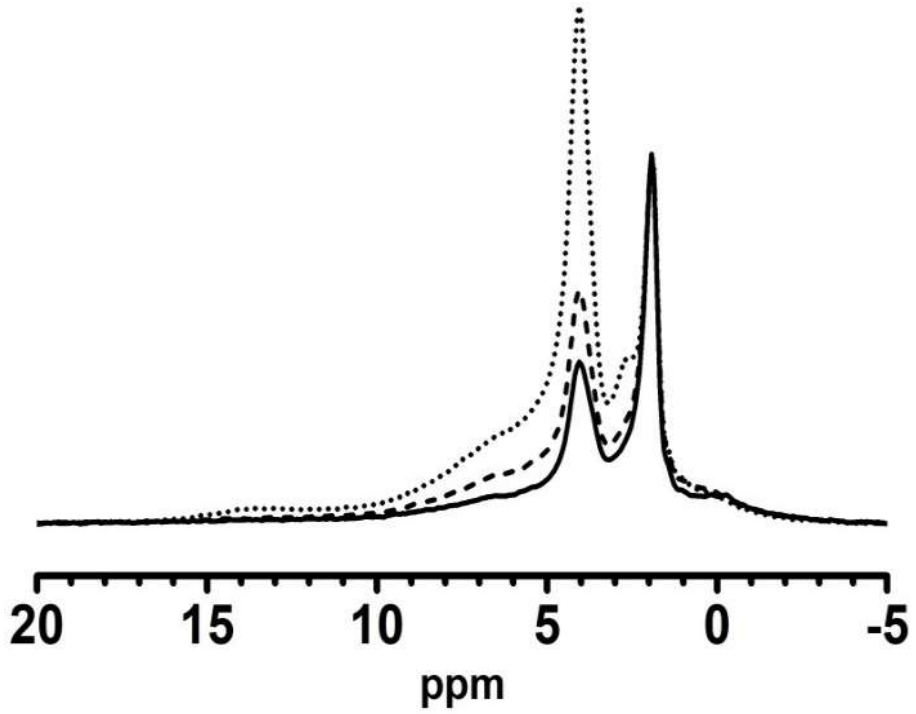

Fig. 4. 5**.** ^{1}H MAS NMR spectra acquired at room temperature for dehydrated Si:Al = 15 HZSM-5 using a spin-echo sequence **(top)** without and with an ^{27}Al r.f. pulse applied during **(middle)** 250-μs and **(bottom)** 500-μs echo evolution periods.

Table 4.3 and Figures 4.2, 4.4, and 4.5 show that framework Al atoms that give rise to BAS are not affected at all by washing with AHFS:Al = 2 solutions, as the 4.2 ppm signal intensity does not decrease. Under the same AHFS treatment conditions, half of the 5-7 ppm signal intensity is eliminated in the Si/Al=15 catalyst. The AHFS washing conditions used here are much milder than those typically reported, in which framework dealumination followed by Si re-insertion occurs over longer washing times and higher solution temperatures.[30,31] Moreover, standard literature methods for the AHFS framework dealumination followed by Si atom reinsertion primarily focus on Y-type of faujasite zeolites, not the MFI structure used here. This is confirmed by the preservation of the 4.2 ppm framework BAS signal, and further supported by XRD data shown in Fig. 4.3. and Table 4.2 showing that 99% of framework crystallinity relative to the starting HZSM-5 is preserved at AHFS:Al = 2, where crystallinity is calculated using the standard ASTM method for powder diffraction on ZSM-5.

4.3.3. Removal of EFAl species by using other chemical washing reagents

Also, other experiments were performed using other chemical-washing methods that are routinely discussed in the literature as effective for extracting EFAl species, including EDTA, HCl, HNO_3, and oxalic acid. As described above, ^{1}H MAS NMR was used to determine the impact of these treatments on the presence of multiple acidic proton species, and whether or not they could remove acidic sites from EFAl species with minimal perturbation to the BAS protons. As shown in Fig. 4.6, none of these methods are effective in removing the H-EFAl species without significant reduction in the framework BAS. It is particularly evident from Fig. 4.6 that EDTA is completely ineffective under the conditions routinely reported in the literature, with essentially all of the H-EFAl intensity remaining in the spectrum after washing. For HNO_3 with two different concentrations and HCl, mostly dealuminatin occurs. Oxalic acid attacks the framework, exhibiting excessive loss of BAS's, and is the only reagent that shows removal of the H-EFAl species at 2.6-

2.8 ppm. ^{27}Al MAS NMR on the EDTA, HCl, HNO_3, and oxalic acid washed HZSM-5 samples are shown in Fig. 4.6f, g, h, k, I in which the 0 ppm signal assigned to EFAl was not detectably reduced by EDTA washing. Only oxalic acid can remove 0 ppm species, and also reduce framework aluminum species at 54 ppm.

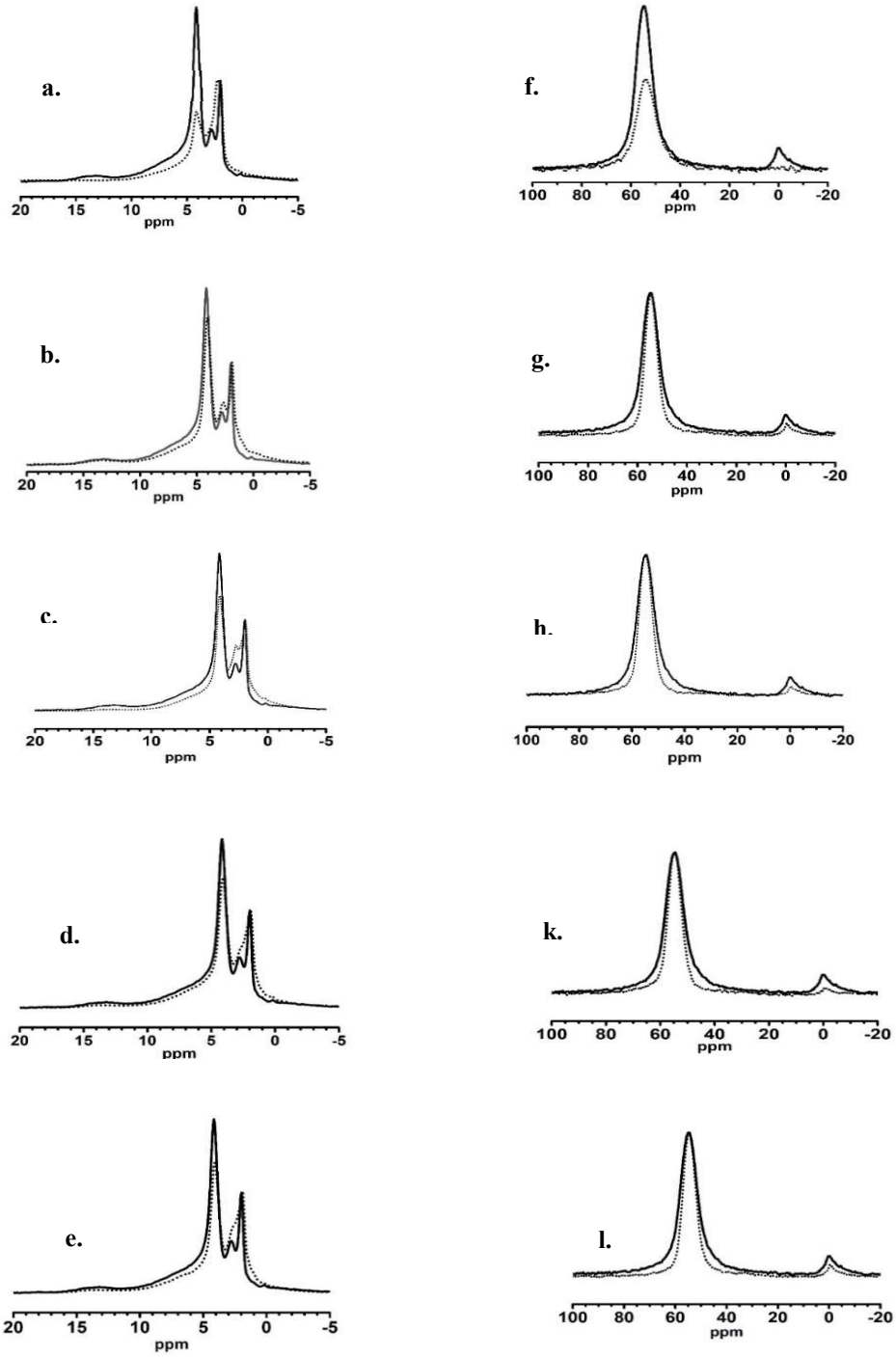

Fig. 4. 6**.** Comparative ^{1}H (left column) and ^{27}Al (right column) MAS NMR spectra acquired following chemical washing (dotted lines) of Si/Al = 15 HZSM-5 with different chemical washing reagents corresponding to **(a,f)** oxalic acid, **(b,g)** EDTA, **(c,h)** 2 M HNO3**, (d,k)** 0.2 M HNO3 and **(e,l)** 0.2 M HCl. The solid line spectra are the control data on the as-prepared HZSM-5 prior to washing.

4.3.4. Re-creation of EFAl species by using mild steaming

Key experimental results that reveal multiple acidic sites exist in a high Al content HZSM-5 catalyst, and that some can be both removed and re-introduced following original synthesis, are shown in Fig.4.7. In addition, Fig. 4.7 also reinforces the prior discussion above that the broad signal in the 5-7 ppm region of Figures 4.1, 4.2, and 4.4 does not originate from water. Comparison of 4.7b and 4.7c shows that following steaming of an AHFS-washed HZSM-5 (Si/Al=15) catalyst, H-EFAl species can be re-introduced as indicated by the re-appearance of the 12-15 ppm signal, signals in the broad 5-7 ppm region, and the 2.6 ppm peak. Again, based on known results for steaming-induced dealumination, these results (a) confirm our previous assignment of the H-EFAl species in Fig. 4.1-4.4, (b) shows that the 5-7 ppm region does not arise from water, and (c) indicates that the two major signals in the 5-7 ppm region shown previously by the deconvoluted peaks in Fig 4.1 (5.1 and 6.5 ppm) can change independently of one another based on sample history. Recall both components were observed in both the Si/Al = 15 and Si/Al = 40 catalysts in Fig. 4.1. Those same peaks are indicated by the dotted lines in Figures 4.7a-c, with the solid arrows identifying the 5.1 and 6.5 ppm components. The area ratio of the 6.5:5.1 ppm peaks in 6a, 6b, and 6c is 2.4, 0.4, and 0.9, respectively. These differences are visually striking in the raw spectra prior to any deconvolution, as indicated by the red arrows in Fig. 4.7, and suggest that the species at 5.1 ppm is enhanced by mild steaming relative to the H-EFAl species represented by the peak at 6.5 ppm. Given that the catalyst in 4.7b is much less reactive than the catalyst in 4.7a, as shown by the data in Fig. 4.8, and that this catalyst contains the lowest amount of H-EFAl species, one must conclude that the distribution of species giving rise to the H-EFAl peaks are critical to catalyst understanding. That such species can be re-introduced by mild steaming (4.7c) but with different acid function distributions will be a focus of future work. These data support recent work showing that the H-EFAl species themselves function as Brönsted sites[18], and that acid function in even a relatively simple zeolite structure like MFI is complex. This is true both for the Si/Al = 15 and Si/Al = 40 catalysts examined here, but likely extends to many other commercially-produced MFI

catalysts. Stated simply, Brönsted acidity in HZSM-5 cannot be characterized merely by framework BAS's.

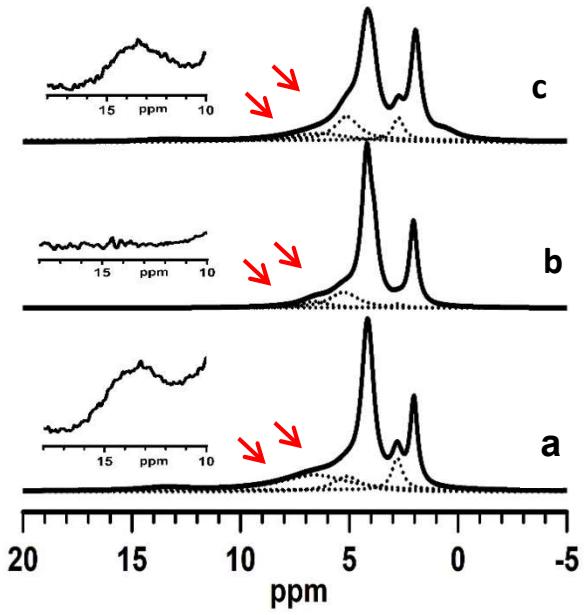

Fig. 4. 7. ^{1}H MAS NMR spectra of **(a)** HZSM-5 with Si/Al = 15; **(b)** same as (a) treated with AHFS:Al = 2; **(c)** same as (b) following the steaming procedure. The expansions ions show signal elimination and creation in the 12−15 ppm region. Note the two red arrows showing evolution of 5.1 and 6.5 ppm H-EFAl components with catalyst treatments.

4.3.5. H/D exchange reaction

However, isotopic exchange experiments with benzene-d_6 and HZSM-5 catalysts before and after AHFS washing reveals that the H-EFAl species that were removed by AHFS have a significant impact on catalyst reactivity. Fig. 4.8 shows representative spectra obtained at the same time point during in-situ exchange experiments at 296 K following adsorption of 1 eqv of benzene-d_6 on activated Si/Al = 15 HZSM-5 catalysts, before and after washing the catalyst with AHFS and also the steamed sample. Spectra were collected as a function of reaction time every five minutes during

the first 30 minutes, and every 30 minutes to an hour thereafter up to a total reaction time of 19 hours in the HZSM-5/AHFS case. In Fig. 4.8, it is clear that a very large C_6H_6 peak exists after only 8 minutes of room-temperature reaction on the starting material HZSM-5 catalyst, the latter of which is characterized by the solid-line spectrum in Fig. 4.1a. Prior to reaction, no benzene peak is expected as it is perdeuterated, and Fig. 4.8 shows that for the HZSM-5/AHFS catalyst, little exchange has occurred after 8 minutes, but the peak continues to increase albeit on much longer timescales than the untreated HZSM-5. Additional spectra from the total set of time-dependent results are shown in Fig. 4.9. The acid site peak(s) become broad and are shifted downfield from the normal BAS chemical shift of 4.2 ppm, as was previously reported following benzene adsorption on HZSM-5.[32] The shift and peak broadening for the acid peak arises from hydrogen bonding and neighboring group anisotropy contributions to the chemical shift from benzene. As usual, the SiOH peak is invariant.

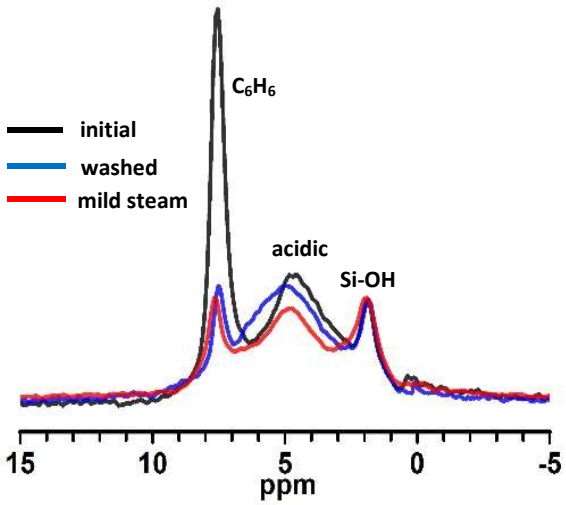

Fig. 4. 8. Representative benzene/catalyst H/D exchange spectra acquired 8 minutes after adsorption of benzene-d_6 on three initial, washed, and mild steamed samples.

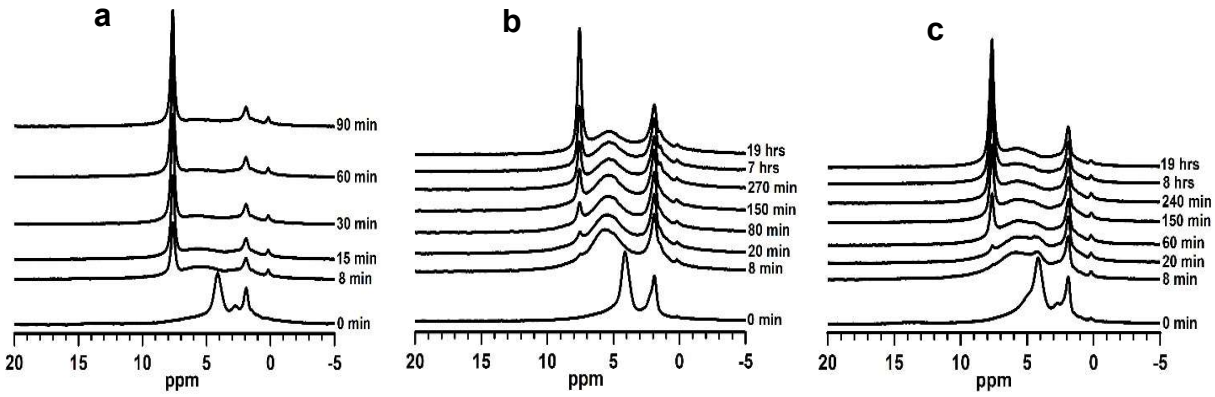

Fig. 4. 9. Representative in-situ ^{1}H magic-angle spinning (MAS) NMR spectra at 296 K as a function of time following adsorption of 1-eqv benzene-d_6 on (a) HZSM-5-15, (b) HZSM-5-15 treated with AHFS/Al=2, and (c) HZSM-5-15 treated with AHFS/Al=2 and steamed.

The benzene/HZSM-5 isotopic exchange probe reaction experimental approach and rate analysis was recently described in detail in the context of water impact on reaction rates,[24] and the same experimental method was used to obtain the data summarized by the rate plots in Fig. 4.10 below. The signal intensity on the y-axis is given in arbitrary units. Rates are extracted via an initial-growth approximation to the linear region of the growth curve, as shown by the dotted lines, and are reported along with [BAS] in the figure legend. Clearly, the initial HZSM-5 catalyst is most active, and the signal growth curve fits well to the expected first order $I(t) = I(\infty)[1- e^{(-kt)}]$ function, where $I(\infty)$ represents the equilibrium signal intensity at long exchange time. Due to experimental limitations, it is difficult to acquire data points earlier than 7 or 8 minutes, but control experiments in which benzene-d_6 is adsorbed onto a non-acidic silica show that there is no proton signal intensity arising from impurities in the benzene, thereby validating the assumption that the signal intensity at time zero is zero and that the fit curve should go through the origin, as it does. Since the benzene signal increases over an order of magnitude slower for the washed and mild-steamed samples, the initial rate is determined by a linear least squares fit through the data points as shown by the two

dashed lines at the bottom of Fig. 4.10. Comparing the exchange rates from the initial rate approximation along with the BAS concentration in Fig. 4.10 for each catalyst reveals that the exchange rate does not depend on BAS concentration. Since the NMR signal intensity units are arbitrary (denoted a.u.), the reported rates are normalized to the smallest initial slope value, i.e., the washed HZSM-5, at R=1 (a.u.)·s^{-1}. The exchange rate for the initial HZSM-5, which has essentially the same [BAS], is R=23 (a.u.)·s^{-1}. Finally, the mild-steamed catalyst is characterized by an exchange rate R = 1.9 (a.u.)·s^{-1}. Thus, even though the initial and washed HZSM-5 catalysts have the same concentration of framework bridging acid sites, there is a ca. 20-fold difference in their reaction rates as determined via an initial-rate analysis of the slope of the line fit to a first-order model. The benzene exchange data on the initial HZSM-5 catalyst was collected out to a reaction time of 90 minutes, which is shown along with the fitting curve in Figure S3 for reference to further validate the fitting out to long reaction times.

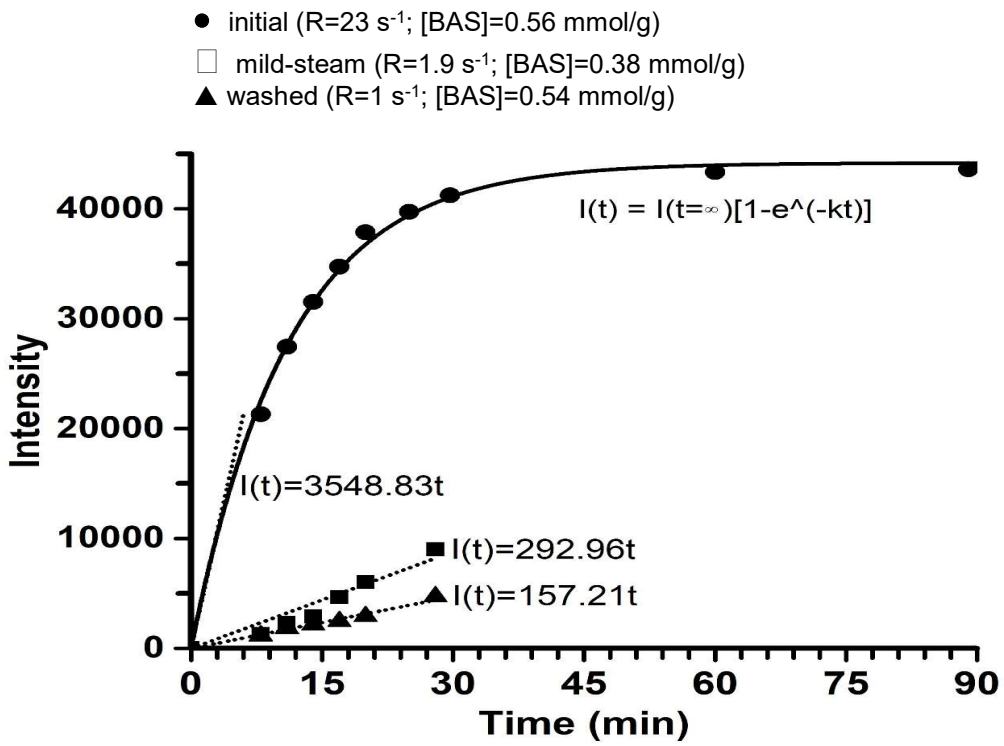

Fig. 4. 10. Representative rate plots for the total integrated areas of the benzene peak at 7.5 ppm in the 296 K in-situ NMR experiments, as a function of reaction time in the Si/Al=15 catalyst before and after AHFS washing and mild steaming. The dashed line is the regression fit.

Thus, the simplest explanation for the identity of at least half of the acidic proton species giving rise to the 5-7 ppm data, i.e., the 50% removed by mild AHFS treatment, is for protons associated with EFAl species or H-EFAl as denoted earlier. When removed, catalytic activity decreases significantly as shown in Fig. 4.10. If one assumes that the Al atoms to which the 5-7 ppm protons are associated reside in the framework, and are removed by the mild AHFS treatment while the known framework BAS species are not affected, then the more complex explanation requires invoking a model where ca. 20-30% fraction of framework Al atoms are much easier to extract by the mild AHFS washing than other framework sites. Given that the structure of HZSM-5 is well-known and there is no indication of weaker AlO_4 bonding sites in the lattice, we find the latter explanation unlikely.

4.4. Conclusion

Combining quantitative spin-counting MAS NMR methods with chemical extraction and mild-steaming techniques reveals that Brönsted acid function in HZSM-5 is complex, including contributions from framework BAS as well as protons associated with extra-framework aluminol species (H-EFAl). For high-acid density HZSM-5, only 50-60% of the aluminum atoms yield framework BAS's with the remaining contributing to the formation of reactive protons associated with EFAl. The distribution of active species can be changed by post-synthetic chemical extraction methods, with AHFS representing the only effective option for removing H-EFAl species while also preserving BAS's. Many other routinely used chemical extraction methods in the literature, including EDTA, HNO_3, HCl, and oxalic acid are much less effective. H-EFAl species that are removed by AHFS washing can be re-introduced using mild steaming, and their presence leads to catalysts with enhanced reactivity versus catalysts where H-EFAl species have been removed. This is true for both the Si/Al = 15 and Si/Al = 40 catalysts investigated here, but is likely general to ZSM-5. As such, recent ideas surrounding the importance of variable framework acid site location in HZSM-5 may have to be re-evaluated in the context of acidic contributions from H-EFAl species.

4.5. References

1. Janda, J.; Bell, A. T.; Effects of Si/Al Ratio on the Distribution of Framework Al and on the Rates of Alkane Monomolecular Cracking and Dehydrogenation in H-MFI, *J. Am. Chem. Soc.* **2013**, *135*, 19193−19207.

2. Schallmoser, S.; Ikuno, T.; Wagenhofer, M. F.; Kolvenbach, R.; Haller, G. L.; Sanchez-Sanchez, M.; Lercher, J. A., Impact of the Local Environment of Brönsted Acid Sites in HZSM-5 on the Catalytic Activity in n-Pentane Cracking, *J. Catal.* **2014**, *316*, 93-102.

3. Dedecek, J.; Sobalik, Z.; Wichterlova, B., Siting and Distribution of Framework Aluminum Atoms in Silicon-Rich Zeolites and Impact on Catalysis, *Cat. Rev. Sci. Eng.* **2012**, *54*, 135-223.

4. Sohn, J. R.; DeCanio, S. J.; Fritz, P. O.; Lunsford, J. H., Acid Catalysis by Dealuminated Zeolite Y: The Roles of Aluminum, *J. Phys. Chem.* **1986**, *90*, 4847-4851.

5. Fritz, P. O.; Lunsford, J. H., The Effect of Sodium Poisoning on Dealuminated Y-Type Zeolites, *J. Catal.* **1989**, *118*, 85-98.

6. Niwa, M.; Sota, S.; Katada, N., Strong Brönsted Acid Site in HZSM-5 Created by Mild Steaming, *Catalysis Today,* **2012**, *185*, 17-24.

7. Zhao, Z.; Xu, S.; Hu, M. Y.; Bao, X.; Peden, C. H. F.; Hu, J., Investigation of Aluminum Site Changes of Dehydrated Zeolite H-Beta during a Rehydration Process by Solid-State NMR, *J. Phys. Chem. C* **2015**, *119*, 1410-1417.

8. Chen, K.; Kelsey, J.; Zhang, L.; Resasco, D.; White, J. L. Water Interactions in Zeolite Catalysts and Their Hydrophobically-Modified Analogues, ACS Catalysis **2015**, *5*, 7480-7487.

9. Paolucci, C.; Khurana, I.; Parekh, A. A.; Li, S.; Shih, A. J.; Li, H.; Di lorio, J. R.; Albarracin-Caballero, J.; Yezerets, A.; Miller, J. T.; Delgass, W. N.; Ribeiro, F. H.; Schneider, W. F.; Gounder, R., Dynamic Multinuclear Sites Formed by Mobilizing Single Atoms: A New Concept in Heterogeneous Catalysis, *Science* **2017**, *357*, 898-903.

10. Yang, C-T.; Janda, A.; Bell, A. T.; Lin, L-C., Atomistic Investigations of the Effects of Si/Al Ratio and Al Distribution on the Adsorption Selectivity of n-Alkanes in Brönsted-Acid Zeolites, *J. Phys. Chem. C* **2018**, *122,* 9397-9410.

11. Knott, B. C.; Nimlos, C. T.; Robichaud, D. J.; Nimlos, M. R.; Kim, S.; Gounder, R., Consideration of the Aluminum Distribution in Zeolites in Theoretical and Experimental Catalysis, *ACS Catal.* **2018**, *8*, 770-784.

12. Song, C.; Chu, Y.; Wang, M.; Shi, H.; Zhao, L.; Guo, X.; Yang, W.; Shen, J.; Xue, N.; Peng, L.; Ding, W., Cooperativity of Adjacent Brönsted Acid Sites in MFI Channels Lead to Enhanced Polarization and Cracking of Alkanes, *J. Catal.* **2017**, *349*, 163-174.

13. Jones, A. J.; Carr, R. T.; Zones, S. I.; Iglesia, E., Acid Strength and Solvation in Catalysis by MFI zeolites and Effects of the Identity, Concentration and Location of Framework Heteroatoms, *J. Catal.* **2014,** *312*, 58-68.

14. Corma, A.; Fornes, V.; Rey, F., Extraction of Extra-Framework Aluminum in Ultrastable Y Zeolites, *Appl. Catal.* **1990**, *59*, 267-274.

15. Muller, M.; Harve, G.; Prins, R., Comparison of the Dealumination of Zeolites Beta, Mordenite, ZSM-5, and Ferrierite by Thermal Treatment, Leaching with Oxalic Acid, and Treatment with $SiCl_4$, *Micropor. Mesopor. Mater.* **2000**, *34,* 135-147.

16. Liu, C.; Li, G.; Hensen, E. J. M.; Pidko, E. A., Nature and Catalytic Role of Extraframework Aluminum in Faujasite Zeolite: A Theoretical Perspective, *ACS Catal.* **2015,** *5* (11), 7024-7033.

17. Fan, Y.; Bao, X.; Lin, X.; Shi, G.; Liu, H., Acidity Adjustment of HZSM-5 Zeolites by Dealumination and Realumination with Steaming and Citric Acid Treatments. *J. Phys. Chem. B* **2006,** *110* (31), 15411-15416.

18. Chen, K.; Abdolrhamani, M.; Sheets, E.; Freeman, J.; Ward, G.; White, J. L**.,** Direct Detection Of Multiple Acidic Sites in Zeolite HZSM-5**,** *J. Am. Chem. Soc.* **2017,** *139*, 18698-18704.

19. Woolery, G. L.; Kuehl, G. H.; Timken, H. C.; Chester, A. W.; Vartuli, J. C., On the nature of framework Brönsted and Lewis acid sites in ZSM-5. *Zeolites* **1997,** *19* (4), 288-296.

20. Wang, X.; Coleman, J.; Jia, X.; White, J. L., Quantitative Investigations of Transient Acidity in Zeolites and Molecular Sieves, *J. Phys. Chem. B.* **2002**, *106*, 4941-4946.

21. Gola, A.; Rebours, B.; Milazzo, E.; Lynch, J.; Benazzi, E.; Lacombe, S.; Delevoye, L.; Fernandez, C., Effect of Leaching Agent in the Dealumination of Stabilized Y Yeolites. *Microporous and Mesoporous Materials* **2000,** *40* (1), 73-83.

22. Apelian, M. R.; Fung, A. S.; Kennedy, G. J.; Degnan, T. F.; Dealumination of Zeolite β via Dicarboxylic Acid Treatment, *J. Phys. Chem.* **1996**, *100*, 16577-16583.

23. Ryder, J. A.; Chakraborty, A. K.; Bell, A. T., Density Functional Theory Study of Proton Mobility in Zeolites: Proton Migration and Hydrogen Exchange in ZSM-5, *J. Phys. Chem. B.* **2000**, *104*, 6998-7011.

24. Chen, K.; Gumidyala, A.; Abdolrhamani, M.; Villines, C.; Crossley, S.; White, J. L., Trace Water Amounts can Increase Benzene H/D Exchange Rates in an Acidic Zeolite. *J. Catal.***2017,** *351*, 130-135.

25. Jentoft, F. C.; Krohnert, J.; Subbotina, I. R., Kazansky, V. B. Quantitative Analysis of IR Intensities of Alkanes Adsorbed on Solid Acid Catalysts, *J. Phys. Chem. C* **2013**, *117*, 5873-5881.

26. Hunger, M., Multinuclear Solid-State NMR Studies of Acidic and Non-Acidic Hydroxyl Protons in Zeolites. *Sol. St. Nuc. Magn. Reson.* **1996,** *6* (1), 1-29.

27. Brunner, E.; Ernst, H.; Freude, D.; Hunger, M.; Krause, C. B.; Prager, D.; Reschetilowski, W.; Schwieger, W.; Bergk, K. H., Solid-State NMR and Catalytic Studies of Mildly Hydrothermally Dealuminated HZSM-5, *Zeolites* **1989**, *9*, 282-286.

28. Beck, L. W.; White, J. L.; Haw, J. F., 1H{27Al} Double-Resonance Experiments in Solids: An Unexpected Observation in the 1H MAS Spectrum of Zeolite HZSM-5. *J. Am. Chem. Soc.* **1994,** *116* (21), 9657-9661.

29. Huo, H.; Peng, L.; Grey, C. P., Low Temperature 1H MAS NMR Spectroscopy Studies of Proton Motion in Zeolite HZSM-5. *J. Phys. Chem. C* **2009,** *113* (19), 8211-8219.

30. Breck, D. W.; Blass, H.; Skeels, G. W., Silicon Substituted Zeolite Compositions and Processes for Preparing Same, *U. S. Pat.4503023*, **1985**.

31. Garralón, G.; Fornés, V.; Corma, A., Faujasites Dealuminated with Ammonium Hexafluorosilicate: Variables Affecting the Method of Preparation, *Zeolites* **1988,** *8* (4), 268-272.

32. White, J. L.; Beck, L. W.; Haw, J. F., Characterization of Hydrogen-Bonding in Zeolites by Proton Solid-State NMR Spectroscopy, *J. Am. Chem. Soc.* **1992,** *114*, 6182-6189.

33. van Eck, E. R. H.; Janssen, R.; Maas, W. E. J. R.; Veeman, W. S., A Novel Application of Nuclear Spin-Echo Double-Resonance to Aluminophosphates and Aluminosilicates, *Chem. Phys. Lett.* **1990**, 174, 428-432.

34. Grey, C. P.; Vega, A. J., Determination of the Quadrupole Coupling Constant of the Invisible Aluminum Spins in Zeolite HY with $^{1}H/^{27}A1$ TRAPDOR NMR, *J. Am. Chem. Soc.* **1995**, *117*, 8232-8242.

35. Kalwei, M.; Koller, H., Quantitative Comparison of REAPDOR and TRAPDOR Experiments by Numerical Simulations and Determination of H-Al Distances in Zeolites, *Sol. St. Nucl. Magn. Reson.* **2002**, *21*, 145-157.

36. Greiser, S.; Hunger, M.; Jäger, C., $^{29}Si\{^{27}Al\}$ TRAPDOR MAS NMR to Distinguish Q^n (mAl) Sites in Aluminosilicates: Faujasite-Type Zeolites, *Sol. St. Nucl. Magn. Reson.* **2016**, *79*, 6-10.

37. Luo, Q.; Yang, J.; Hu, W.; Zhang, M.; Yue, Y.; Ye, C.; Deng, F., Unambiguously Distinguishing Si[3Si,1Al] and Si[3Si,1OH] Stuctural Units in Zeolite by $^{1}H/^{29}Si/^{27}Al$ Triple Resonance Solid-State NMR Spectroscopy, *Solid State Nucl. Magn. Reson.* **2005**, *28*, 9-12.

38. ASTM D5758-01 Standard Test Method for Determination of Relative Crystallinity of Zeolite ZSM-5 by X-Ray Diffraction, **2015**.

CHAPTER V

SYNERGISTIC EFFECT OF WATER AND ACIDIC PROTONS ASSOCIATED WITH EXTRA-FRAMEWORK ALUMINOL SPECIES IN BENZENE H/D EXCHANGE REACTION

5.1. Introduction

HZSM-5 a family of MFI zeolite has an influence on number of industrially significant reactions such as the conversion of methanol to aromatic rich, gasoline-range hydrocarbons.[1-4] Recently, the quantitative ^{1}H MAS NMR spectroscopic detection showed that the distribution of reactive Brönsted acid site protons arising from framework and extraframework moieties can be complex.[5-9] Beside the traditional bridging acid sites (SiOHAl) associated with four coordinate framework aluminum, several forms of the EFAL species such as cationic species such as Al^{3+}, AlO^{+}, $Al(OH)_2^{+}$ and $AlOH^{2+}$, and neutral or polymeric species such as AlOOH, $Al(OH)_3$ and Al_2O_3 are acidic and reactive. It was suggested that the spatial proximity and interaction between the EFAl species and the bridging acid site can be responsible for the Brönsted -Lewis synergy for the enhancement of the catalytic activity of the HZSM-5 zeolite.[10] Alternatively, Iglesia et al. proposed that the activity enhancement is mainly associated with the smaller effective void size of the supercage in USHY zeolite due to the presence of EFAl rather than to changes in intrinsic strength of BAS.[11-12]

The EFAl species can be originated from dealumintion of framework aluminum with a hydrothermal or thermal treatments such as mild/ severe steaming methods.[13-16] During the steaming, Although, some authors reported that the EFAl species have a negative effect on activity

of the steamed zeolite samples, many others authors suggested that the EFAl species themselves contribute Brönsted acid sites that are as, or even more, reactive than framework bridging acid sites.[9,17-19]

Recently published reports including variations in synthesis, catalytic testing, computation, and spectroscopic investigations indicate that different Al sites in the catalyst framework exist, and that the details of Al siting, e.g. at channel intersections or in straight channels, can be critical to catalyst performance.[20-22]

New solid acid catalyzed upgrading of renewable feedstock in the liquid-phase demonstrates the catalytic diversity of zeolite structures. Water can be incorporated in the reaction system in the feed or evolved as a side product inside the solid acid catalyst during reaction. It has been recently discovered that the degree to which water positively or negatively influences reaction chemistries should be dependent on the relative water loading present near the solid acid site in a zeolite under reaction conditions.[23-25]

In this contribution, Brönsted proton siting in HZSM-5 catalysts two different Si/Al's (15, 40) are examined through a combination of post-synthetic chemical washing, steaming, and in-situ probe molecule reactivity, and direct spectroscopic inspection of the Brönsted proton active sites. Quantitative spin-counting NMR results on HZSM-5 catalysts with Si/Al ratios of 15 before and after washing with AHFS (ammonium hexafluorosilicate) and steaming at two different temperature 500ºC and 600ºC reveal that while proximate Brönsted sites within the framework do exist and increase with decreasing Si/Al as expected, Brönsted proton sites from non-crystalline and/or extra-framework species are required for maximum activity. In addition to including acidic EFAl species or protons from non-crystalline regions similar to amorphous silica-alumina, the term "defect" as used here also include possible acidic sites in the zeolite framework where three-coordinate Al atoms (or possibly penta-coordinate Al species) bonding with proximate silanols. In

this latter case, such sites experience large deviations from the normal tetrahedral framework geometry, and their Al signals are not observable in dry zeolite catalysts, but their associated Brönsted acid proton can be detected.

When acidic non-crystalline and/or EFAl hydroxyls are present along with framework BAS's, reaction rates for room-temperature H/D exchange between an aromatic probe molecule and the catalyst are maximum. While, the EFAl species are removed using known chemical washing methods, reaction rates decrease dramatically. Following their removal, the Brönsted protons from EFAl and non-crystalline species can be re-introduced to the catalyst by mild steaming as shown by direct NMR observation, with concomitant increase in reaction rates. Room-temperature reaction rate constants for benzene H/D exchange are a strong function of the concentration of defect Brönsted acid sites. In total, this contribution helps address several key questions in the current literature, including the role of paired active sites in high Al content HZSM-5 zeolite catalysts, types of defect Brönsted sites, contributions to acid-catalyzed chemistry from these defect acid sites, and synergistic contributions from water in the presence of defect acid sites.

5.2. Experimental sections

5.2.1. Catalyst preparation

Zeolite ZSM-5 (Si/Al = 15, CBV3024E) sample was obtained from Zeolyst in the $NH4^+$-exchanged form. Calcined zeolite samples were prepared in a glass reactor body using a gradual, stepwise vacuum calcination up to a final temperature of 500°C to yield acidic HZSM-5. For reference, in the HZSM-5 with Si/Al = 15, the expected framework BAS density based on total Al content is 1.04 mmol/g.[23] This sample is named by parent-HZSM-5. Three different samples were prepared by future post-synthetic treatments as described below:

Washed sample with AHFS treatments: As previously reported, 1 gr of $NH4^+$ZSM5 zeolite was mixed with deionized water at a concentration of 30 g/L to prepare the initial solution. Then, 5 mL

of 0.4 M AHFS solution (AHFS/Al molar ratio is 2:1) was added to the mixture at 90°C and stirred for 4 h. The mixture was then filtered, washed with warm deionized water three times, and dried overnight at 120°C. The final sample was followed by vacuum stepwise dehydration in the same way as the parent-HZSM-5 sample.[9,13]

Mild steamed sample: The washed sample was further treated by steaming with 21 Torr water vapor in nitrogen flow at 12 mL/min in a flow reactor, heated stepwise to a final temperature of 500°C, and held there for 72 h. After steaming, the samples were dehydrated using the flow reactor with nitrogen gas at 500°C for 5 h.[9]

Severe steamed sample: This procedure is same as the mild steaming method, but the washed sample was steamed at 600°C for 72 h. After steaming, the samples were dehydrated using the flow reactor with nitrogen gas at 500°C for 5 h.

5.2.2. Water and C_6D_6 adsorption method

A vacuum line equipped with a CAVERN type apparatus was used for quantitative adsorption, following previously published procedures.[23,26] First, the dehydrated zeolite samples were sealed inside the glovebox into the 4-mm zirconia MAS NMR rotor which was placed in the CAVERN. After evacuation in the vacuum line, the water vapor loading ranging from 0.05 to 0.3 eqv were introduced in the vacuum line to an initial pressure. A desired pressure drop is used to control the adsorption quantity after exposure to the catalyst. Each catalyst with water loading was sealed overnight to allow water diffusion and equilibration within the catalysts, and then characterized by ^{1}H MAS NMR to confirm the water loadings. After NMR characterization, they were opened inside the glove box to avoid exposure to any additional water, immediately inserted to the CAVERN body, sealed, and transferred to the vacuum line for subsequent C_6D_6 adsorption. To adsorb C_6D_6, same procedure was done on the zeolite samples with the different amount of water loading. For example, to adsorb C_6D_6 (%99.6 atom% deuterium, Aldrich) onto ZSM-5 with Si/Al = 15, 20 mg

of catalyst was loosely packed into the rotor in the CAVERN device. For example, 21 torr of initial pressure and 3.9 torr of pressure drop were used to determine when 1 eqv of benzene was adsorbed. The rotor was capped using the CAVERN device. Brönsted acid site densities are calculated from Si/Al ratios (e.g. acid density = 1.04 mmol/g for Si/Al = 15). For reference and to aid the reader, one equivalent of adsorbate corresponds to 6 molecules per unit cell for Si/Al = 15.

5.2.3. H/D exchange experiments

All samples loaded with different water loading and 1 eqv of C_6D_6 were characterized by ^{1}H MAS NMR to confirm H/D exchange reactions. The H/D exchanges took place immediately after adsorptions, while the adsorption processes usually took 3-5 minutes for completion. The initial H/D exchange spectra were typically acquired 6-8 minutes following the initial exposure. The following spectra were then taken with 6-7 min intervals to follow the reactions.

5.2.4. NMR measurements

^{1}H MAS NMR data for spin counting were collected on a Bruker AVANCE 400 spectrometer operating at 9.05 T and for tracking H/D exchange reactions were collected on Bruker DSX-300 MHz spectrometer, with spinning rate of 10 kHz with a 4 mm double-resonance MAS probe. Recycle delays were 10 s for dry zeolites. Rotors were spun with −54°C dew point dry air and periodically compared to dry N_2 spinning; no differences in spectra or relaxation times were observed. Spinning speeds of 10 or 15 kHz, 32 scans and 3.4−3.9 μs π/2 pulses were used for single-pulse acquisition spectra with samples packed in zirconia rotors and sealed with grooved Teflon spacers. Extremely dry HZSM-5 catalysts of the type used here can have T_{1H} values of up to 15 s for the terminal silanol SiOH species, but the T_{1H} values for all framework and extra-framework protons were always 10 s or slightly shorter. As such, spectra were acquired with a 50 s delay, as all quantitative analyses focused on acidic protons and not the inert silanol species.[25] The spin-counting or standard addition method to quantify the distribution of protonic species in HZSM-5 based on the addition of a known amount of inert polydimethylsiloxane (PDMS) follows the

procedure previously published.[9,27] All samples were loaded in the glovebox and typically included 20−30 mg of zeolite with 20−40 μg of PDMS in restricted volume MAS rotors.

^{27}Al MAS NMR data were acquired on a Bruker AVANCE 400 spectrometer on samples that were exposed to ambient moisture to eliminate lattice strain and enable detection of framework Al atoms. Large quadrupole coupling constants arising from lattice distortions and whose magnitude is on the order of several megahertz precludes Al observation in completely dehydrated catalysts. For this reason, ^{27}Al NMR is not a quantitatively reliable method for following how acid sites are impacted by postsynthetic treatments. Even though multiple-quantum NMR methods can help identify some "NMR-invisible" aluminum species, the quantitative distribution of acidic proton sites must be interrogated in completely dry catalysts as even ambient water levels can enable proton exchange on intermediate timescales causing signal loss. Trace water does exist as proton exchange on the slow-exchange timescale occurs,[25] albeit in amounts that do not impact the spectral lineshapes.[28] ^{1}H MAS NMR provides the best experimental route to this information, because Brönsted acid sites are themselves protons, not Al atoms.

Crystallinity and elemental analysis measurements. XRD was used to calculate the HZSM-5 crystallinity following some post-synthetic chemical treatments using a Philips PW 1830 diffractometer operating with a Cu Kα radiation (λ = 1.5418 Å) source. Data was gathered in the 5−70° 2θ range with step width and scanning speed set to 0.02° and 0.5 sec/step, respectively. Al and Si contents were determined via standard ICP-AES methods from Galbraith Laboratories.

5.3. Results and discussion

The key benefit in using ^{1}H solid-state NMR to interrogate protonic species in zeolites is that it provides a direct, quantitative signal from all species including Brönsted acid site protons.[20-31] ^{1}H solid-state NMR does not suffer from the limitations of ambiguous extinction coefficient and

scattering effects associated with infrared spectroscopy of powders, and has been recently discussed in the literature as a way to calibrate the latter.[32] Fig. 5.1 shows high-resolution ^{1}H MAS NMR spectra for HZSM-5 catalysts in their dry, protonic form, i.e., in the absence of atmospheric exposure. Peaks are labeled according to previously reported assignments,[9,25] with 5.1a-d and 5.1e corresponding to Si/Al=15 and 40, respectively. The two largest peaks in each of the spectra, excluding the spectrum in 1d, correspond to the well-known crystalline BAS's (4.2 ppm) in the framework and the silanol hydroxyl groups (1.8-2 ppm) at crystallite termini. In comparing the bottom spectrum in 5.1a, corresponding to as-prepared Si/Al = 15, to the spectrum in 5.1e for the similar Si/Al=40, the relative intensity of these two peaks are reversed due to the much lower BAS density in the latter, as expected. The main purpose in showing the data in Fig. 5.1, however, is to demonstrate the populations of additional protonic species whose identity and function are less well understood, indicated by the relatively narrow peak at 2.8 ppm, and the broad peaks from ca. 5-7 ppm and 12-15 ppm. These peaks can be easily deconvoluted from the rest of the spectrum, as shown by the dashed lines in Fig. 5.1a. For clarity, they are not shown in 5.1b -5.1e. Previously, the 2.6 and recently-discovered 12-15 ppm peaks were assigned to hydroxyl groups from EFAl species (H-EFAl), as they are easily removed by chemical washing.[15] The broad shoulder slightly downfield of the BAS peak, visible from 5-7 ppm, has been recently assigned as arising from a combination of EFAl hydroxyl species and framework acid sites with uniquely distorted or coupled bonding environments,[9,25] the latter of which was originally proposed in 1994.[33] Previously, the 5-7 ppm region was also assigned to framework BAS's that were hydrogen bonded.[30] The assignment of the protons giving rise to the intensity in the 5-7 ppm region, which is a significant fraction of the total proton intensity, continues to be debated in the literature, with some relatively recent reports claiming it as residual water.[34] Recent quantitative spin-counting analysis of several HZSM-5 catalysts eliminated the possibility that this peak arises from residual water.[9] Figure 5.1a shows that the deconvoluted 5-7 ppm peak requires at least two components to accurately fit, which will be discussed in more detail later in the contribution. With the exception of the SiOH terminal

silanol species represented by the 1.8-2 ppm peak in Figure 5.1, all other species have been recently shown to act as Brönsted acid sites in room-temperature H/D exchange reactions with a hydrocarbon reagent.[25]

Note that the distribution of species is very different in 5.1a and 5.1e for the as-synthesized Si/Al = 15 and Si/Al = 40 catalysts, respectively. In addition, within the series of spectra for the former, the relative contribution of each of the species varies dramatically with sample history. To be clear, there are at least five different types of protons as indicated by the five different peaks in 5.1a-d. In going from 5.1a to 5.1b, the as-received commercial catalyst following slow, stepwise vacuum dehydration (5.1a) was washed using ammonium hexafluorosilicate (AHFS) (5.1b), yielding a spectrum devoid of the H-EFAl groups and thus no 2.8 and 12-15 ppm peaks. However, Fig. 5.1c shows that these species can be reintroduced following the mild steaming procedure defined in the Experimental section, since both the 2.8 and 12-15 peaks reappear, while still preserving most of the BAS's as indicated by the 4.2 ppm signal. Similar behavior is seen for the Si/Al = 40 catalyst in 5.1e, which does not have any detectable H-EFAl species in the initial catalyst. Following mild steaming, however, small contributions from the species giving rise to the 2.8 and 12-15 ppm peaks can be observed in the red overlay spectrum in 5.1e, with concomitant decrease in the BAS signal intensity. Finally, Fig. 5.1d shows that severe steaming eliminates almost all BAS's, and in addition to the previously discussed H-EFAl species, generates additional non-crystalline protons indicated by the 1-ppm signal that is not observed in other catalysts

The result in 5.1e indicates that even in relatively low Al content HZSM-5 which have nothing other than crystalline BAS's in the as-synthesized form, the H-EFAl species can be introduced by appropriate treatment. While the amounts of the 12-15 and 2.8 ppm peaks shown in the red spectrum of 5.1e appear very small, their impact is significant.

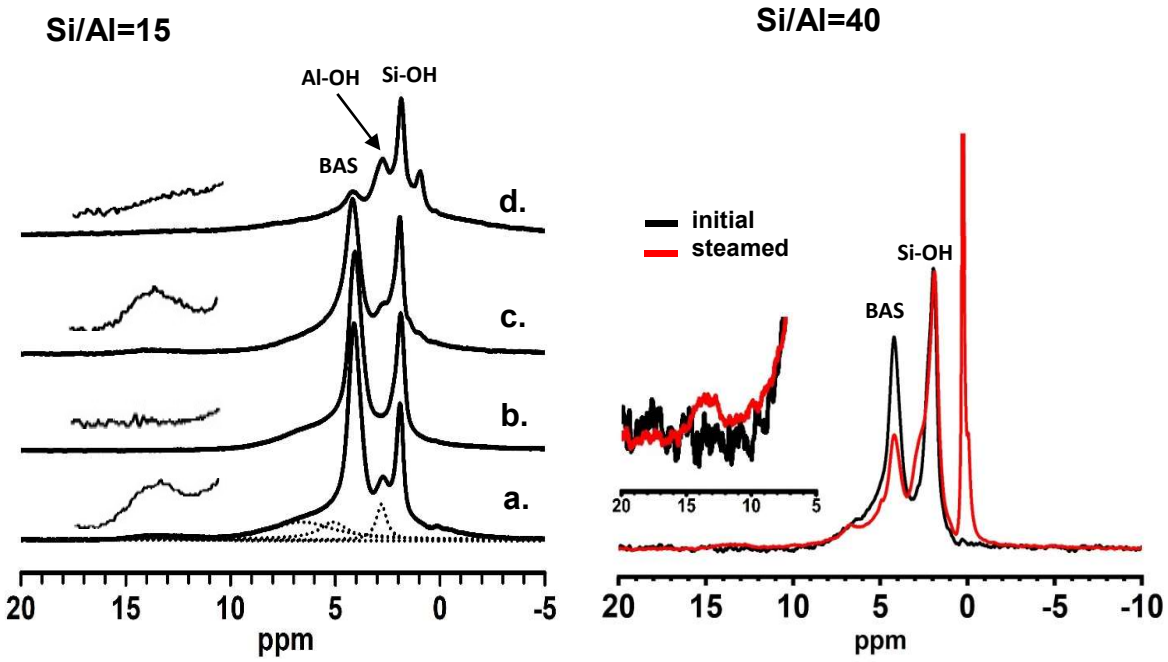

Fig. 5. 1. [1]H MAS NMR spectra of (a) as-prepared HZSM-5 with Si/Al = 15 following step-wise vacuum dehydration; (b) same as (a) treated with AHFS:Al = 2; (c) same as (b) following a mild steaming procedure; (d) same as (b) following the severe-steaming procedure; (e) Si/Al = 40, with the as-prepared catalyst shown in black and the mild-steamed catalyst shown in red along with the PDMS intensity standard. The insets show signal originating from elimination and creation of acidic H-EFAl species (12−15 ppm region).

The amounts of all species can be quantified using the spin-counting standard-addition method, in which a known amount of an inert PDMS (polydimethylsiloxane) in the solid state is added to the rotor with the catalyst, as shown by the presence of the intense peak at 0 ppm in the all samples. Using this method, the BAS concentration in the steamed Si/Al = 15 catalyst in Fig. 5.2c and 5.2d decreases by a factor compared to the washed catalyst, and the extra-framework species at 2.7ppm, 5-7 ppm, and 13 ppm increase. Given that the details of the spin-counting method have been previously published,[9] the raw spin-counting solid-state NMR data for each of the other samples

shown in Fig. 5.2 (1a-d), yielding quantitative population distributions for each proton type (*vide infra*).

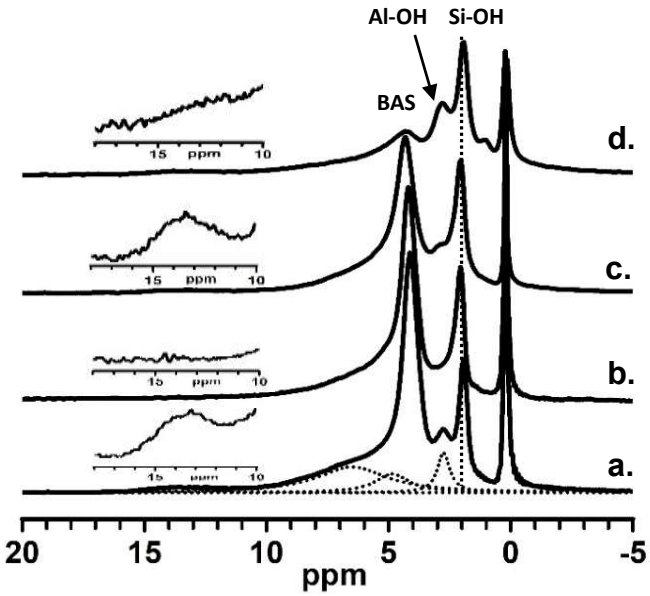

Fig. 5. 2. ^{1}H MAS spin-counting NMR spectra of (a) HZSM-5 with Si/Al = 15; (b) same as (a) treated with AHFS/Al = 2; (c) same as (b) following the mild steaming procedure; (d) same as (b) following the severe steaming. All peaks are normalized based on silanol peak at 1.9 ppm.

For convenience, the accompanying ^{27}Al MAS NMR spectra are also shown in Fig. 5.3 for the same samples in their hydrated forms, i.e., exposed to ambient moisture. The spectra of all samples shows the signals at 0, 54, and a broad shoulder at 30 ppm assigned to Al atom located in extra-framework (VI), framework (IV), and distorted framework tetrahedral coordinated aluminum species respectively, as shown in Fig. 5.3. By increasing the steaming temperature from 500^{o}C to 600^{o}C, the line width of signal of the Al (IV) became broad and 30ppm lines appear in the spectrum. Silaghi et al. suggested that penta-hedral or distorted tetrahedral Al atoms created in the intermediate steps for the formation of EFAL. These Al species are supposed to be at the initiation of aluminum dislodgement to extra-framework positions.

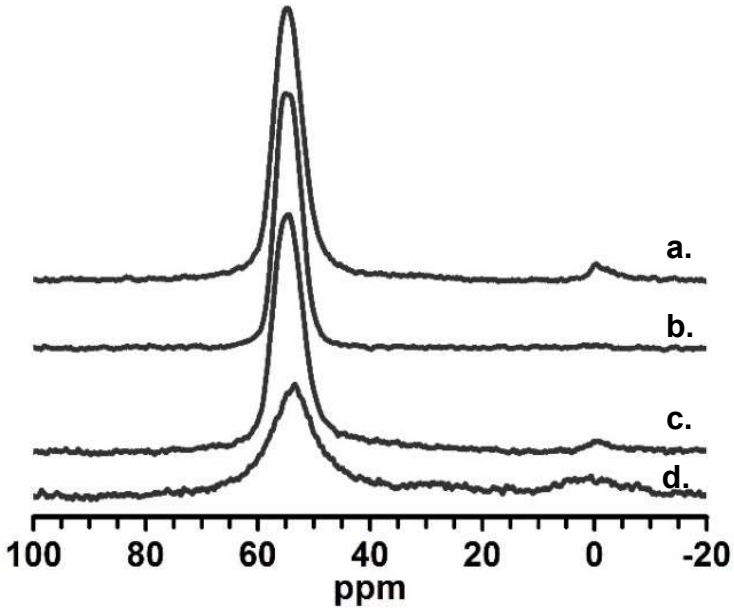

Fig. 5. 3. ^{27}Al MAS NMR spectra of (a) HZSM-5 with Si/Al = 15; (b) same as (a) treated with AHFS/Al = 2; (c) same as (b) following the mild steaming procedure; (d) same as (b) following the severe steaming. All peaks are normalized based on silanol peak at 1.9 ppm.

XRD patterns of four different catalysts are presented in Fig. 5.4 that show the crystalline structure of washed sample is preserved but for the steamed samples, the crystallinity is reduced by increasing the steaming temperature. The large reduction in crystallinity for the sever steamed catalyst can be observed.

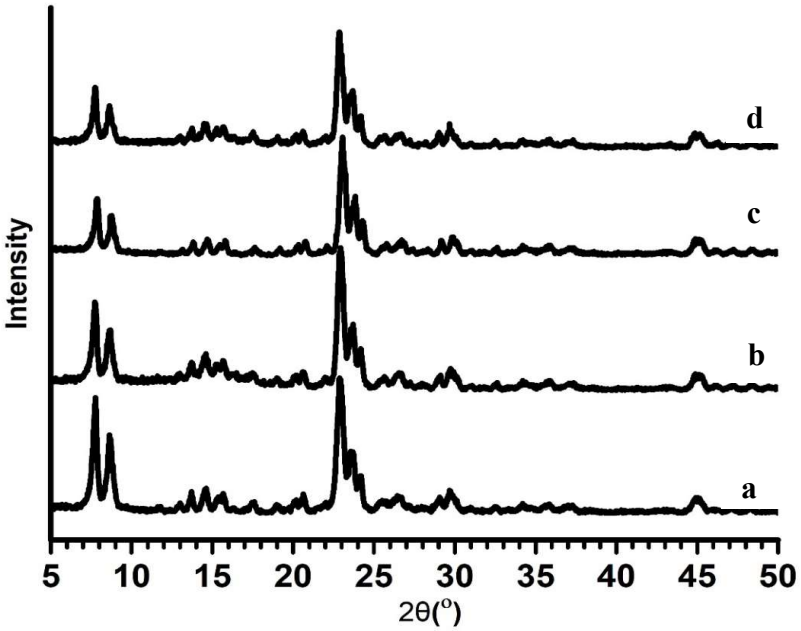

Fig. 5. 4**.** X-ray powder diffraction of (a) HZSM-5 with Si/Al = 15; (b) same as (a) treated with AHFS/Al = 2; (c) same as (b) following the mild steaming procedure; (d) same as (b) following the severe steaming.

Relative crystallinity is calculated for all samples using the standard ASTM method for powder diffraction on ZSM-5.[35] Relative crystallinity and elemental analysis for the HZSM-5, washed HZSM-5, mild-steamed HZSM-5, and severe-steamed HZSM-5 are shown in Table 5.1. These data show the large reduction in crystallinity for the severe-steamed catalysts. Also, elemental analysis for aluminum concentration is in good agreement with quantitative ^{1}H MAS NMR spin-counting shown in Table 5.2.

Table 5. 1. Powder x-ray crystallinity and elemental analysis data for all catalysts.

Catalyst	Relative Crystallinity (%) normalized to as-received	%Al*
As-received	100	0.90
AHFS-washed	99.0	0.57
Mild-steam	94.2	0.57
Severe-steam	88.7	---

*Elemental analysis provided by Galbraith Laboratories.

From quantitative spin-counting experiments, concentrations of each protonic component for the four Si/Al = 15 catalysts were calculated and are listed in Table 5.2 below. The total concentration of all non-SiOH (i.e., excluding silanol groups) protonic species in the initial HZSM-5 catalyst is 1.1 mmol/g, very near the expected value of 1.04 mmol/g based on total Al content. As expected, this total decreases with subsequent treatments, due to the combined effects of extraction of H-EFAl species with AHFS and condensation/dihydroxylation associated with the steaming steps. The very small increase in SiOH (first column) with subsequent steps is trivial compared to the loss of all other species, and in particular to the almost order of magnitude decrease in the BAS concentration. As shown in Table 5.2, by varying the steaming temperature on the washed sample with AHFS, two samples with different concentration of multiple Brönsted OH species are produced. Further increase in the temperature changes the composition of protonic species. In contrast to the washed sample with the lowest ratio of BAS-EFAl to BAS-FAl, the severe steamed sample has the highest ratio. This sample is a good candidate to investigate the reactivity of BAS arising from EFAl in the hydrocarbon reactions in presence of different loading of water. As seen in Table 5.2, the concentration of EFAl aluminol species increases and BAS

species at 4.2 ppm decreases as the steaming temperature increases. This reveals that more aluminum transfers from framework to the extra-framework.

Table 5. 2.Distribution of species, in units of **mmol/g**, obtained from quantitative ^{1}H MAS NMR spin-counting spectra of the HZSM-5 Si/Al = 15 catalysts shown in Figure 5.1.

Catalyst	SiOH 1.9 ppm	H-EFAl 2.8ppm	H-EFAl/non-xtal/defect 5-7ppm	H-EFAl 12-15ppm	H-EFAl 1 ppm	sum of all species except SiOH	BAS 4.2 ppm	Sum of H^+ defect species
Initial	0.18 ±0.01	0.09 ±0.01	0.45±0.037	0.059 ±0.0.025	0	1.1*	0.56±0.018	0.59
AHFS-washed	0.20 ±0.01	0.030 ±0.003	0.28±0.019	0	0	0.84	0.54±0.020	0.31
mild-steamed	0.20	0.080	0.32	0.021	0	0.80	0.38	0.42
severe-steamed	0.21	0.17	0.25	0.018	0.029	0.53	0.064	0.46

Water present in either vapor or liquid phases can dramatically impact zeolite chemistries, ranging from unexpected increases in reactivity to deleterious impacts on framework stability.[23-24] Fig. 5.5 shows the results from the control experiments in which water is adsorbed on different samples with different amount of H-FAl and H-EFAl species. In all samples, a strong interaction between water and framework and extra-framework protons are observed. As water loading increases, the narrow acid site peaks merge to the downfield region and broadens due to water diffusion and the dynamic exchange between water protons and heterogeneous acid site protons. However, the water peak continuously shifts downfield with further exposure. In the parent HZSM-5 sample, the water peak is getting broader than other samples, because of the exchange between more acid sites and water peak. Based on the results from spin-counting, the parent sample has the highest amount of protonic species coming from the extra-framework and framework moieties in the range of 4-7 ppm, so the effect of proximate water and protonic species moves the chemical shift to more

downfield to 7 ppm at higher water loadings. At dry conditions, shown by the bottom spectra of Fig. 5.5a and 5.4d for the parent and severe steamed HZSM-5 samples respectively, the parent shows a more apparent trend of the downfield shift of the water peak. In the severe steamed sample, the chemical shift is toward up field where the chemical shift of original water peak is 4.8 ppm. For the washed sample, Fig. 5.5b, the acidic Brönsted sites arising from EFAl aluminol species are less than other samples, so by increasing water loading, the chemical shift to the downfield is smaller than the parent sample. For 0.2 eqv H_2O, the chemical shift for parent and washed samples are 6.50 and 6.30 ppm, respectively. It can be concluded that a strong interaction/reaction between H_2O and the Brönsted acidic sites arising from FAl and EFAl species is observed even at very small amount of added water, 0.05 eqv Also, the narrow and intense acid site peak detected in the dry catalysts broadens and shifts due to water diffusion and the dynamic exchange between protons of water and the acidic sites.

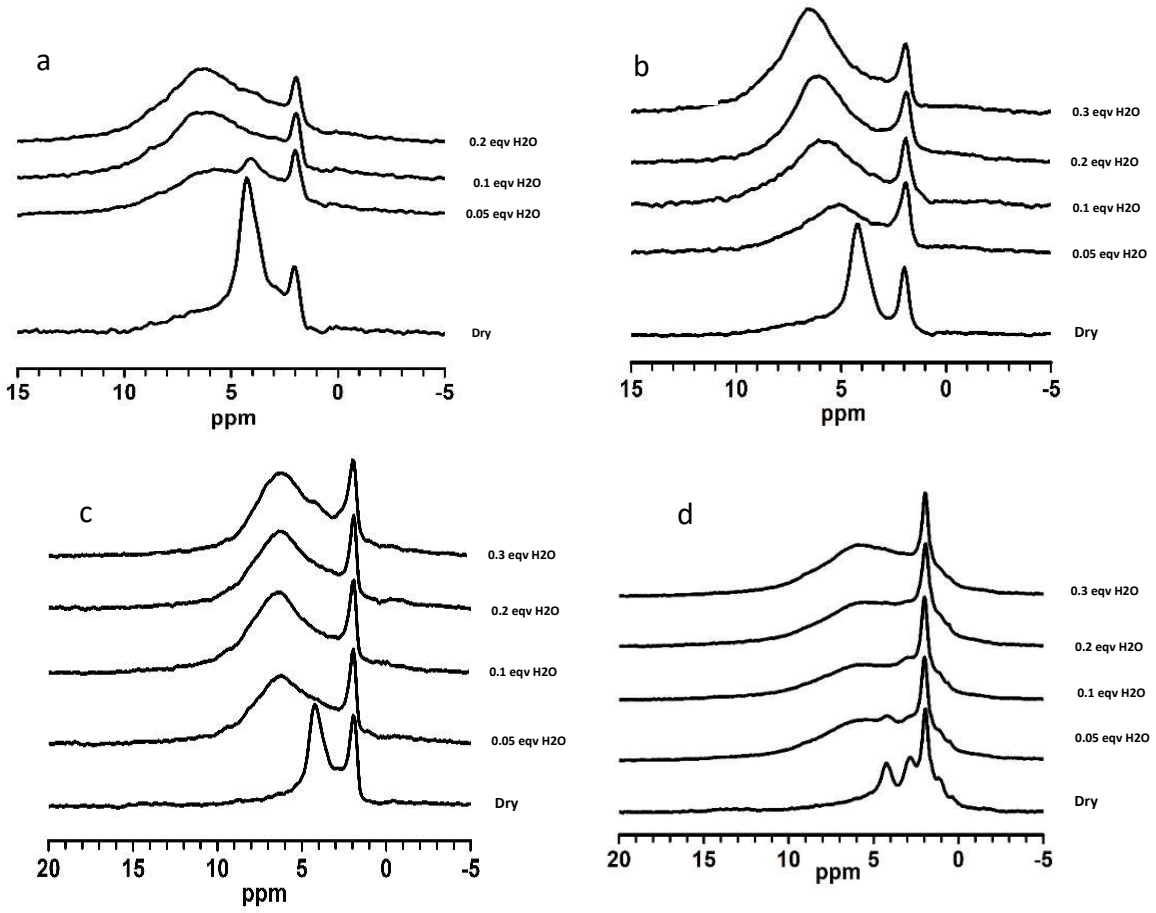

Fig. 5. 5. ^{1}H MAS NMR at 296 K of solid HZSM-5 (Si/Al = 15) catalysts as a function of controlled water loading, as noted, in number of equivalents relative to the acid site concentration for (a) HZSM-5 with Si/al=15, (b)treated with AHFS/Al=2, (c)mild steamed samples, and (d) severe steamed samples.

For all samples, as water loading increases up to 0.3 eqv, the exchange-averaged chemical shifts move downfield to 7 ppm, representing that the proximity of water molecule to Brönsted acid sites causes partially positive character in comparing to the dry samples. The exchange-averaged chemical shifts for each samples with different water loading is listed in Table 5.3.

Table 5. 3. Chemical shift of adsorbing different loading of water

Samples	Dry	0.05 eqv	0.1 eqv	0.2 eqv	0.3 eqv
Parent-HZSM-5-15	4.23	5.80	6.30	6.50	-
Washed-HZSM-5-15	4.20	6.11	6.03	6.30	6.54
Mild steamed-HZSM-5-15	4.23	6.20	6.32	6.43	6.50
Severe steamed-HZSM-5-15	4.21	5.80	5.89	6.01	6.10

For further explore the connection between the distribution of acidic protons in different samples, benzene-d_{10} was used as a reactivity probe molecule. The control experiments acquired at room temperature as a function of the adsorption of 1 eqv of benzene-d_6 (C_6D_6) in the course of reaction time on four samples in the dry condition are shown in Fig. 5.6. For all samples, after the adsorption of C_6d_6, the bridging acid site shifted to downfield and broadened, where the acid site resonance shifted from 4.2 ppm to 5 ppm. This broadening can be related to the of H-pi bonding between acid protons and benzene rings. The area from benzene peak centered at 7.5 ppm peak increases as proton/deuterium exchange happens, with a consequent decrease of total protonic species arising from FAl and EFAl.

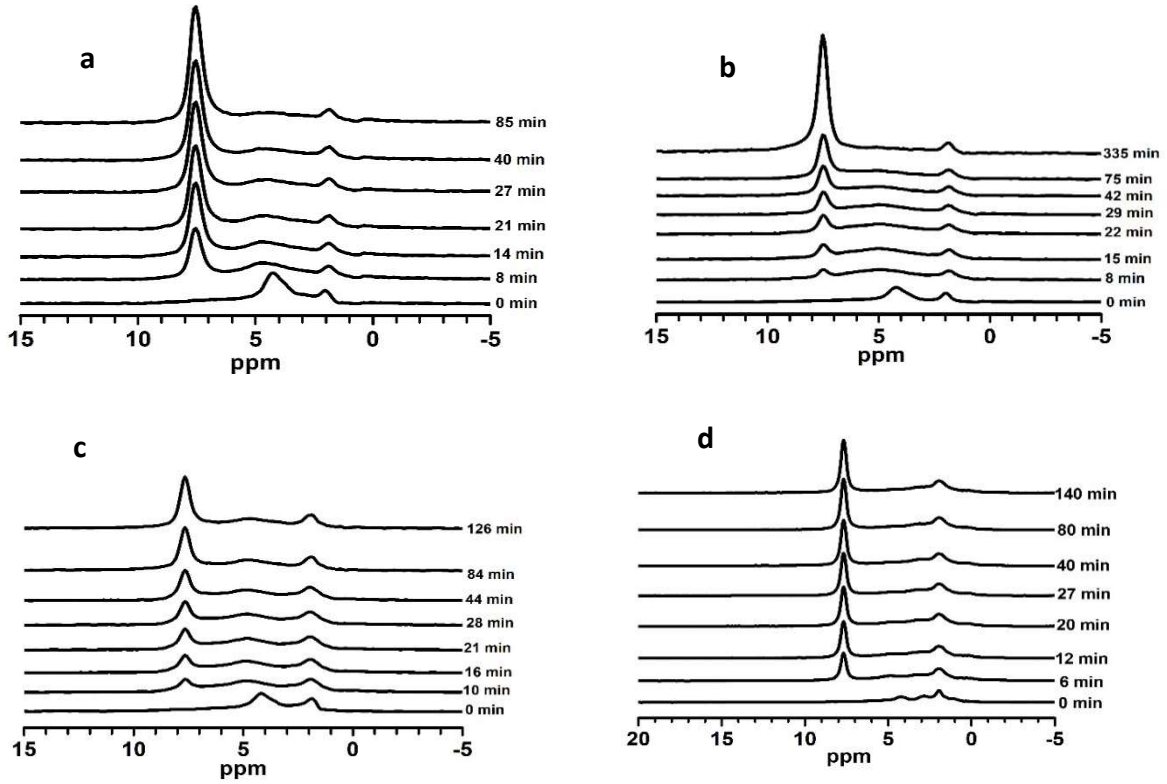

Fig. 5. 6**.** Representative in-situ ^{1}H magic-angle spinning (MAS) NMR spectra at 296 K as a function of time following adsorption of 1-eqv benzene-d_6 on dry (a) HZSM-5 with Si/Al = 15; (b) same as (a) treated with AHFS/Al = 2; (c) same as (b) following the mild steaming procedure; (d) same as (b) following the severe steaming. All peaks are normalized based on silanol peak at 1.9 ppm.

Fig. 5.7 represents the NMR spectra as a function of time following adsorption of 1-eqv benzene-d_6 in the presence of co-adsorbed water (0.1 eqv H_2O). It is concluded from Fig. 5.6 and Fig. 5.7 that the ratio of the benzene peak to the silanol peak centered at 2.0 ppm is much larger in the parent HZSM-5 than other samples. Although the concentration of bridging acid site arising from FAl in the severe steamed sample is the smallest, its H/D exchange rate for the benzene is very high. It is resulted that H-EFAl species are very reactive and involved in the exchange reactions. For the washed sample with the smallest concentration of H-EFAl species, the reaction rate constant for the growth of benzene peak is very slow and at least one order of magnitude smaller than the parent

sample in the dry condition. In the mild steamed sample, H-EFAl species can be partially recreated as indicated by the re-appearance of the 12−15 ppm signal, signals in the broad 5−7 ppm region, and the 2.7 ppm peak and H-FAl species are decreased in comparison with the washed sample.

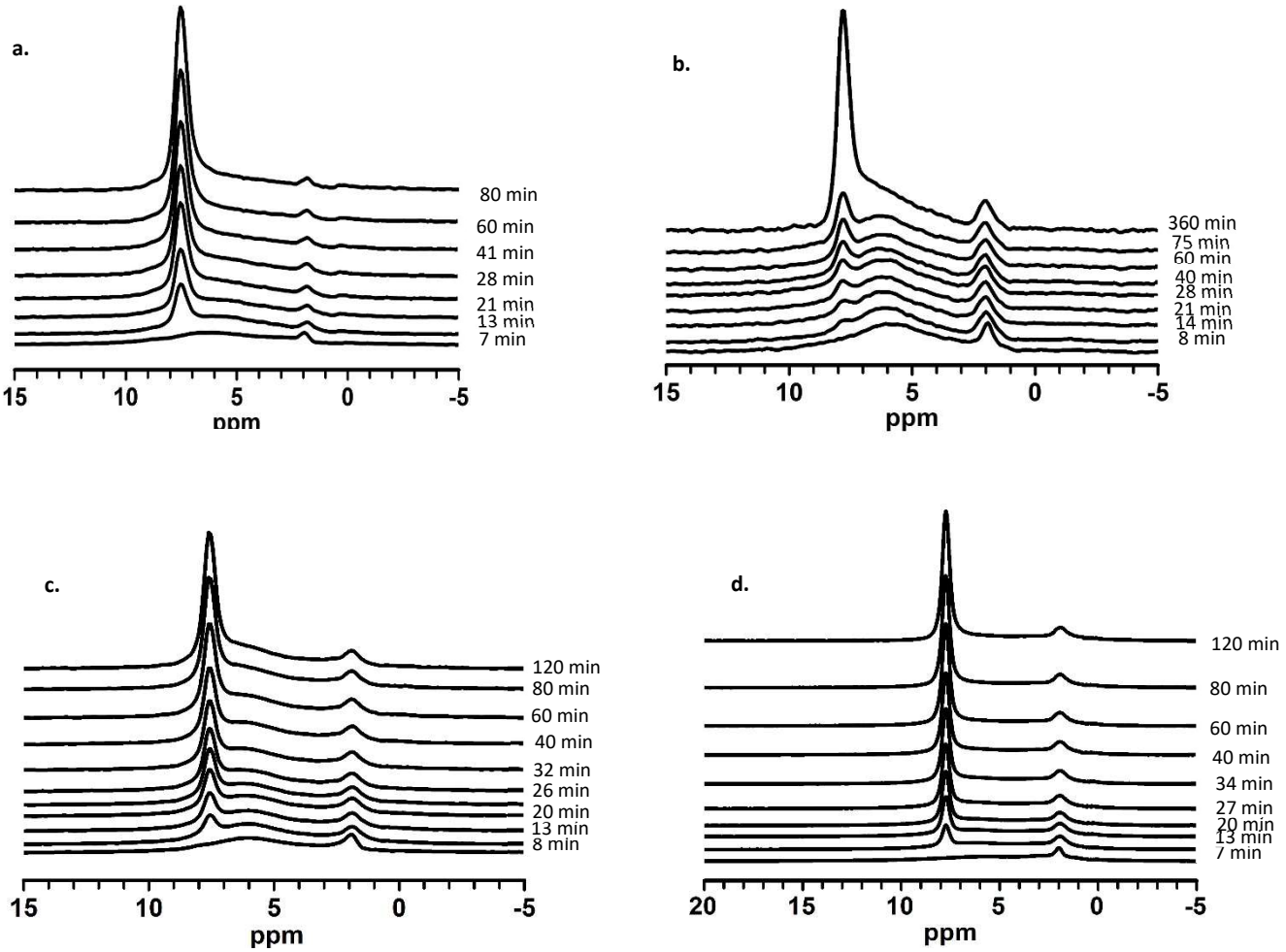

Fig. 5. 7. Representative in-situ ^{1}H magic-angle spinning (MAS) NMR spectra at 296 K as a function of time following co-adsorption of 1-eqv benzene-d_6 and 0.1 eqv H_2O on (a) HZSM-5 with Si/Al = 15; (b) same as (a) treated with AHFS/Al = 2; (c) same as (b) following the mild steaming procedure; (d) same as (b) following the severe steaming. All peaks are normalized based on silanol peak at 1.9 ppm.

H-FAl and H-EFAl species in the absence and presence of different water loadings are calculated and summarized in Table 5.2. Also, rate constant for different water loadings on each sample

acquired at 296 K are presented in Table 5.4. Results from Table 5.4 represents that the rate of hydrogen/deuterium exchange between benzene and four different treated HZSM-5 samples is significantly larger in all cases, except the washed sample, where 0.1 eqv water is adsorbed. For the washed sample, adding a small amount of water is slightly increasing the rate of reaction at 0.05 eqv and reducing at any amount of loading higher than 0.05 eqv. Two conclusions come from the data in Table 5.4: First, the rate of reaction for the samples with more Brönsted acid sites associated with EFAl/non-crystalline species is fast. It means that the species that are removed from HZSM-5 via AHFS washing and recreated by steaming procedures contribute significantly to the catalyst activity. Second, adding 0.1 eqv of water can increase the rate of reaction for the samples having H-EFAl species. It proves the synergistic effect of water molecule and H-EFAl/non-crystalline species.

Table 5. 4. Rate constant versus water loading for the reaction obtained from the full kinetic rate plots on each sample for data acquired at 296 K. Individual numbers were calculated by time-dependent analysis of peak integrals of rising benzene 1H signal following isotopic exchange with the acid sites.

Samples		Rate of reaction constant ($10^{-4} \times s^{-1}$)
Parent-HZSM-5-15	dry	19.88
	0.05 eqv. H_2O	22.33
	0.1 eqv. H_2O	28.00
	0.2 eqv. H_2O	11.87
Washed-HZSM-5-15	dry	2.17
	0.05 eqv. H_2O	2.73
	0.1 eqv. H_2O	0.58
	0.2 eqv. H_2O	0.55
	0.3 eqv. H_2O	0.17

Mild steamed -HZSM-5-15	dry	3.00
	0.05 eqv. H_2O	3.20
	0.1 eqv. H_2O	4.97
	0.2 eqv. H_2O	3.73
	0.3 eqv. H_2O	2.50
Severe steamed-HZSM-5-15	dry	12.60
	0.05 eqv. H_2O	18.67
	0.1 eqv. H_2O	21.13
	0.2 eqv. H_2O	13.00
	0.3 eqv. H_2O	8.78

Fig. 5.8 indicates that the reaction rate constant for the benzene H/D exchange probe reaction decreases by an order of magnitude for the washed sample following removal of the H-EFAl species, due to an integrated effect arising from Lewis-Brönsted and Brönsted - Brönsted synergy effects. It has been reported that the turnover rate and selectivity in propane oligomerization depend on the site proximity in the MFI zeolite. One could argue that the increase in amount of H-EFAl/non-crystalline species that coincided with increased benzene reactivity could be explained by a simultaneous Lewis- Brönsted synergy arising from EFAl species and framework BAS's. Given its large proton affinity, it is not reasonable that initiation step for benzene H/D would include hydride abstraction. This is supported by recently published mechanism for benzene activation via protonation, in which it was shown that benzene/catalyst H/D exchange reactions are good probe molecules for zeolite catalyst acidity[36]. These data support that the defect Brönsted sites including H-EFAl species themselves play an important role as Brönsted acid sites. It can be concluded that both BAS's and acidic protons from EFAl and non-crystalline sites, i.e., defect sites, must be present for maximum reactivity, suggesting that a BAS/defect site Brönsted -Brönsted acid

site synergy is important. The reactivity of the signal at 0.9 ppm is shown here for the first time. These species, created at severe steaming condition, are very reactive active sites and involve in the H/D exchange reactions. Therefore, the turnover rate for the severe steamed sample with the highest ratio of defect sites to BAS's species is larger than the other samples.

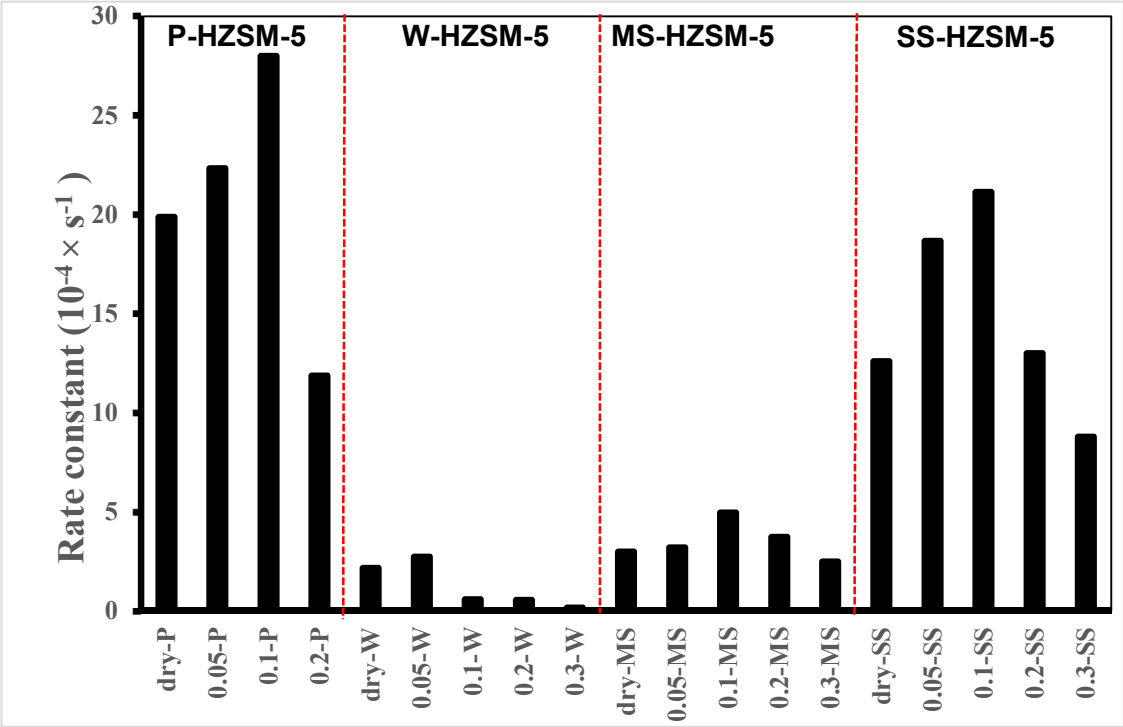

Fig. 5. 8. Rate constant versus water loading for the reaction obtained from the full kinetic rate plots on each sample for data acquired at 296 K; P, W, MS, and SS represent parent HZSM-5-15, washed HZSM-5-15, mild steamed and severe steamed HZSM-5-15 samples.

First order dependence of the reaction rate of H/D exchange between benzene and heterogonous acid sites is related to the concentration of the defect Brönsted sites including H-EFAl arising from the steaming. If we consider the Brönsted acid sites from framework aluminum the only species involved in the reaction, their reaction rate is not the first order. Therefore, the defect Brönsted species concentration can be dominant in the reaction rate calculation for the first order assumption.

It ca be concluded that water shows positive effect in enhancing the reaction rate only for catalysts have both BAS and defect site species.

5.4. Conclusions

Combined spectroscopic, reactivity, and post-synthetic treatments indicated that paired-Brönsted acid sites in the framework contribute less to overall catalyst activity in room-temperature probe reactions than do proximate framework and defect Brönsted sites. Reaction rates for several experiments involving HZSM-5, Si/Al = 15 catalysts indicated that the rate does not correlate well with framework BAS concentration, but depends more on the concentration of Brönsted acid sites arising from defect sites. Brönsted-Brönsted synergies do not preclude Brönsted-Lewis synergies arising from EFAl species, but the fact that protons from EFAl species are also active means that the overall catalyst acidity is more complex than a BAS activated by a proximate non-framework Al atom and that mechanistic proposals must be understood in the context of Brönsted acid site distributions. Also, proximate framework and defect Brönsted sites play a significant role in water synergies. Our data proves that adding substoichiometric amounts of water can enhance the H/D echange reaction rates in zeolite HZSM-5, suggesting that only H-EFAL active sites respond to water addition. For the washed sample with single type of acid site, adding water suppress the rate of reaction.

5.5. References

1. Anderson, J. R.; Mole, T.; Christov, V., Mechanism of some conversions over ZSM-5 catalyst. *Journal of Catalysis* 1980, *61* (2), 477-484.

2. Corma, A. Inorganic Solid Acids and Their Use in Acid-Catalyzed Hydrocarbon Reactions. *Chem. Rev.* **1995**, *95*, 559-614.

3. Thomas, J. M.; Thomas, W. J. *Principles and Practice of Heterogeneous Catalysis* **2005**, VCH Publishing, Weinheim, Germany.

4. Derouane, E. G.; Védrine, J. C.; Pinto, R. R.; Borges, P. M.; Costa, L.; Lemos, M. A. N. D. A.; Lemos, F.; Ribeiro, F. R. The Acidity of Zeolites: Concepts, Measurements, and Relations to Catalysis. *Catal. Rev.* **2013**, *55*, 454-515.

5. Cheng, Y.-T.; Jae, J.; Shi, J.; Fan, W.; Huber, G. W. Production of Renewable Aromatic Compounds by Catalytic Fast Pyrolysis of Lignocellulosic Biomass with Bifunctional Ga/ZSM-5 Catalysts. *Angew. Chem. Int. Ed. Eng.* **2012**, *51*, 1387-1390.

6. Ennaert, T.; Van Aelst, J.; Dijkmans, J.; De Clercq, R.; Schutyser, W.; Dusselier, M.; Verboekend, D.; Sels, B. F. Potential and Challenges of Zeolite Chemistry in the Catalytic Conversion of Biomass. *Chem. Soc. Rev.* **2016**, *45*, 584-611.

7. Zapata, P. A.; Faria, J.; Ruiz, M. P.; Jentoft, R. E.; Resasco, D. E. Hydrophobic Zeolites for Biofuel Upgrading Reactions at the Liquid-Liquid Interface in Water/Oil Emulsions. *J. Am. Chem. Soc.* **2012**, *134*, 8570-8578.

8. Pagan-Torres, Y.; Wang, T.; Gallo, J. M. R.; Shanks, B. H.; Dumesic, J. A. Production of 5-Hydroxymethyfurfural from Glucose Using a Combination of Lewis and Brönsted Acid Catalysts in Water in a Biphasic Reactor. *ACS Catal.* **2012**, *2*, 930-934.

9. Abdolrahmani, M.; Chen, K.; White, J. L., Assessment, Control, and Impact of Brönsted Acid Site Heterogeneity in Zeolite HZSM-5. *The Journal of Physical Chemistry C* 2018, *122* (27), 15520-15528.

10. Pidko, E. A.; Almutairi, S. M. T.; Mezari, B.; Magusin, P. C. M. M.; Hensen, E. J. M., Chemical Vapor Deposition of Trimethylaluminum on Dealuminated Faujasite Zeolite. *ACS Catalysis* 2013, *3* (7), 1504-1517.

11. Gounder, R.; Jones, A. J.; Carr, R. T.; Iglesia, E., Solvation and acid strength effects on catalysis by faujasite zeolites. *Journal of Catalysis* 2012, *286*, 214-223.

12. Jones, A. J.; Carr, R. T.; Zones, S. I.; Iglesia, E., Acid strength and solvation in catalysis by MFI zeolites and effects of the identity, concentration and location of framework heteroatoms. *Journal of Catalysis* 2014, *312*, 58-68.

13. Zhang, S.; Gong, Y.; Zhang, L.; Liu, Y.; Dou, T.; Xu, J.; Deng, F., Hydrothermal treatment on ZSM-5 extrudates catalyst for methanol to propylene reaction: Finely tuning the acidic property. *Fuel Processing Technology* **2015,** *129*, 130-138.

14. Wang, Q.; Han, W.; Hu, H.; Lyu, J.; Xu, X.; Zhang, Q.; Wang, H.; Li, X., Influence of the post-treatment of HZSM-5 zeolite on catalytic performance for alkylation of benzene with methanol. *Chinese Journal of Chemical Engineering* **2017,** *25* (12), 1777-1783.

15. Silaghi, M.-C.; Chizallet, C.; Sauer, J.; Raybaud, P., Dealumination mechanisms of zeolites and extra-framework aluminum confinement. *Journal of Catalysis* **2016,** *339*, 242-255.

16. Ong, L. H.; Dömök, M.; Olindo, R.; van Veen, A. C.; Lercher, J. A., Dealumination of HZSM-5 via steam-treatment. *Microporous and Mesoporous Materials* **2012,** *164*, 9-20.

17. Pashkova, V.; Sklenak, S.; Klein, P.; Urbanova, M.; Dedecek, J., Location of Framework Al Atoms in the Channels of ZSM-5: Effect of the (Hydrothermal) Synthesis. *Chem. Eur. J.* **2016**, *22*, 3937-3941.

18. Holzinger, J.; Beato, P.; Lundegaard, L.; Skibsted, J., Distribution of Aluminum over the Tetrahedral Sites in ZSM-5 Zeolites and Their Evolution after Steam Treatment. *J. Phys. Chem. C* **2018**, *122*, 15595-15613.

19. Dib, E.; Mineva, T.; Veron, E.; Sarou-Kanian, V.; Fayon, F.; Alonso, B., ZSM-5 Zeolite: Complete Al Bond Connectivity and Implications on Structure Formation from Solid-State NMR and Quantum Chemistry Calculations. *J. Phys. Chem.* Lett. 2018, 9, 19-24.

20. Schallmoser, S.; Ikuno, T.; Wagenhofer, M. F.; Kolvenbach, R.; Haller, G. L.; Sanchez-Sanchez, M.; Lercher, J. A., Impact of the local environment of Brönsted acid sites in ZSM-5 on the catalytic activity in n-pentane cracking. Journal of Catalysis 2014, 316, 93-102.

21. Dedecek, J.; Balgová, V.; Pashkova, V.; Klein, P.; Wichterlová, B., Synthesis of ZSM-5 Zeolites with Defined Distribution of Al Atoms in the Framework and Multinuclear MAS NMR Analysis of the Control of Al Distribution. Chemistry of Materials 2012, 24 (16), 3231-3239.

22. Li, C.; Vidal-Moya, A.; Miguel, P. J.; Dedecek, J.; Boronat, M.; Corma, A., Selective Introduction of Acid Sites in Different Confined Positions in ZSM-5 and Its Catalytic Implications. ACS Catalysis 2018, 8 (8), 7688-7697.

23. Chen, K.; Gumidyala, A.; Abdolrhamani, M.; Villines, C.; Crossley, S.; White, J. L., Trace water amounts can increase benzene H/D exchange rates in an acidic zeolite. *Journal of Catalysis* **2017,** *351*, 130-135.

24. Chen, K.; Kelsey, J.; White, J. L.; Zhang, L.; Resasco, D., Water Interactions in Zeolite Catalysts and Their Hydrophobically Modified Analogues. *ACS Catalysis* **2015,** *5* (12), 7480-7487.

25. Chen, K.; Abdolrhamani, M.; Sheets, E.; Freeman, J.; Ward, G.; White, J. L., Direct Detection of Multiple Acidic Proton Sites in Zeolite HZSM-5. *Journal of the American Chemical Society* **2017,** *139* (51), 18698-18704.
26. Munson, E. J.; Ferguson, D. B.; Kheir, A. A.; Haw, J. F., *J. Catal.* **1992**, *136*, 504-509.
27. Wang, X.; Coleman, J.; Jia, X.; White, J. L., Quantitative Investigations of Transient Acidity in Zeolites and Molecular Sieves, *J. Phys. Chem. B.* **2002**, *106*, 4941-4946.
28. Ryder, J. A.; Chakraborty, A. K.; Bell, A. T. Density Functional Theory Study of Proton Mobility in Zeolites: Proton Migration and Hydrogen Exchange in ZSM-5. J. Phys. Chem. B 2000, 104, 6998− 7011.
29. Hunger, M. Solid State Nucl. Magn. Reson. 1996, 6, 1-29.
30. Brunner, E.; Ernst, H.; Freude, D.; Hunger, M.; Krause, C. B.; Prager, D.; Reschetilowski, W.; Schwieger, W.; Bergk, K. H. Zeolites 1989, 9, 282-286.
31. Batamack, P.; Doremieux-Morin, C.; Fraissard, J.; Freude, D. J. Phys. Chem. 1991, 95, 3790-3796.
32. Gabrienko, A. A.; Danilova, I.; Arzumanov, S.; Pirutko, L.; Freude, D.; Stepanov, A. G., Direct Measurement of Zeolite Acidity by FTIR Spectroscopy: Solid-State 1H MAS NMR Approach for Reliable Determination of Intergrated Molar Absorption Coefficients. J. Phys. Chem. C. 2018, 122, 25386-25395.
33. Beck, L. W.; White, J. L.; Haw, J. F. *J. Am. Chem. Soc.* **1994**, *116*, 9657-9661.
34. Huo, H.; Peng, L.; Grey, C. P. *J. Phys. Chem. C* **2009**, *113*, 8211-8219.
35. ASTM D5758-01 Standard Test Method for Determination of Relative Crystallinity of Zeolite ZSM-5 by X-Ray Diffraction, 2015.
36. Wang, C.; Mao, X.; Caratzoulas, S.; Gorte, R. J., H-D Exchange of Simple Aromatics as a Measure of Brönsted-Acid Site Strengths in Solids. *Catal. Lett.* **2018**, *148*, 3548-3556.

FUTURE WORK

Synthesize HZSM-5 (MFI) and HZSM-22 (TON):

Zeolites with high surface area, different pore sizes and accessible active sites have been prepared for promising applications such as catalysis, medicine, and microelectronics. Their physicochemical properties are dependent on spatial starting reagents, type of structure-directing agents (SDA), temperature, pressure, and reagent sources[1]. The preparation of zeolites is usually carried out using different synthesis methods such as hydrothermal, solvothermal, and ionothermal methods. The hydrothermal methods are mostly applied for synthesis of zeolites using commercial chemicals as the primary source of SiO_2 and Al_2O_3. This method is carried out in the presence of water as solvent, and base solution as mineralizer. The reagents are crystallized inside a Teflon-lined autoclave under pressure and the temperature range is 90-180°C for optimum zeolite production. In solvothermal method, any nonpolar, polar, and hydrophobic solvents such as alcohols, hydrocarbons, and pyridine can be used to prepare zeolites. Ionothermal method is similar to the solvothermal synthesis method in which the solvent used are ionic liquids[2].

The distribution of Al among different voids of a given zeolite influences catalytic reactivity, in spite of the similar acid strength of attendant protons, because reactive intermediates and transition states stabilized at such protons interact with surrounding oxide cavities by van der Waals forces whose strength depends on the geometry of the confining environment. This Al distribution also influences the structural stability of a given zeolite.

As I explained before, the distribution and content of aluminum atoms play important roles in acidities and control the locations of compensative protons which are Brönsted acid sites. There are three different types of Al locations in zeolite structure:

(i) Single Al atoms which only one Al atom (without any nearest neighbor) is located in five- or six membered ring; ($Al{-}O(-Si{-}O)_x{-}Al$, $x \geq 3$),

(ii) Close or paired Al atoms which two Al atoms are located in different framework rings; ($Al{-}O(-Si{-}O)_x{-}Al$, $x = 1, 2$)

Therefore, catalyst synthesis will be a key component of the work, primarily to prepare well-characterized structures at varying Si/Al, to prepare one- versus two-dimensional channel structures with similar topologies (e.g. MFI vs. TON), and to control extraframework Al, silanol defect densities, and tune densities and strength of acid sites in hydrocarbon reactions.

ZSM-5 zeolite catalysts, a member of MFI family, can be synthesized with different Al distribution with different single and close (pairs and single) Al atoms in the framework controlled by using various aluminum sources such as $Al(OH)_3$ and $Al(NO_3)_3$. Also, it has been reported that MFI zeolites synthesized in the presence of only tetrapropylammonium (TPA^+) cations contain higher fractions of Al atoms located in 10-MR channel intersections, within which TPA^+ cations remain occluded in crystalline products, than MFI zeolites synthesized with mixtures of organic TPA^+ and inorganic alkali (Na^+) cations, which reside within straight and sinusoidal 10-MR channels[3].

Aluminosilicate ZSM-22 zeolite with a TON structure possesses a one-dimensional channel system with pore openings of 0.45 × 0.55 nm. The TON framework is rich in five-membered rings and belongs to the mordenite family of zeolites. The unique pore architecture and its mild acidity render ZSM-22 zeolite outstanding catalytic performance in the skeletal isomerization of normal alkanes, selective xylene isomerization, methylation of toluene with methanol to p-

xylene. Zeolites with the TON structure can be synthesized with a wide range of organic "template" known as structure-directing agents[4-5].

We believe that control of acid site density and acid site location will be paramount to determining if and how water can enhance hydrocarbon reactivity in solid acids.

Investigate the effect of EFAl and water loading on C-C bond cleavage by using high-temperature in-situ MAS NMR

Water can be incorporated in the reaction system in the feed or evolved as a side product inside the solid acid catalyst during reaction. We can conduct ^{13}C isotpic exchange reaction in order to investigate whether adding sub-stoichiometric amount of water can increase the reactivity of acidic zeolites with different concentraction of EFAl species on isomerization of n-butane to i-butane.

The isomerization of n-butane to isobutane is one of the important studies to understand the reaction mechanism in acid catalysis. The possible reaction steps contain cracking, dehydrogenation, and isomerization. All of these steps are initiated from the protonation of C-C or C-H bonds of n-butane to form a five-coordinated carbonium ion by proton arising from Brönsted acid sites.

In-situ ^{13}C MAS NMR can be used for investigating the effect of water in presence of different acidic sites arising from BAS and EFAl species.

Modification on Al content in high aluminum zeolite, HZSM-5-11.5

In zeolite with various Si/Al ratios, as the Si/Al ratio decreases, aluminum contents increase and consequently the acidic properties of zeolite is getting stronger.

Our preliminary data of ^{1}H MAS NMR shows that HZSM-5 with Si/Al=11.5 has a different spectrum than other ratios. There are no peaks at 2.6-2.8 ppm and 13-15 ppm which are

originate from hydroxyl groups on aluminum atoms that exist as extra-lattice or extra-framework aluminum (AlOH), most likely as small aluminum oxide moieties.

Also, both mild and severe steaming conditions for this catalyst are different than HZSM-5 with Si/Al=15. Transfering aluminum from framework to produce EFAl species happen at lower temperature and shorter time, which means that HZSM-5 with Si/Al=11.5 is less stable than Si/Al=15 and it is easier to dealuminate.

Fig.1 indicates that dehydration of the catalyst through the flow reactor (500°C –overnight) and the vacuum line can change the concentraction of species located at 5-7 ppm.

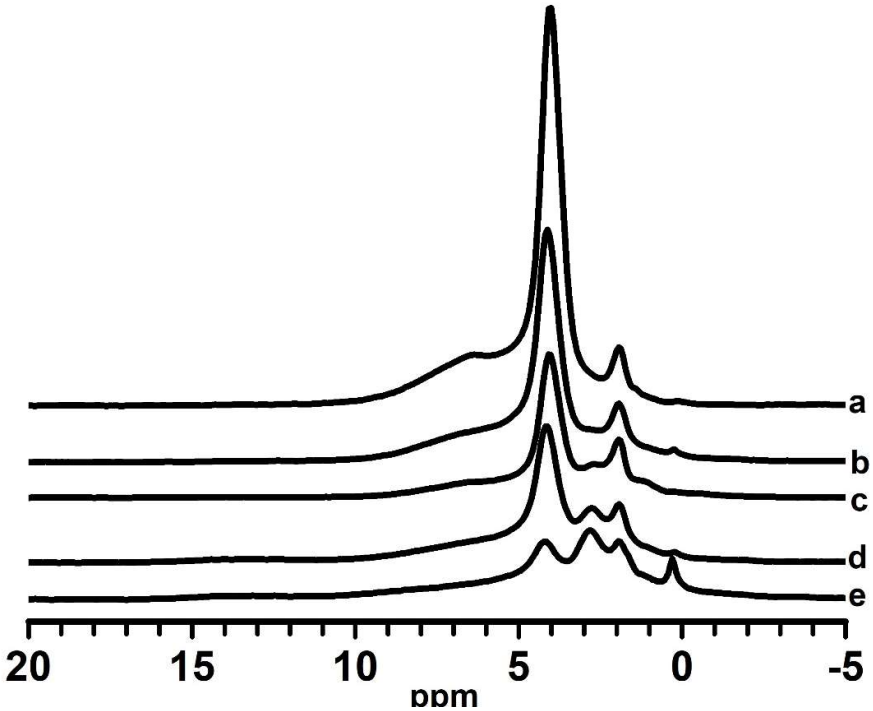

Fig. 1. ^{1}H MAS NMR spectra of HZSM-5 with Si/Al=11.5 acquired at room temperature for (a) dehydrated catalysts prepared under vacuum line heating, (b) dehydrated catalyst in the flow reactor at 500°C –overnight with air, (c) dehydrated catalyst in the flow reactor at 600°C – 5 hrs. with compressed air (from OU group), (d) mild steamed sample, 500°C- 5hrs , 12ml/min (N_2+H_2O), and (e) severe steamed sample, 500°C- 48hrs , 12ml/min (N_2+H_2O).

The new information contained in Fig. 1 is that the peak located at 2.6-2.8 ppm can be produced by dehdration under flow reactor with air and steaming in presence of water. The bridgng acid site for the received sample which is dehydrated under vacuum line is much bigger than the sample which is dehydareted under flow reactor and this signal drops quickly by increasing the steaming time.

For the future, a few suggestions and important questions about HZSM-5 with Si/Al=11.5 that need to be explored are stated below:

1. What are those species at 5-7 ppm?

   - Ammoniom species left from the raw material; for removing the ammonia and making the proton form, it needs longer dehyrdation and/or higher temperature.

   - Defect site species including acidic EFAl protons or protons from non-crystalline regions similar to amorphous silica-alumina.

2. Is the reactivity of HZSM-5 catalyst for Si/Al=11.5 larger than Si/Al=15 based on the density of Brönsted acid sites? (e.g. acid density is 1.36 mmol/g for Si/Al = 11.5 and 1.04 mmol/g for Si/Al = 15 based on Si/Al ratio).

3. What is the reactivity of the received sample (without any EFAl species) in comarision to the steamed samples with both BAS and EFAl species?

References:

1. Luo, Y.; Wang, Z.; Jin, S.; Zhang, B.; Sun, H.; Yuan, X.; Yang, W., Synthesis and crystal growth mechanism of ZSM-22 zeolite nanosheets. *CrystEngComm* **2016,** *18* (30), 5611-5615.

2. Henry E. Mgbemere, I. C. E., Ganiyu I. Lawal, Zeolite Synthesis, Characterisation and Application Areas: A Review. *International Research Journal of Environmental Sciences* **2017,** *6* (10).

3. Di Iorio, J. R.; Gounder, R., Controlling the Isolation and Pairing of Aluminum in Chabazite Zeolites Using Mixtures of Organic and Inorganic Structure-Directing Agents. Chemistry of Materials 2016, 28 (7), 2236-2247.

4. del Campo, P.; Beato, P.; Rey, F.; Navarro, M. T.; Olsbye, U.; Lillerud, K. P.; Svelle, S., Influence of post-synthetic modifications on the composition, acidity and textural properties of ZSM-22 zeolite. *Catalysis Today* **2018,** *299*, 120-134.

5. Ernst, S.; Weitkamp, J.; Martens, J. A.; Jacobs, P. A., Synthesis and shape-selective properties of ZSM-22. *Applied Catalysis* **1989,** *48* (1), 137-148.

VITA

Maryam Abdolrahmani

Candidate for the Degree of

Doctor of Philosophy

Dissertation: BRONSTED ACID SITE HETEROGENEITY IN ZEOLITE HZSM-5 AND SYNERGISTIC EFFECTS WITH WATER IN HYDROCARBON REACTIONS

Major Field: Chemistry

Biographical:

Education:

- Completed the requirements for the Doctor of Philosophy in your major at Oklahoma State University, Stillwater, Oklahoma in May, 2019.
- Completed the requirements for the Master of Science in chemical engineering at University of Science & Technology, Tehran/Iran in 2009.
- Completed the requirements for the Bachelor of Science in chemical engineering at Mohaghegh Ardebili, Ardebil, Iran in 2006.

Experience:

Oklahoma State University (January 2014- May 2019)

- Preparation of different zeolite structures and characterization of acid sites of zeolite by using solid state MAS NMR.
- Extraction and creation of extra-framework aluminum species from HZSM-5 by using different post-synthetic methods such as chemical washing and steaming.
- Investigation of the role of water in the reaction mechanisms of benzene, a single ring aromatic in methanol to hydrocarbon chemistry, on HZSM-5 zeolite catalysts by using In-situ MAS NMR.

IRANDELCO (October 2007 – September 2012)

- Experienced in Catalyst preparation and Characterization Techniques and instruments (TPR, PSA, BET, XRF, AAS, XRD, ICP, Catalytic activity tests, Aging and stability tests).